Analysis of D^0 - $\bar{D}^0$ Mixing in the $K\pi$ Channel

Mark Mattson and Paul Karchin
Wayne State University
CDF/DOC/BOTTOM/CDFR/7116
Version 1.5

March 6, 2006

Abstract

The CDF Run II experiment has collected a substantial sample of $D^* \to \pi D^0$, $D^0 \to K\pi$. This data will be used to investigate the ratio of the $D^0 \to K^+\pi^-$ wrong-sign (WS) decay rate to the $D^0 \to K^-\pi^+$ right-sign (RS) decay rate. The Cabibbo favored (CF) D^0 decay will produce RS signal. The WS signal will be composed of the doubly Cabibbo suppressed D^0 decay, and $D^0 - \bar{D}^0$ mixing. The backgrounds for the wrong-sign sample are examined. Of specific interest is the contamination from right-sign D^*s, where the D^0 kaon and pion assignments are swapped. The studies from data and toy Monte-Carlo show that we understand how the right-sign sample transforms in the wrong-sign plot. A cut was found that removed most of the background, with only a modest cost to signal.

A technique is presented where the right-sign and wrong-sign D^* signals can be cleanly seen against a background of fake D^* candidates. A set of ntuple cuts are presented that would improve the signal to background. A cut optimization method is shown, to be used when the wrong-sign D^* signal region is blinded. An older data set (hbot0h) was used to test the methods. With approximately $\int \mathcal{L} \sim 60\, pb^{-1}$, the wrong-sign D^* yield is 254 ± 47. For the full set of data (xbhd0d), the blinded results predict that the CDF II measurement of the time-integrated WS/RS D^0 ratio will be 3.6 (assumed) ± 0.21 (stat.) ± 0.11 (sys.) $\times 10^{-3}$.

With approximately $\int \mathcal{L} \sim 350\, pb^{-1}$, the time-integrated ratio of WS to RS D^0s is 4.05 ± 0.21 (stat.) ± 0.11 (sys.) $\times 10^{-3}$. This measurement is competitive with the current world-best results, and consistent with the world average.

Contents

List of Figures

List of Tables

1 Introduction

This CDF note is intended to provide details on the D-Mixing analysis being done by members of the Wayne State group. There have been a number of talks so far at the B-Hadronic meetings [1, 2, 3, 4, 5, 6, 7]. This note provides more details of the analysis.

The CDF experiment has collected a large sample of charm mesons during Run II. The first published Run II result was the mass difference between the D_s and D^+ in the $KK\pi$ mode.[8] The $D^* \to \pi D^0$ sample, where the D^0 decays to a kaon and a pion, has a large, clean signal. This sample is in use for several analyses[9, 10, 11], and will be used to investigate $D^0 - \bar{D^0}$ mixing. D mixing can also be investigated by using CP-even and CP-odd final states, such as $D^0 \to KK$ or $\pi\pi$, or semi-leptonic decays. This analysis will focus on the decays to $K\pi$.

1.1 Theory

A good introduction to $D^0 - \bar{D^0}$ mixing was written by Alexey Petrov[12]:

> One of the most important motivations for studies of weak decays of charmed mesons is the possibility of observing a signal from new physics which can be separated from the one generated by the Standard Model (SM) interactions. The low energy effect of new physics particles can be naturally written in terms of a series of local operators of increasing dimension generating $\Delta C = 1$ (decays) or $\Delta C = 2$ (mixing) transitions. For D^0-$\bar{D^0}$ mixing these operators, as well as the one loop Standard Model effects, generate contributions to the effective operators that change D^0 state into $\bar{D^0}$ state leading to the mass eigenstates $|D_{1,2}> = p\,|D^0> \pm q\,|\bar{D^0}>$, where the complex parameters p and q are obtained from diagonalizing the D^0-$\bar{D^0}$ mass matrix. The mass and width splittings between these eigenstates are parameterized by $x \equiv (m_2 - m_1)/\Gamma$, $y \equiv (\Gamma_2 - \Gamma_1)/(2\Gamma)$, where $m_{1,2}$ and $\Gamma_{1,2}$ are the masses and widths of $D_{1,2}$ and the mean width and mass are $\Gamma = (\Gamma_1 + \Gamma_2)/2$ and $m = (m_1 + m_2)/2$. Since y is constructed from the decays of D into physical states, it should be dominated by the Standard Model contributions, unless new physics significantly modifies $\Delta C = 1$ interactions. On the contrary, x can receive contributions from all energy scales, so it is usually conjectured that new physics can significantly modify x leading to the inequality $x \gg y$. As we discuss later, this signal for new physics is lost if a relatively large y, of the order of a percent, is observed.

The known properties of the D^0 are available from the Particle Data Group[13]. The 75 page PDF file includes an overview of D mixing, starting on the 2nd page. Unlike kaon and beauty mixing, the D mixing proceeds very slowly. Figure 1 was from a talk by Petrov at CDF[14], that illustrates why charm mixing is expected to be much smaller than beauty mixing.

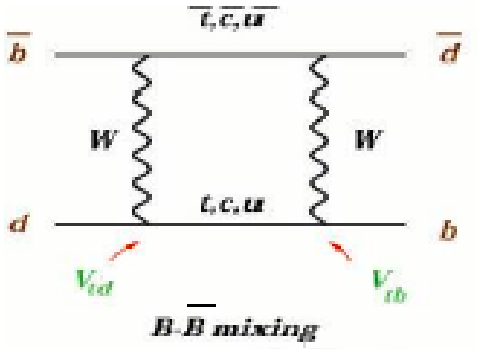

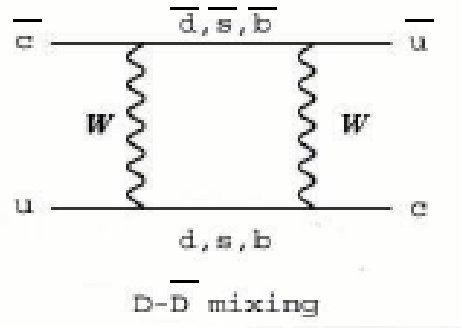

$\overline{D^0} - D^0$ mixing	$\overline{B^0} - B^0$ mixing
• intermediate down-type quarks • SM: b-quark contribution is negligible due to $V_{cd}V_{ub}^*$ • $rate \propto f(m_s) - f(m_d)$ (zero in the SU(3) limit)	• intermediate up-type quarks • SM: t-quark contribution is dominant • $rate \propto m_t^2$ (expected to be large)
1. Sensitive to long distance QCD 2. Small in the SM: New Physics! (must know SM x and y)	1. Computable in QCD (*) 2. Large in the SM: CKM!

(*) up to matrix elements of 4-quark operators

Figure 1: The figures are on page 5 of the slides[14]. Charm mixing is expected to be very small, unlike strange and beauty mesons. Petrov contrasts the charm and beauty mixing box diagrams.

Petrov also examined the double penguin ("di-penguin") operator.[15] This is topologically distinct from the box diagram, and both contribute to the short-distance meson mixing amplitude. It was shown to be marginally important for strange mixing, and completely negligible for beauty. He demonstrated that the operator contributes to D-meson mass difference at the same order of magnitude as the usual box diagram. It also has a sign opposite to the box diagram, which implies that the short-distance piece will be smaller that previous estimates (based only on the box diagram contribution). He also stressed that $D^0 - \bar{D}^0$ mixing is dominated by long distance pieces, not by the short distance box diagram contribution. An example of a long distance process is shown in figure 2.

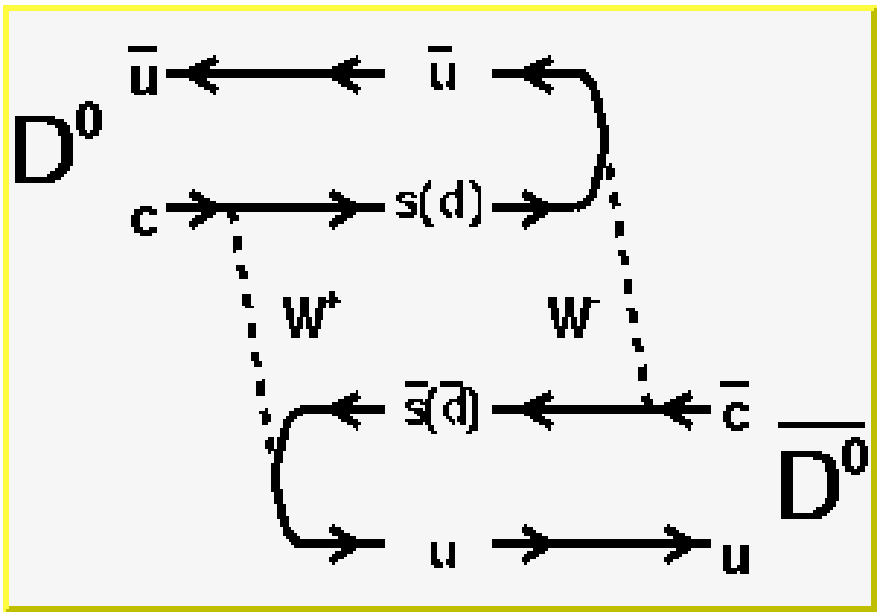

Figure 2: Both the D^0 and $\bar{D}^0$ can decay to the same final state (either 2 kaons or 2 pions). This allows the particle to oscillate to the anti-particle through a virtual state of kaons (or pions).

The theoretical predictions of x and y have large uncertainties, mostly because the charm quark mass m_c does not fit the light or heavy approximations. Depending on the assumptions, most calculations yield $x, y < 10^{-3}$.

1.2 Term Definitions

To measure mixing, the particle and anti-particle decays need to be kept straight. This requires the definition of some terms, starting with right-sign (RS) and wrong-sign (WS). The literature for D-mixing uses RS and WS heavily. For the decay $D^{*+} \to \pi^+ D^0$, the pion from the D^* decay is used to tag whether the meson was a D^0 or a $\bar{D}^0$. The D^0 then decays to a kaon and a pion, resulting in a kaon and two pions being observed in the detector. For

RS decays, both pions have the same charge, while for WS decays, the pions have opposite charge. (For all decays, the charge conjugate decay is included, unless otherwise mentioned. So $D^{*-} \to \pi^- \bar{D}^0$ is also used.)

The first step is usually to get the ratio of wrong-sign decays to right-sign decays, for the D^0 decay to a kaon and a pion. There are three decay paths that will contribute signal events for this analysis. The Cabibbo favored (CF) decay $D^0 \to K^-\pi^+$ (fig 3) will be signal in the right-sign mass plots. The wrong-sign signal will be composed of the doubly Cabibbo suppressed (DCS) decay $D^0 \to K^+\pi^-$ (fig 4) and D-mixing. D-mixing is where the D^0 oscillates to a $\bar{D}^0$ (or vice versa), then the D meson has a CF decay.

Without particle identification, each two-track combination will form both a RS and a WS candidate, depending on which track is assigned a kaon mass (with the other track being given the pion mass). This means that a Cabibbo favored decay can show up as a signal event in the RS mass plots (correct kaon and pion particle assignments) and as background in the WS mass plots (wrong kaon and pion assignments).

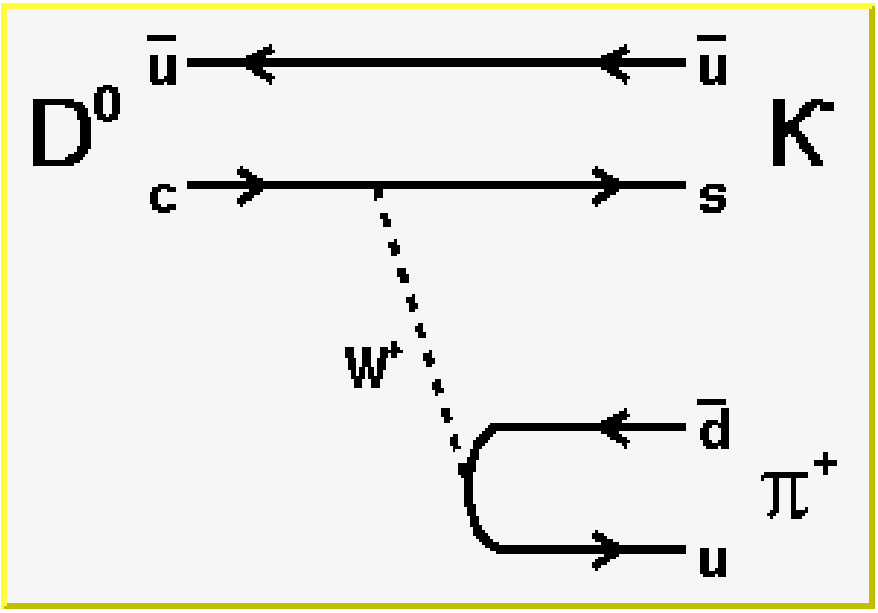

Figure 3: Right-Sign CF D^0 decay by a W emission.

The parameters x and y (that were defined in Petrov's introduction as $x \equiv (m_2 - m_1)/\Gamma$, $y \equiv (\Gamma_2 - \Gamma_1)/(2\Gamma)$) cannot be measured directly, as there can be a strong phase difference (δ) between DCS and CF decay amplitudes. This results in parameters $y' = y\cos\delta - x\sin\delta$, $x' = x\cos\delta + y\sin\delta$. The term R_D is the time-integrated rate of the direct DCS decay relative to the RS decay. $R_M = \frac{1}{2}(x^2+y^2) = \frac{1}{2}(x'^2+y'^2)$ is a term for the mixing rate. In the limit of CP conservation, the ratio of the time-dependent wrong-sign compared to integrated right-sign D^0 decays is $r_{WS}(t) = \Gamma(D^0(t) \to K^+\pi^-)/\Gamma(D^0 \to K^-\pi^+) = e^{-t}(R_D + \sqrt{R_D}y't + \frac{1}{2}R_M t^2)$. The time unit t is the proper time of the D^0 decay in units of the D^0 lifetime. The time-

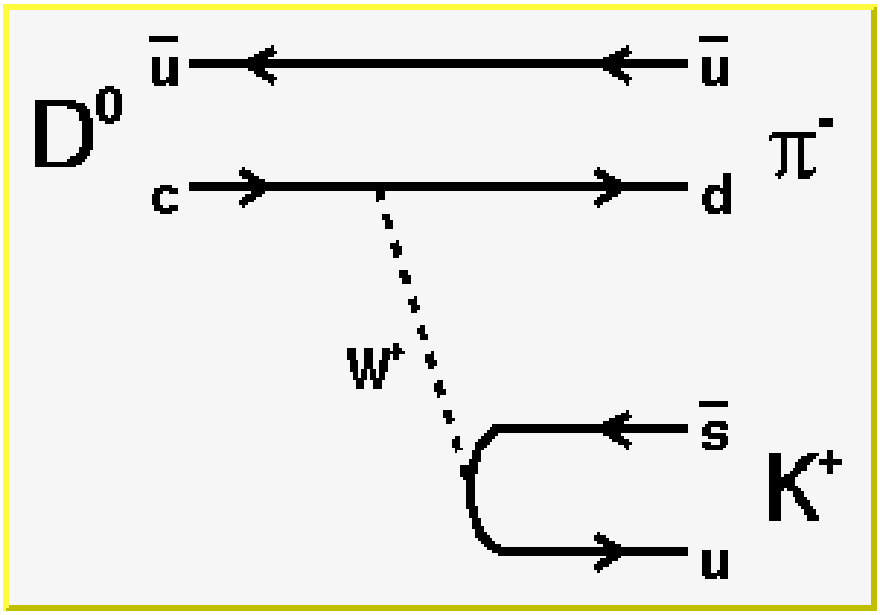

Figure 4: Wrong-Sign DCS D^0 decay by a W emission.

integrated ratio will be $R_{WS} = \int_0^\infty r_{WS}(t)dt = R_D + \sqrt{R_D}y' + R_M$.

1.3 Results From Other Experiments

Once a good WS signal is present, the time-independent ratio is usually measured first. In the limit of no mixing, the WS signal is the same as the DCS signal. Recent results of the time-integrated ratio are given in table 1, with the assumption that $R_{WS} = R_D$. The Belle[16, 17] and BABAR[18] experiments have the most statistics. Their published results will be used for guidance in this analysis. The CDF experiment has a comparable number of tagged D^0 already written to tape. The other experiments have an advantage that their analysis used particle identification with good single track efficiency ($\sim 85\%$) and low single track fake rates ($\sim 5\%$).

Once the data is understood in more detail, a time-dependent analysis can be done to obtain the mixing parameters. Results from other experiments are consistent with no mixing, within uncertainties.

1.4 Analysis Strategy

This study will proceed in two parts. The analysis will start with an older dataset (hbot0h), to develop and refine methods that will be used for the analysis. The wrong-sign signal will be observed, to see what techniques work and which do not. When possible, data will be used instead of Monte Carlo. Essentially, this data is being used to practice. The results of

Experiment (Luminosity)	# of RS D^0	# of WS D^0	Ratio of WS / RS
PDG values[13]	BR (3.80 ± 0.09) %	BR (1.38 ± 0.11) x 10^{-4}	0.362 ± 0.029 %
CLEO[19] 9.0 fb^{-1}	13527 ± 116	$44.8^{+9.7}_{-8.7}$	$0.332^{+0.063}_{-0.065} \pm 0.040$ %
FOCUS[20]	36760 ± 195	149 ± 31	$0.404 \pm 0.085 \pm 0.025$ %
Belle[16] 46.2 fb^{-1}	120795 ± 371	450 ± 31	$0.372 \pm 0.025^{+0.009}_{-0.014}$ %
BABAR[18] 57.1 fb^{-1}	120000	430	$0.357 \pm 0.022 \pm 0.027$ %
Belle[17] 90 fb^{-1}	227721± 497	845 ± 40	$0.381 \pm 0.017^{+0.08}_{-0.16}$ %

Table 1: Results by Other Experiments For the Time-Integrated Ratio

this study will be present internally to CDF, to give an idea of what is possible.

Once the methods have been finalized, the analysis will switch to dataset xbhd0d. That data is processed with the most recent CDF offline software. This dataset is about 6 times larger than hbot0h, and contains the data events that went into hbot0h. The more recent dataset will be used to generate final (hopefully blessed) results. The wrong-sign signal region will be blinded while the cut optimization is being done, to reduce bias.

Although only the $D^0 \to K^-\pi^+$ is mentioned, the charge-conjugate decay $\bar{D}^0 \to K^+\pi^-$ is also reconstructed. All plots and discussions will include the charge-conjugate decay mode, unless specifically mentioned otherwise.

2 Analysis Settings

This section outlines the path from the accelerator collisions to the generated ROOT ntuples. Detector information is gathered during collisions (online), processed later in a computer farm (offline), then run through a user-specific program. The results of that program are in a ROOT file, which is used to generate the final plots. These details are common to most charm (or B) analyses, and provided in case others wanted to repeat this study. For people familiar with generating D^* ntuples, they might want to skip to the next chapter, when details that are specific to the D-mixing analysis start.

2.1 Online Data Taking

The $D^0 \to K^-\pi^+$ data will show up in the data stream taken by the B-Charm trigger path. It was designed for B physics, but has been found to be efficient for charm as well. Details have been written in the CDF Note 6526.[21] The trigger path is often called the Two Track Trigger (TTT).

The basic idea is that B and charm hadrons have high mass, long lifetimes compared to the random combinatorial background, and small lifetimes compared to strange particles. The trigger looks for a detached vertex (to avoid background from the primary interaction), with characteristics consistent with the decay of a high mass particle.

The Level 1 trigger requirements are listed next. XFT stands for "eXtremely Fast Tracker", and is designed to find tracks in the COT for the L1 trigger.

- a pair of tracks with opposite charge
- 4 XFT layers per track
- XFT p_T greater than 2.04 GeV for both tracks
- angle between the tracks is between 0 and 135 degrees
- scalar sum of the p_Ts of the tracks is greater than 5.5 GeV

The Level 2 trigger requirements are a little more complicated. For the data being used, the requirements changed part of the way through the sample. SVT stands for "Silicon Vertex Trigger", and finds tracks in the silicon detectors. "d_0" is the impact parameter, how far the track misses the primary vertex when it has been extrapolated back. The initial requirements were:

- two tracks
- SVT $\chi^2 < 25$
- d_0 between 0.1 and 1.0 mm
- p_T greater than 2.04 GeV for both tracks

After about 9 pb^{-1}, the following additional requirements were added to L2:

- d_0 between 0.12 and 1.0 mm
- angle between the tracks is between 2 and 90 degrees
- scalar sum of the p_Ts of the tracks is greater than 5.5 GeV
- the intersection point in the $r - \phi$ plane projected along the net momentum vector of the two tracks must be greater than 200 μm from the beam line

The Level 3 executable matches SVT tracks to COT tracks based on curvature and angle. Once matches are made, the cuts (similar to what was required in L1 and L2) are applied.

The TTT note listed other B-Charm trigger paths (such as low-p_T and high-p_T), which were used during data taking. When the data rate is too high, the triggers are prescaled to match what the DAQ (data acquisition) can handle. The idea was to have a tight trigger (high-p_T) which is scaled very little, and a loose trigger (low-p_T) that can be heavily prescaled. Since this analysis is measuring a ratio of branching fractions and not an absolute number, we are not concerned about the prescales. In addition, the events from the low-p_t trigger will not pass momentum requirements that are imposed when the events are re-analyzed offline.

2.2 Offline Processing

At a later time, the data is processed offline. Any advantages to detector alignment, improved tracking code, and so forth, are applied at this time. Besides various CDF notes, the Offline computing web page has links for data handling, farms, datafile catalog, and the database browser.

The data being used for this analysis belong to the hbot0h sample, which was processed with the 4.8.4 CDF software version. In addition to the normal offline processing, certain data blocks that are not used by the B Group were removed. This allowed the file size to be smaller, and the data could be kept on local disks. This reduces the time delay caused by retrieving data from tape.

2.3 User Created Executable

The hbot0h sample is enriched for charm particles, but is still too large for everyday work. Understanding the data often involves trying many different cuts and selections. There are significant time savings for having a small file that can be run through in minutes, instead of the entire hbot0h sample which would take days (for each change). The data is processed by a user created executable, with the following goals:

- Select events that have reconstructed $D^* \to \pi D^0$, $D^0 \to K\pi$; avoid other charm and B reconstructions

- Store only the quantities needed for this analysis, and write out the results as a ROOT tree (ntuple)

The code was built on the 4.9.1hpt3 CDF software. The relevant code for this analysis resides in a collection of routines called CharmMod, which holds code used for the various charm analyses. The CharmMod Reference Manual is available as a CDF note.[22] TCL files are used to hold parameter and executable settings. These settings can be changed relatively easily, which avoids the need to recompile the entire executable.

The TrackSelectorModule was used to choose which tracks were used in vertexing. The tracks were refit using the KAL method, with the "HelixFit" and "PhysicalError" settings on. Silicon L00 and ISL hits were dropped. The tracking selected two groups of tracks. One group will become the candidates for the daughter tracks of the D^0. The second group will become candidates for the pion produced by the D^*. The major settings are listed in table 2.

Name	Setting	Notes
min COT axial hits	20	All Tracks
min COT stereo hits	20	
min axial superlayers	0	
min stereo superlayers	0	
max $\|\eta\|$	2.0	
min Si hits	3	Group 1 Tracks
min p_T	2.0 GeV	
min Si hits	0	Group 2 Tracks
min p_T	0.35 GeV	

Table 2: These are the important selections used by TrackSelectorModule to get a list of tracks, which will be used by the D1 and D2 VertRecoModules. Group 1 tracks will be used for the D^0 daughter tracks, while Group 2 will be used for the D^* pion.

The D1VertRecoModule was used to reconstruct a two-track vertex, which will become the Cabbibo-favored decay $D^0 \to K^-\pi^+$. A negative sign in front of the particle ID uses the antiparticle instead of the particle. No mass constraint was used. The charge conjugate mode was also found. The daughter tracks had to pass the TTT requirements. Primary Vertex Pointing Constraint was set to false. The other settings are listed in table 3.

The D2VertRecoModule was used to reconstruct a vertex formed from a track and another vertex, which will become the decay $D^{*+} \to \bar{D^0}\pi^+$. This module requires that D1VertRecoModule was run first, to produce a D^0 vertex. The RS decay is to $D^0\pi^+$, but by asking for the $\bar{D^0}$ we could ask for the wrong-sign decay. No mass constraint was used. The charge conjugate mode was also found. Primary Vertex Pointing Constraint was set to false. The other settings are listed in table 4.

The hbot0h sample was divided into 200 segments, and 200 jobs were submitted to the computer farm. Four of those jobs crashed, but were successful when run again. Seven jobs

Name	Setting	Notes
D^0 ID	421	
K^- ID	-321	K^+ would be 321
π^+ ID	211	π^- would be -211
Mass limits	1.7 to 2.0 GeV	
$\Delta\phi$ limits	0. to 2.0 rad	track pair
Δ R max	3.	
Δ Z max	8. cm	
p_t min	5.5 GeV	
L_{xy} min	0.0 cm	
d_0 limits	-999. to 999.	vertex

Table 3: This is a list of important selections used to get a two-track vertex. The tracks are given $K\pi$ particle assignments, to form the D^0 candidates. Some of these cuts are listed in D1VertRecoModule.hh, others are inherited from DFilterModule.hh.

Name	Setting	Notes
D^* ID	413	
D^0 ID	421	$\bar{D^0}$ would be -421
π^+ ID	211	π^- would be -211
Mass Difference limits	0. to 0.17 GeV	
$\Delta\phi$ limits	0. to 4.0 rad	track pair
Δ R max	4.	
Δ Z max	8. cm	
p_t min	5.5 GeV	
L_{xy} min	-999. cm	
d_0 limits	-999. to 999.	vertex

Table 4: This is a list of important selections used to get a vertex formed from a track plus a D1 vertex. This list will become the candidates for $D^* \rightarrow \pi D^0$. The track is given a pion particle assignment. The D^0 vertices come from the D1VertRecoModule. Some of these cuts are listed in D2VertRecoModule.hh, others are inherited from DFilterModule.hh.

failed every time they were submitted to the farm. This suggests a problem with the data, or a subtle code bug. This analysis uses the 193 ROOT files that were written out by the jobs that completed without error.

2.4 ROOT Tree Selections

The ROOT files were filled by the routine DStarD0piAnalModule.cc. The local version of that file should be examined to find the full list of available variables for the ROOT tree (ntuple). Table 5 is a list of variables and cuts that are used most often for this analysis. By convention, all the variables start with "p". The variable letters are related to the physical quantity. For example,"MD" is the D^0 mass, while "MDS" is the mass of the D^*. The addition of "WS" to the name refers to the "Wrong-Sign" mass computed, when the kaon and pion mass assignments are changed. So if we wanted to plot the wrong-sign D^* mass, we would use the variable "pMDSWS".

The wrong-sign quantities are found by taking the D^* candidate found by D2VertRecoModule, and swapping the K and π assignments of the D^0 candidate. We do not find the WS and RS samples separately. Since the RS D^0 has a mass selection between 1.7 and 2.0 GeV, we need to apply this same selection in ROOT to the WS $K\pi$ mass. The ROOT cut "abs(pMDWS-1.85) $<$ 0.15 " will do this. Table 5 gives a list of the most common ROOT cuts and a brief description.

ROOT Command	Description
abs(pMDWS-1.85) $<$ 0.15	WS mass window same as RS mass range
abs(pMD-1.864) $<$ 0.030	"Good" RS D^0s, a selection that will contain some background and the majority of the signal
abs(pMD-1.864) $>$ 0.030	Opposite assignment cut, rejecting "good" RS D^0s
abs(pMDWS-1.864) $>$ 0.030	Opposite assignment cut, rejecting "good" WS D^0s
abs(pMDS-pMD-0.1454) $<$ 0.0020	RS D^* tag, require good $(D^* - D^0)$ mass difference
pMkk $<$ 1.894	Select events consistent with $D^0 \to KK$
pMpipi $>$ 1.834	Select events consistent with $D^0 \to \pi\pi$

Table 5: This is a partial list of selections used when examining the events stored in the ROOT files.

2.5 Dataset xbhd0d

Eventually, the analysis will switch from hbot0h ntuples to xbhd0d. The improved software and calibrations are expected to improve the mass resolution. More variables will be added to the ROOT output, in case they can improve the signal/background discrimination. Although the events that make up hbot0h are a subset of xbhd0d, reprocessing with a different software

version will change the output. The processing code will use many of the same cuts and selections. Differences will be listed in a table, in this note, when the 0d processing starts.

3 Backgrounds in the D^* and D^0 Mass Distributions

The analysis started by reconstructing the all-hadronic mode $D^{*+} \to D^0\pi^+$, $D^0 \to K^-\pi^+$. (Unless otherwise mentioned, all modes include the charge conjugate decay.) The soft pion from the D^* tagged whether the D meson was produced as a D^0 or a $\bar{D^0}$. The kaon and pion charges determined what the particle was when it decayed.

This section presents results using the CDF hbot0h data sample. The data was taken from Oct 2002 through Feb 2003, covering runs 138808-1546487. The selected good runs represent roughly 60 pb^{-1} of luminosity.

Besides the $K\pi$ mass distribution, another common plot will be the mass difference between the D^* candidate and (mass(D^0) + mass(π)). Although the D^* mass could be plotted instead, the mass difference has a much narrower signal peak, which will help reduce background. Most of the systematics that contribute to the mass resolution of both the D^* and the D^0 will cancel out in the mass difference.

The previous chapter mentioned the minimum cuts that are present for all candidates that are written to the ROOT ntuple. A "good D^* tag" means selecting events that have the mass difference very close to the measured value ($m_{D^*} - m_{D^0} - m_\pi = 5.83$ MeV). For the hbot0h data, that window is $\pm$ 2 MeV. A "good D^0" means that the candidate mass is close to ($m_{D^0} = 1.8645$ GeV). For the hbot0h data, that window is $\pm$ 30 MeV. "Cosine Kaon" is the cosine of the decay kaon direction, in the D^0 rest frame, relative to the direction of the D^0 in the lab frame.

One virtue of this analysis is that we have a clear RS D^* signal. Figure 5 shows the RS mass distributions. Both plots have large signal compared to background. The "good D^* tag" was applied to the left plot, and the "good D^0" selection was applied to the right plot. The WS D^* should have the same properties as the right-sign signal (except for branching rate and a miniscule lifetime difference). This chapter will examine the background sources that will be present in the wrong-sign distributions. The next chapter will deal finding selections that will have a high efficiency for signal, and reduce background.

To obtain an accurate count of the WS signal, we need to understand what type of events go into our analysis.

- Signal events - Correctly reconstructed $D^* \to \pi D^0$, $D^0 \to K\pi$ events. These will be from either a doubly Cabibbo suppressed decay, or from mixing ($D^0 \to \bar{D^0}$ oscillation followed by a Cabibbo favored decay).

- Random pion - Real $D^0 \to K\pi$ events, where the tagging pion used to form the D^* candidate is not associated with the D^0.

- CF D^* misidentification - A Cabibbo favored D^* decay where the kaon and pion assignments of the D^0 daughter tracks swapped (double particle misidentification). This will be a background in the WS plots.

- Single misidentification - A $D^0 \to KK$ or $\pi\pi$ decay where one of the tracks is misidentified, to form a $K\pi$ candidate.

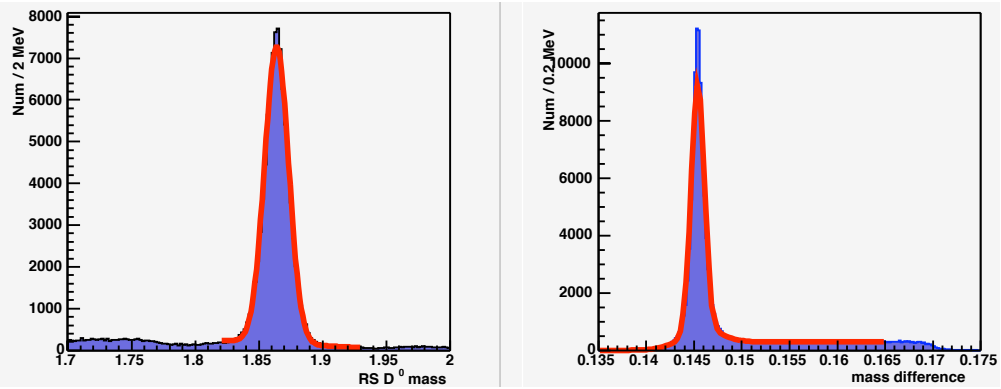

Figure 5: The left plot is the $K\pi$ mass for candidates with a good D^* tag. The x-axis is in units of GeV. The peak fit has 84K events, with a gaussian width of 9.47 MeV. The right plot is the mass difference $(D^* - D^0)$ for good D^0s. Two gaussians where used to fit the peak. The narrow gaussian has a fixed width of 0.72 MeV, and has 79K events. The wider fit has a fixed width of 2.2 MeV, and has 14K events.

- Combinatoric background - One or both tracks for the D^0 candidate do not belong to a $D^0 \to K\pi$ decay. This may be random tracks from the primary vertex, but may include partially reconstructed charm decays.

3.1 Signal

The $D^0 \to K\pi$ distribution will show up as an almost gaussian peak, with a width around 10 MeV. The actual shape is narrower at the center and wider in the tails, compared to a single gaussian. An earlier study of D^0 mesons by CDF[23] describes a procedure to model the distribution. We will use a double-gaussian or other simple approximation for this signal shape, unless it becomes necessary to use a more complex (and accurate) model.

For the D^* distribution, it is common to plot the mass difference ($M_{D^*} - M_{D^0}$ or $M_{D^*} - M_{D^0} - M_\pi$) rather than the mass of the D^*. Systematics that contribute to the D^0 peak width will cancel in the mass difference, resulting in a narrower peak.

Figure 5 gives examples of the signal peaks, for the RS $K\pi$ mass and D^* mass difference distributions.

3.2 Random Pion

This background has a D^0 that combines with an unassociated pion to form a (fake) D^* candidate. These random pions could be from the primary vertex, or some other decay that is independent of the D^0. There are two cases: where the D^0 is reconstructed correctly, and where the D^0 has double misidentification. Although they are D^0 decays, these events are background for this analysis since they are not D^*s.

In figure 5, the right plot has the RS mass difference distribution. The candiates outside the signal peak are mostly combinatoric background and fake tag events. For a correctly assigned D^0 with a fake tag, the $K\pi$ distribution will show a normal D^0 signal, while the $(D^* - D^0)$ mass difference will not have a peak. For a D^0 with $K\pi$ misidentification, the $K\pi$ mass distribution will be smeared out, almost a flat background.

3.3 CF D^* Background

The basic reconstruction does not have particle identification. This implies that every $K^-\pi^+$ reconstruction can also have the mass assignments reversed, to generate a $K^+\pi^-$ candidate. A correct mass assignment will result in a narrow peak, the width being determined by detector resolution. (The physical D^0 width is negligible compared to detector resolution.) Cabibbo favored decays that have the kaon and pion particle assignments swapped will produce wrong-sign background events.

Figure 6 shows candidates plotted with both RS and WS interpretations. The CF D^0 decays, which appear as a broad distribution along the WS axis, dominate the plot. Any WS signal would be completely obscured by these candidates. The use of the WS D^* tag still retains a lot of CF D^* decays (although it is not as efficient as using the RS D^* tag). The use of the D^* tag will still accept background events, where a real D^0 and a random π track happened to form a candidate that survived the selection. The plot also has clustering of events in the high mass (upper right) and low mass (lower left) regions. These are $\pi\pi$ and KK events, which will be discussed in section 3.4.

The data is plotted in figure 7, with a narrower D^0 mass range, to avoid $KK, \pi\pi$ background events. As expected, the CF D^* background events dominate the WS plot. If a WS signal is to be seen, this is a very important background to reduce.

To make sure that we understand the WS plot, we constructed a toy model. A particle with the D^0 mass decays to a kaon and a pion in the rest frame, with the track directions known. The daughter tracks are boosted to the lab frame. The kaon and pion assignments are swapped, and the new invariant mass is calculated. The difference in mass is shown in Figure 8. The kaon and pion will be boosted differently, when transforming from rest to lab frame. The largest difference in mass will occur when the kaon decays parallel or anti-parallel to the direction of the D^0 momentum. In figure 9, a scatter plot of the data is shown, with the theoretical curve drawn. The data is dominated by RS decays. At any particular decay angle of the kaon, the mass distribution is determined by the detector resolution. It is the sum over all decay angles which causes the integrated CF D^0s to have a broad distribution when reflected into the WS mass plot.

The model was modified to start with a D^*. The angle of the D^* pion is recorded, as well as the kaon angle of the D^0. The results are in figure 10, which shows the change in the mass difference $(D^* - D^0)$ when the kaon and pion from the D^0 have their mass assignments swapped. The model implies that the RS D^* background will have a mass difference peak with a width of one or a few MeV, which is suggested by the data.

There will also be WS D^* signal events that show up as background in the RS plots, when

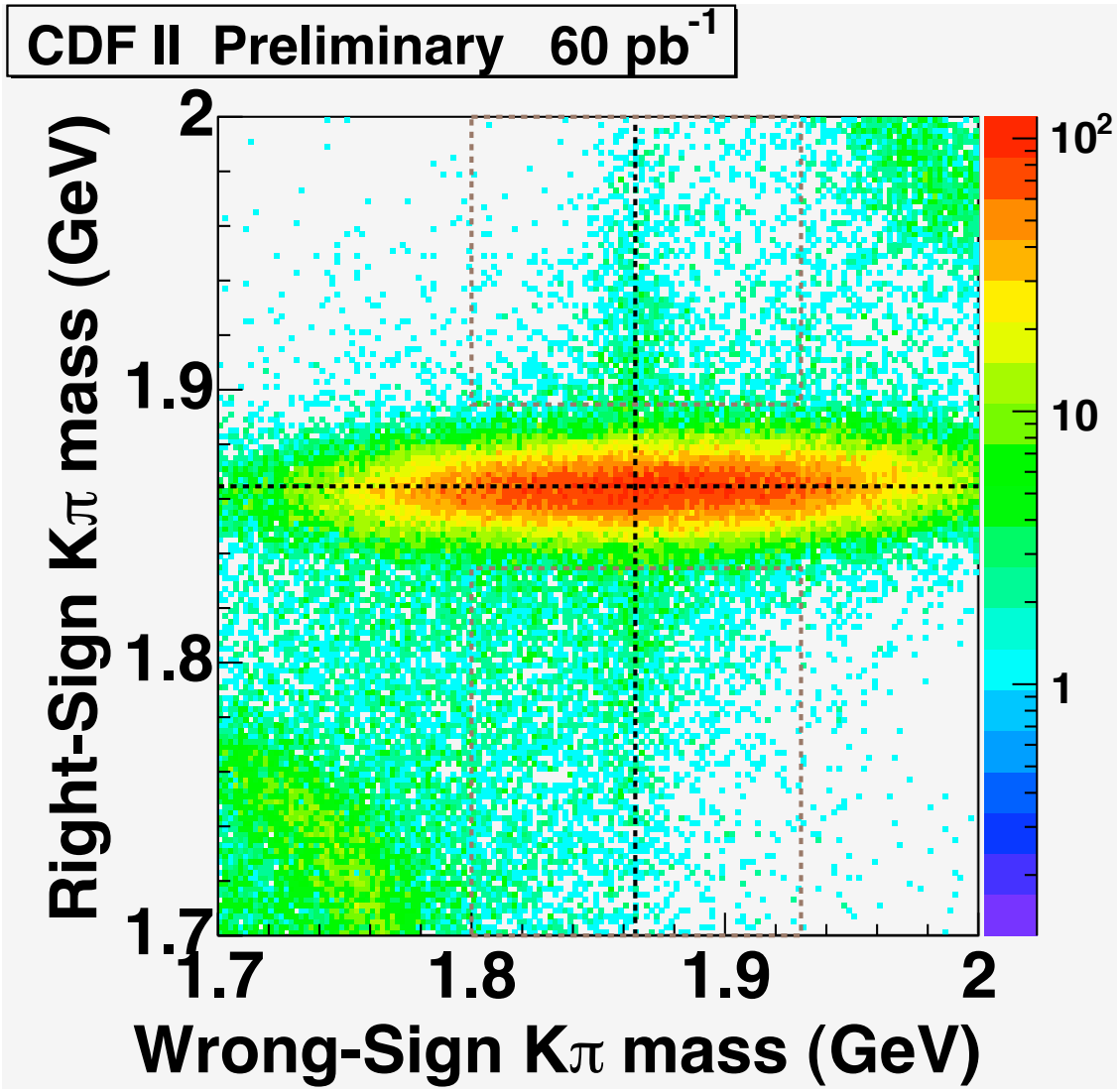

Figure 6: Candidates are plotted with both RS and WS interpretations. The dashed lines are the PDG D^0 mass of 1.8645 GeV. A cut requiring a good (WS) D* tag is used to reduce background. The bins are 3 MeV wide, along each axis. The regions surrounded by the brown dashed lines will be used to get the WS signal in chapter 4.

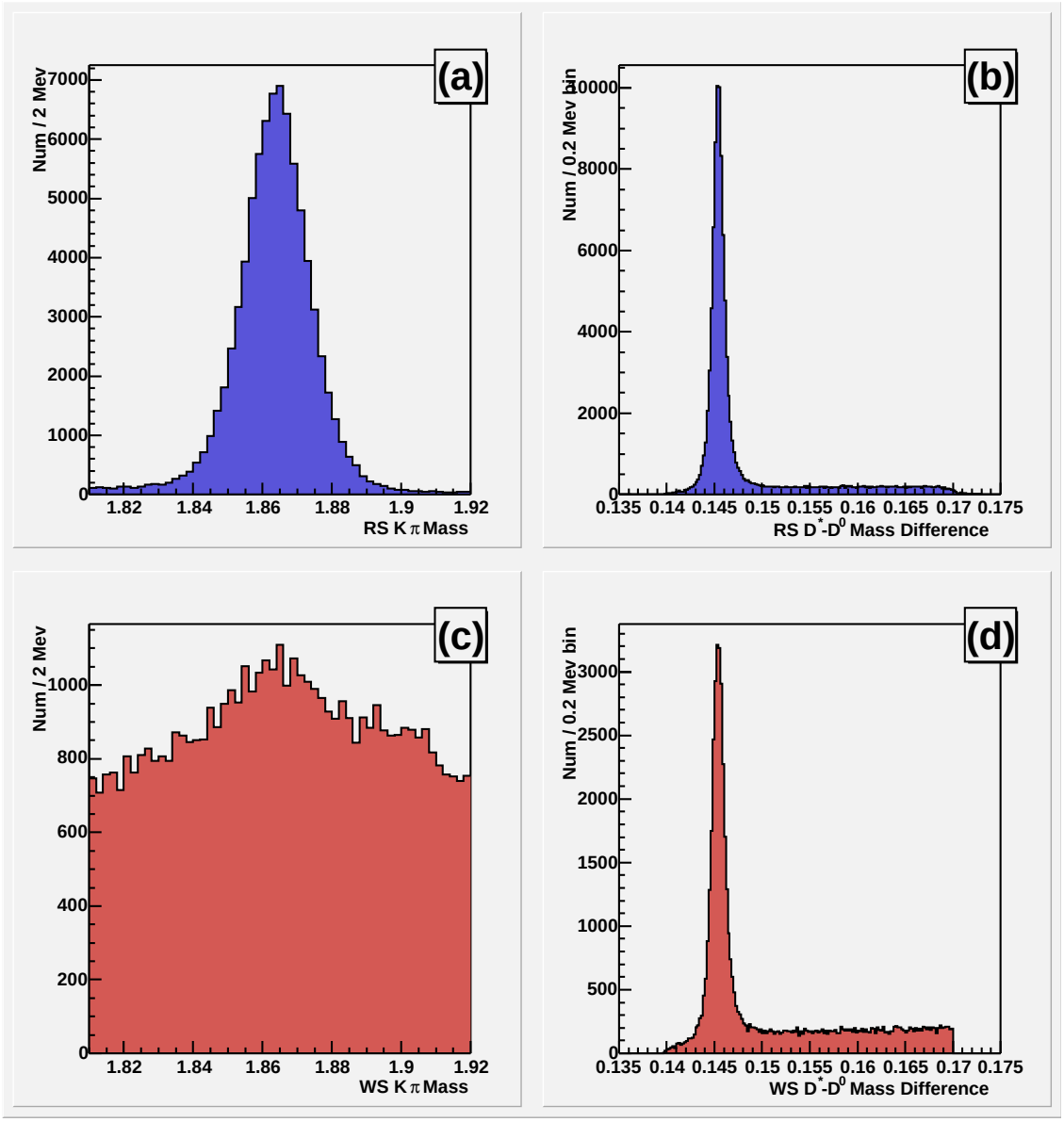

Figure 7: These plots show the RS (top row, a and b) and WS (bottom row, c and d) candidates from data. The left side (a and c) has $K\pi$ mass candidates, requiring a good D^* tag. The mass range is smaller than figure 5 to avoid contribution from $KK, \pi\pi$ events. The right side (b and d) shows the $(D^* - D^0)$ mass difference, requiring a good D^0.

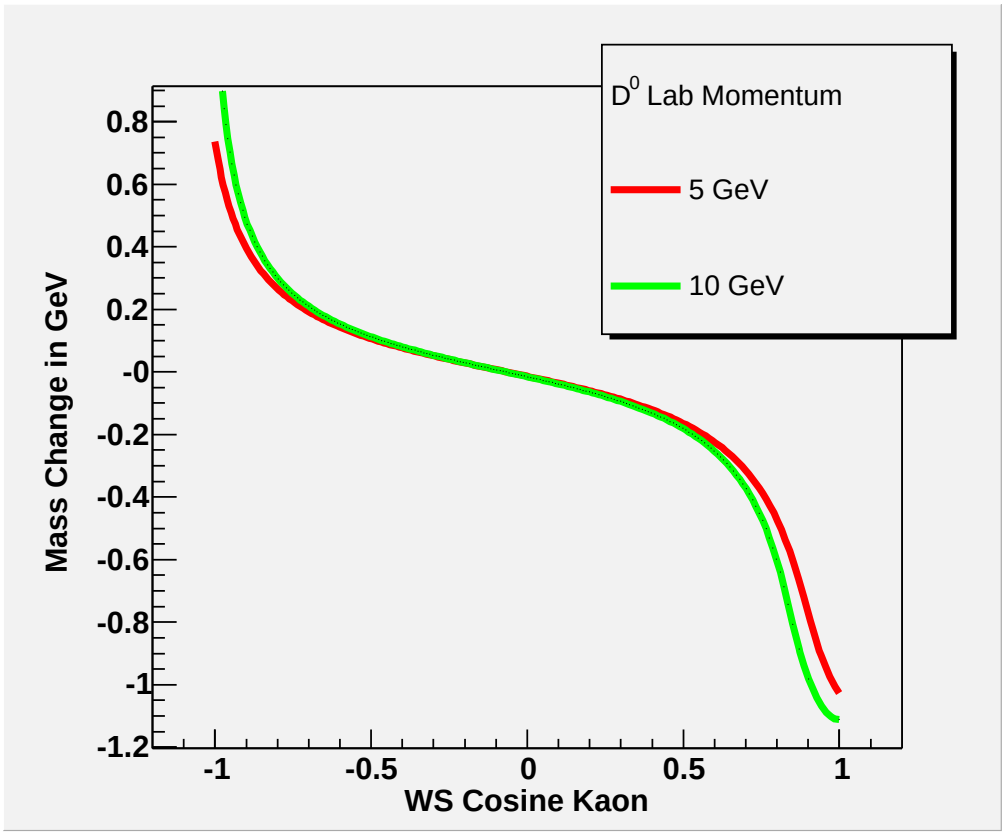

Figure 8: The plot is the change in mass, when the kaon and pion tracks from a simulated CF D^0 have their mass assignments switched. The cosine kaon is the cosine of the angle of the WS kaon in the rest frame of the WS D^0, with respect to the D^0 direction. The red curve is a D^0 with 5 GeV of momentum in the lab frame, the green curve is a 10 GeV D^0.

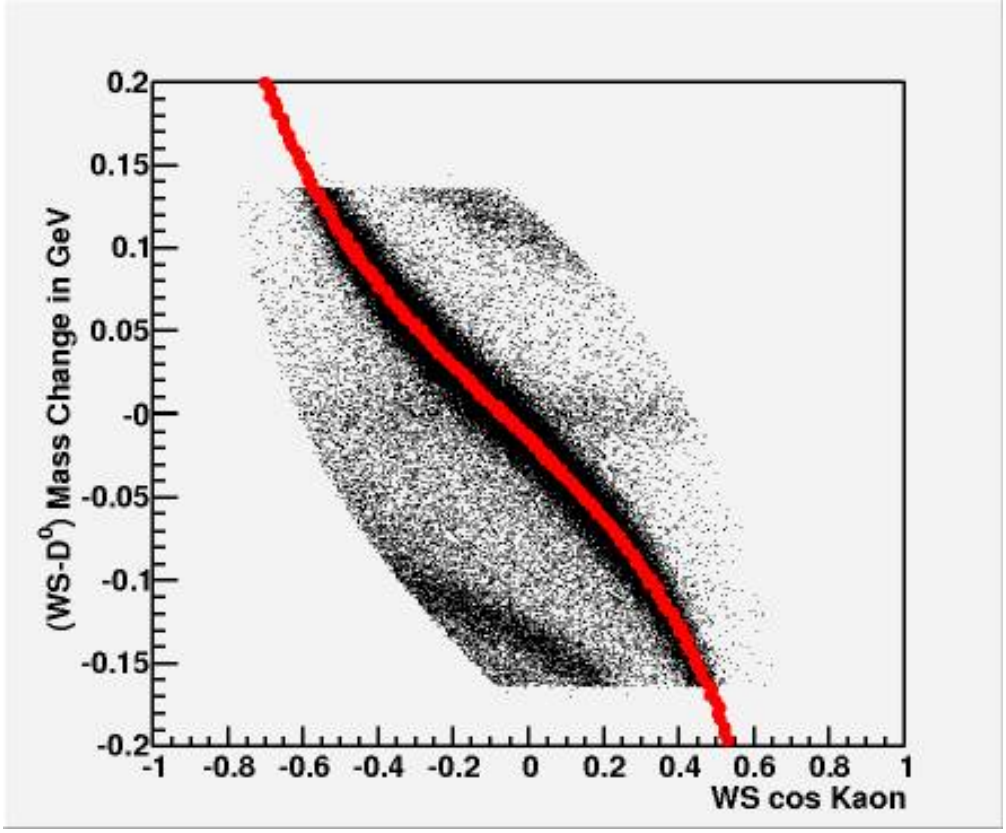

Figure 9: This is a data scatter plot of the WS mass (in GeV) with the mean fit D^0 mass subtracted. The $K\pi$ mass is limited to the range from 1.7 to 2.0 GeV. The cosine kaon is the cosine of the angle of the WS kaon in the rest frame of the WS D^0, with respect to the D^0 direction. The red line uses the same model as figure 8, with 7 GeV momentum.

the kaon and pion tracks are mis-assigned. Due to the difference in branching fractions, these DCS and mixing events will produce negligible background in the RS mass plots, compared to the CF signal.

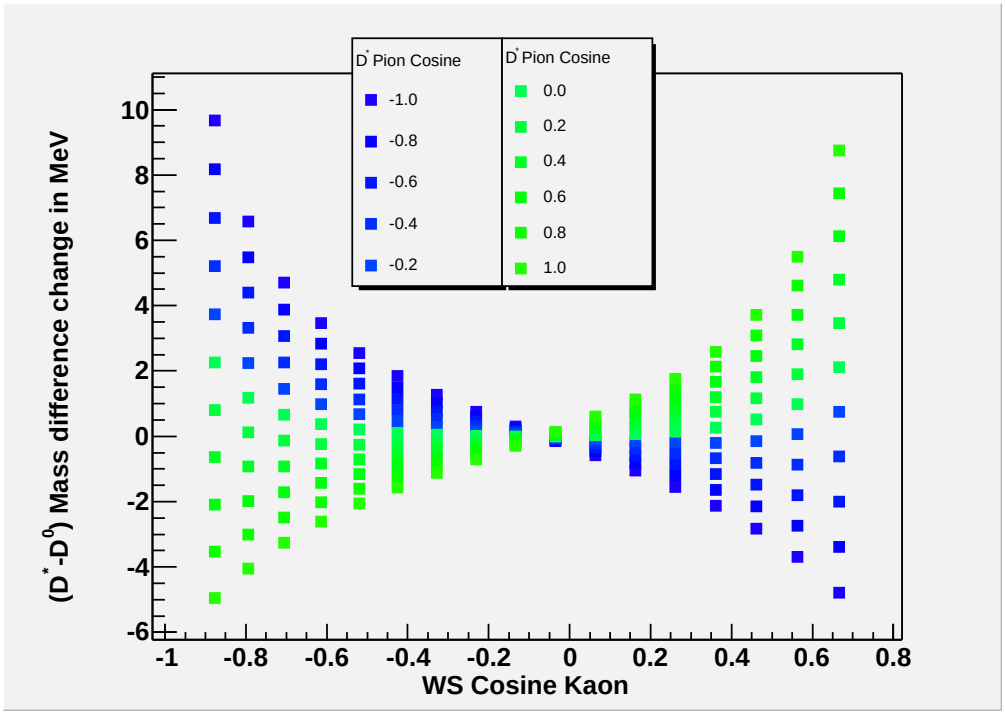

Figure 10: A simulated $D^* \to \pi D^0, D^0 \to K\pi$ decay has the kaon and pion (from the D^0) mass assignments switched. The change in reconstructed $(D^* - D^0)$ mass difference is plotted versus cosine kaon. At each value of cosine kaon are 11 data points, which correspond to values (from -1. to 1.) of the D^* pion cosine, with respect to the D^* direction.

3.4 $D^0 \to KK, \pi\pi$ Misidentification

In figure 6, besides the large number of events in the middle due to RS D^0s, there is enhancement in the upper right and lower left corners. These are due to $D^0 \to KK, \pi\pi$ events. When transforming the data candidates into those mass plots, peaks at the D^0 mass are clearly shown, as seen in figure 11. These candidates are distinct from both the RS and WS signal. We can avoid confusion from these events by limiting the D^0 mass range from 1.80 - 1.93 GeV.

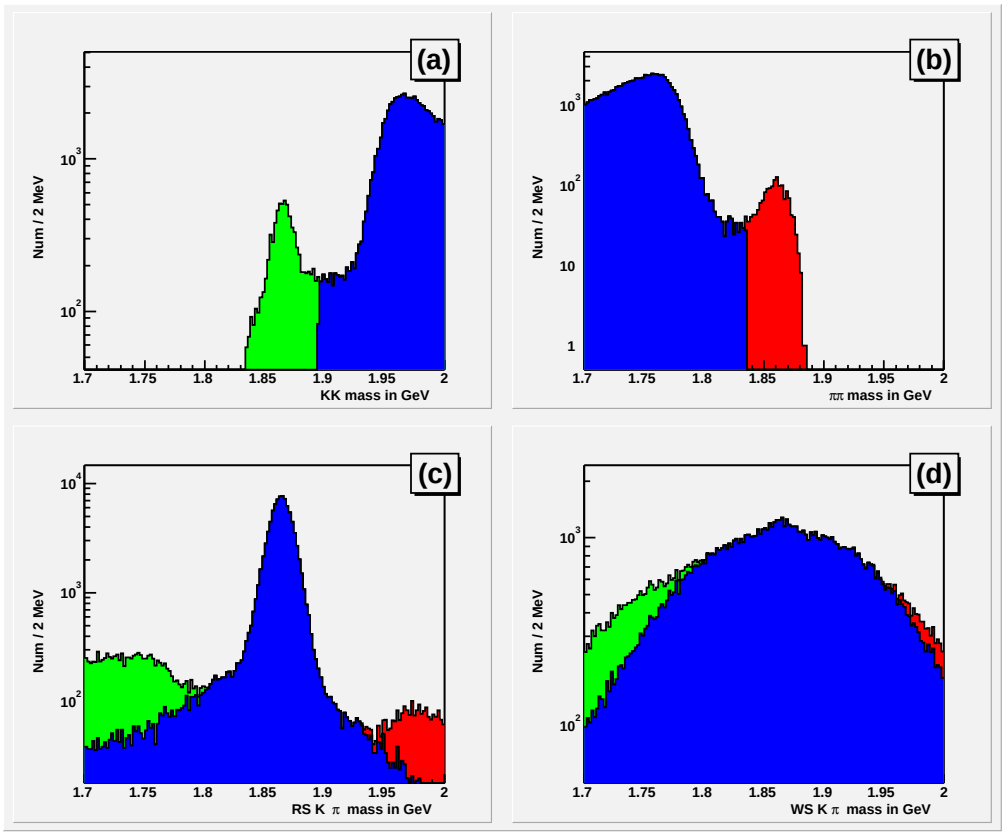

Figure 11: Data events have their invariant mass recalculated, assigning the tracks as KK (a) or $\pi\pi$ (b). Events within 30 MeV of the D^0 mass in (a) are colored green. Events within 30 MeV of the D^0 mass in (b) are colored red. All others are colored blue. Those events are then shown as cumulative distributions for RS $K\pi$ candidates (c) and WS $K\pi$ candidates (d).

3.5 Combinatoric Background

Pure combinatoric background has candidates formed from a random selection of tracks, which happen to pass our selection criteria. This is a well understood phenomena in any physics analysis. The mass plots from this background are featureless (beyond statistical fluctuations), and are modeled by a linear or simple polynomial fit for the D^0 mass plot.

We need to consider other events where one or both tracks do not belong to a $D^0 \to K\pi$ decay. Most other charm-like decay modes will not cause any problems. As seen with the $KK, \pi\pi$ modes, assigning the wrong particle mass to the decay tracks, will move the reconstructed mass out of the search window. One concern is where wrong mass assignments are not that different from the correct choices. A possible example is $D^0 \to K^-\mu^+\nu_\mu$. The muon is only slightly lighter than a pion. The $K\pi$ hypothesis will result in a slightly higher mass, but the missing energy from the ν_μ could bring the candidate back into the search region. Another mode which might have problematic reflections is $D^0 \to \pi^+\pi^-\pi^0$. One of the pions will be assigned a kaon mass (increasing the mass), but the neutral pion will not be observed (decreasing the mass). It is possible that these two effects will almost cancel out, leaving a reflection near our expected signal.

These charm-like events may need to be investigated with Monte Carlo, from a model, or from real data with a clean sample of each mode. For now, we will assume that a linear fit will describe the combinatoric background. An earlier study of D^0 mesons by CDF[23] did not consider these backgrounds. It appears that BABAR[18] did the same. The Belle[17] results suggest that these backgrounds will not cause a noticeable deviation from the linear background fit in the $K\pi$ plot.

3.6 Summary

Figure 12 has a table that lists the expected mass distribution shapes for the various types of events. For the $K\pi$ distribution, the shapes are peaked (about 10 MeV wide) for real D^0s that are correctly identified. For real D^0s where the kaon and pion mass assignments are switched, the distribution is wide (80 MeV). For the mass difference, the signal has a narrow peak (around 0.7 MeV wide). Mis-ID D^0s have a slightly wider peak (around 2 MeV wide). Events that are not D^* will have a broad distribution. The combinatoric background will contain both D^* (where the D^0 does not decay to $K\pi$) and non-D^* events, so the mass difference distribution will be a mix of shapes. The signal is peaked in both $K\pi$ and mass difference distributions.

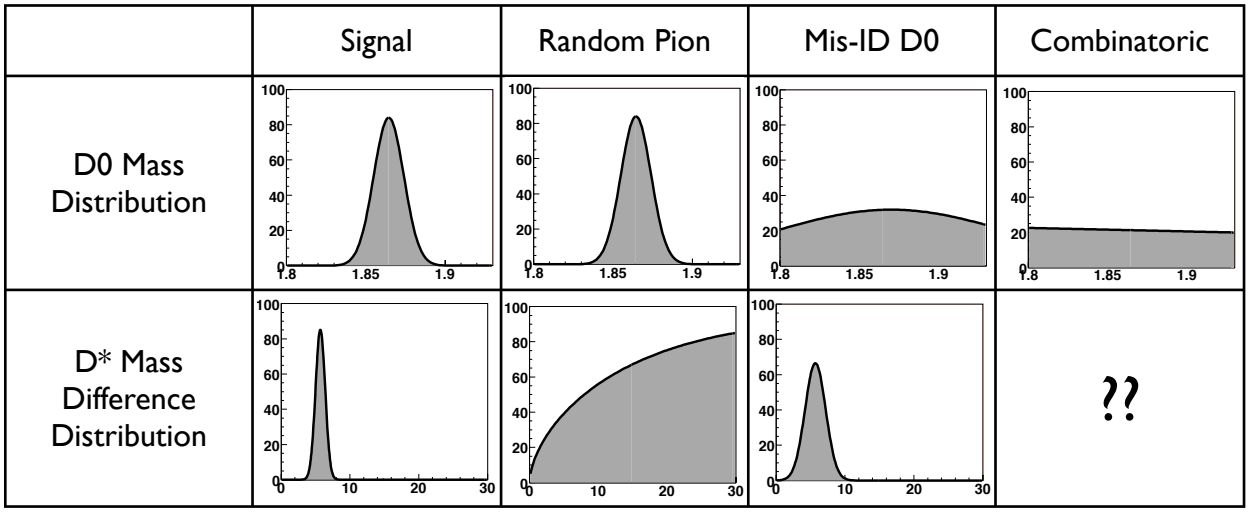

Figure 12: The table in this figure shows the expected mass distributions of the events. The plots are cartoons, not actual data. The D^0 $(K\pi)$ mass distribution has the range from 1.80 to 1.93 GeV. The $(D^* - D^0 - \pi)$ mass distribution has the range from 0 to 30 MeV. The combinatoric background will contain both D^* (where the D^0 does not decay to $K\pi$) and non-D^* events, so the mass difference distribution will be a mix of shapes.

4 Signal Optimization

The last chapter described the primary backgrounds that are in the D^0 and D^* mass plots. This chapter describes the methods used to deal with them. The hbot0h WS signal was used to test the effectiveness of the cuts, but the methods were developed with the idea of using them with data where the WS signal region is blinded. The CDF data set xbhd0d will be WS signal region blinded during the signal optimization process, to reduce bias.

Chapter 2 discussed the selections that were used while writing candidates to the ROOT ntuple file. These cuts are present in all plots shown, unless the contrary is explicitly mentioned. They will be referred to as the "minimum" or "default" cuts. Any additional ROOT selections will be in addition to the minimum set.

4.1 Fit Functions

There are several functions that are used repeatedly, to fit mass distributions. The simplest is a linear fit, mostly for the combinatoric background in the $K\pi$ mass distribution.

For signal, a variable width gaussian is used. It has the same formula as a regular normal distribution, except that the "sigma" is also a function of mass. The distribution, where x is the mass, has the form

$$(A/\sigma_x)\, exp(-(x-\mu)^2/(2\sigma_x^2))\,,\ \sigma_x = \sigma_0 + B\,|x-C| \tag{1}$$

For the $K\pi$ distribution, $C = \mu$. The mass dependent width allows the distribution to be narrow with longer wings, compared to a normal gaussian. This formula works as well as a double gaussian for the $K\pi$ mass, with one fewer free parameter. For the mass difference, where the shape is not quite symmetric, allowing $C \neq \mu$ allows the shape to be skewed to one side.

The background for the mass difference, where the π^* is a random track attached to a D^0 candidate, is given by the formula

$$A\, x^B\, exp(-Cx) \tag{2}$$

x is the D^* mass minus the D^0 and π mass. This allows the function to rise quickly at small values, and flatten out at larger values. If a simpler function is required, a fractional power like x^n with $n \sim 0.4$ can be used, but the fit will not be nearly as good.

4.2 Opposite Assignment Mass Cut

Figure 7 showed that CF D^* mis-identified background events dominate the WS plot. To reduce that specific background, we use the opposite assignment cut. The opposite assignment refers to switching the K and π assignments of the D^0 tracks. When plotting the WS mass, events are excluded if they have a RS mass consistent with being a D^0. For ROOT, the cut would require events with $|m_{RS} - m_{D^0}| \geq$ (cut value). In the case of plots showing the RS mass, the cut is applied to the candidate's WS mass. Since the wrongly reconstructed

D^0s have a distribution roughly 10 times larger than correct D^0s, this will remove most of background while still retaining most of the correctly reconstructed events.

Figure 13 has plots that were used for setting for the opposite assignment mass cut. The objective is to improve the signal significance, defined as $S'_{RS}/\sqrt{S'_{RS}+B}$. S'_{RS} is the RS signal scaled by 0.36%, which simulates the amount of WS signal. B is the sum of the combinatoric background and misassigned RS background in the WS signal mass window.

Figure 13a shows the RS $K\pi$ mass distribution, taking the mass difference from the PDG value, $|(K\pi - 1.8645)|$. The distribution is assumed to have two components: a sharp (signal) peak, and a linear background. The sideband of the plot allow an estimate of the background level under the signal peak. Sideband subtraction gives the amount of RS signal. The sideband is small compared to the RS signal, but this will not necessarily be true for WS signal.

Figure 13b shows the WS $K\pi$ mass distribution. The plot is dominated by a combination of misassigned CF D^0s and flat background. The real WS signal and various other backgrounds are neglected for this study, as they will be small compared to the two background sources mentioned. The WS flat background is assumed to be at the same scale as the RS sideband. The rest of the events above this flat level will be interpreted as misassigned RS D^0s.

Those two plots give the amount of RS signal, flat background (taken from RS sidebands), and mis-assigned CF background in the WS signal region. Next, the RS distribution is generated with the opposite mass assignment cut at some setting. This new plot is used to get the amount of RS signal and flat background that survive the cut. The amount of misassigned CF D^0s in the WS plot are assumed to scale directly with the number of RS D^0s. So with the cut at some setting (x), the RS signal that survives the cut ($S_{RS}(x)$), the RS signal before applying the cut ($S_{RS}(0)$), and the amount of misassigned RS D^0 background in the WS plot before the cut ($B_m(0)$), the estimated misassigned background is given by

$$B_m(x) = B_m(0) \times S_{RS}(x)/S_{RS}(0) \tag{3}$$

The setting of the cut is changed, to scan a range of values. The results for the scan are shown in figure 13 for the signal significance (plot c), scaled RS signal (d), flat background level (e), and misassigned RS D^0 background (f).

The WS distribution is not used, except to get a no-cut estimate on the mis-assigned CF D^0 background. Once the opposite assignment cut is applied, the WS D^0 signal is no longer negligible compared to the backgrounds. A toy MC study showed that the misassigned RS background shape (in the WS plot) is unchanged when the opposite assignment mass cut is used. (The width of the distribution increases by 5% at a cut value of 30 MeV.) The cut changes the amplitude of the background, and does not produce peaks or valleys in the signal region of the WS plot.

The cut was chosen to be 30 MeV for the hbot0h data. Although the highest possible significance value is around 28-29 MeV, 30 is a nice round number that should work just as well. The brown boxes in figure 6 show the events that will be used to get the WS signal. The central region will be excluded by the opposite assignment cut. The WS $K\pi$ mass range

is limited to 1.80-1.93 GeV, to avoid contamination from $D^0 \to KK, \pi\pi$ events. The studies for the rest of this chapter will include the opposite assignment cut (on top of the minimum cuts), unless specifically mentioned.

Figure 14 shows the effectiveness of the opposite assignment cut, compared to figure 7. With the CF background removed from the WS plot, there is a discernible peak in the WS $K\pi$ mass plot. This peak will have a combination of true WS D^*s and real CF D^0s that are treated as WS due to a fake D^* tags.

4.3 Cut Optimization Using D^0s

The RS D^0s are used to see if there are more cut variables that will reduce the background. Combinatoric background will most likely be affected, since D^* background coming from partially or fully reconstructed charm are unlikely to be affected by cuts this study would use. The objective is to improve the signal significance. The WS signal is estimated by scaling the RS D^0 signal. The RS $K\pi$ distribution is assumed to have two components: a sharp (signal) peak, and a linear background. The sidebands of the plot allow an estimate of the background level under the signal peak. Sideband subtraction gives the amount of RS signal. The opposite assignment cut is used for both RS and WS distributions. With the misassigned CF D^0 background removed, the remaining WS background is taken from the sidebands of the WS $K\pi$ mass distribution. The WS D^0 signal region is blinded

A ROOT script produces plots for each variable, where 50 bins are used to scan possible cut values. (Fifty is a convenience used, even when the variable only assumes integer values up to 6.) The estimated signal significance is generated from the scaled RS signal and the WS sidebands. Most of variables available in the ROOT ntuple do not improve the significance when they are used in a cut.

An exception is cutting on the D^0 vertex L_{xy}/σ_{xy}. Figure 15 shows the signal significance when cutting on the D^0 vertex L_{xy}/σ_{xy}. This cut is a standard in many analyses, designed to reduce fake vertices formed by tracks from the primary vertex. Based on these plots, a cut value of 4 was chosen.

4.4 D^* Yield Technique

Figure 16 shows the wrong-sign $K\pi$ mass versus $(D^* - D^0 - \pi)$ mass difference distribution. A peak is present at the correct PDG values for the D^* and D^0. Besides the general smooth background, we can see sharper backgrounds around the dashed lines for the D^* and D^0. The horizontal band is from real D^0s that are combined with a unrelated π track to form a fake D^* candidate. The vertical band is from real D^*s, where the D^0 does not decay to the WS $K\pi$ mode.

Ideally, the WS signal could be determined by fitting the 2D histogram. The problems are two-fold. The first is that the distributions in both directions would need to be known, for the signal and various backgrounds. Second, an early test showed this fit to be unstable. The ROOT fitter was very sensitive to initial settings, and tended to converge to unreasonable

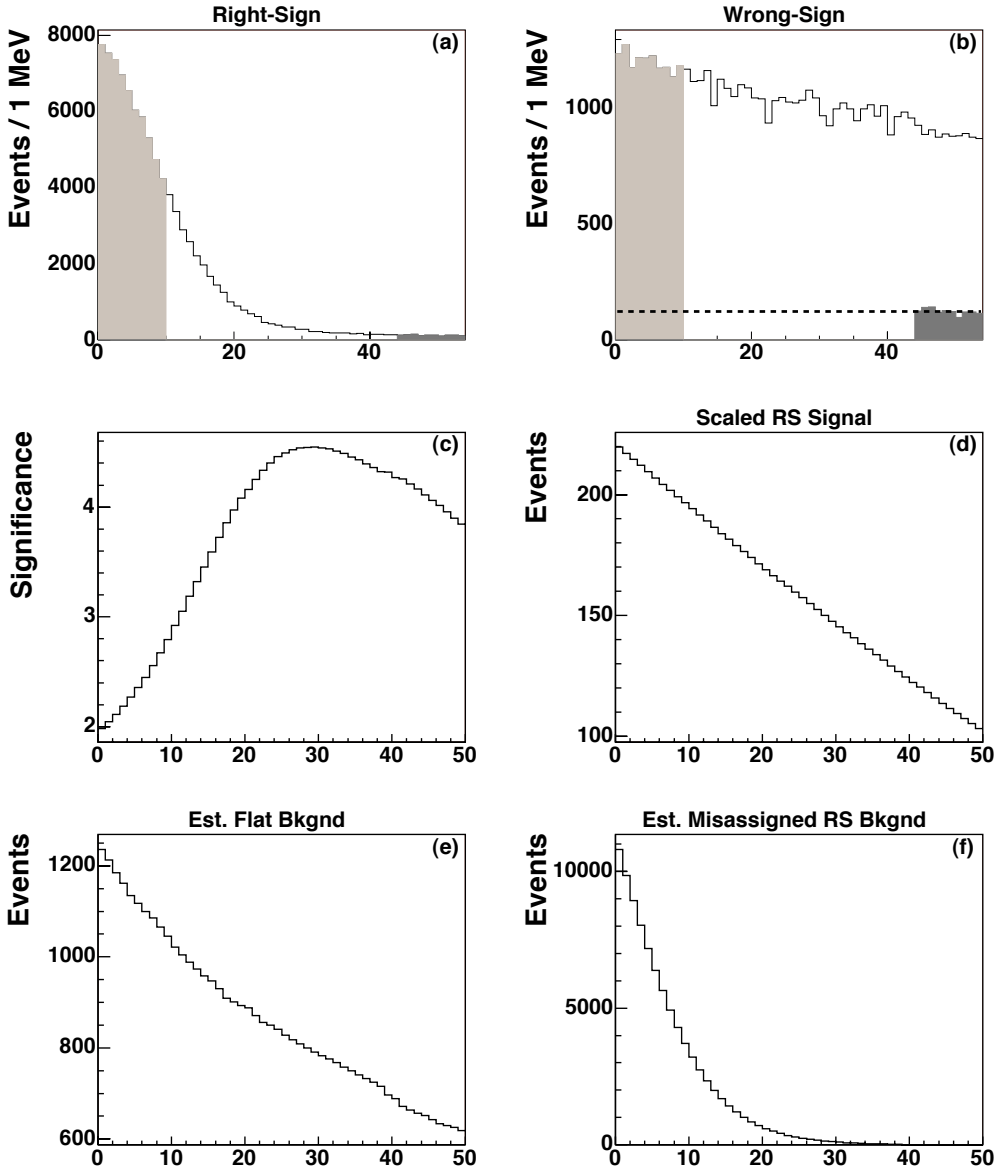

Figure 13: For all plots, the x-axis is $|m_{K\pi} - m_{D^0}|$ in MeV. Candidates with a good D* tag are used. Plots (a) and (b) are the events interpreted as RS and WS, respectively. The signal region (shaded light grey) is defined as any event within 10 MeV of the correct D^0 mass, while the sideband (dark grey) lies 45-55 MeV away. The dark grey region in the WS distribution (b) is a copy of the RS sideband level. The dashed line shows the estimated flat background level in the WS distribution. Plot (c) is the estimated signal significance as a function of the opposite assignment mass cut value. Plots (d-f) show the scaled RS signal, flat background, and misassigned RS background as a function of the cut value.

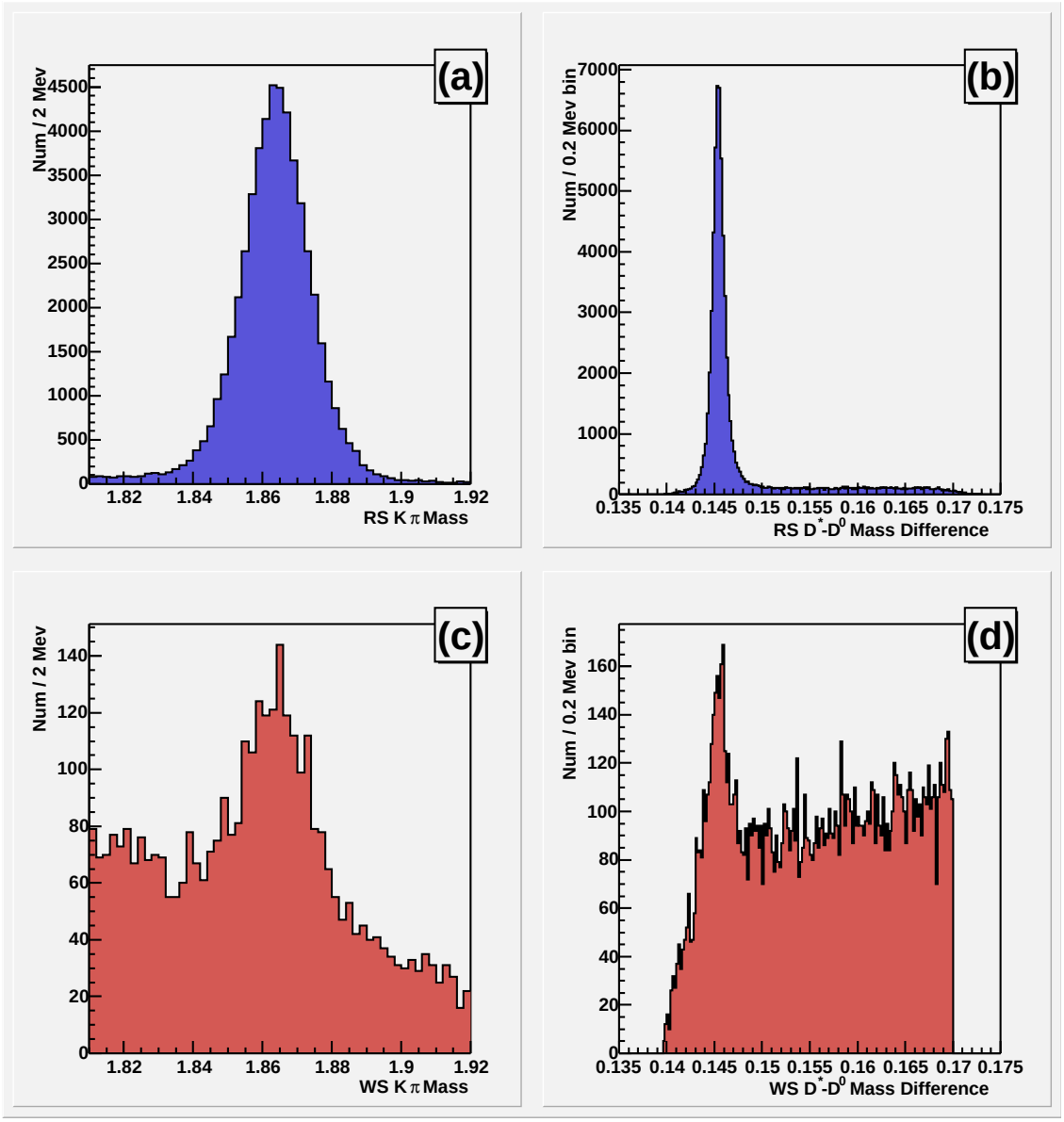

Figure 14: These plots show the RS (top row, a and b) and WS (bottom row, c and d) candidates from data. The opposite assignment cut has been applied. The left side (a and c) has $K\pi$ mass candidates, requiring a good D^* tag. The right side (b and d) shows the $(D^* - D^0)$ mass difference, requiring the candidate to lie in the D^0 signal window.

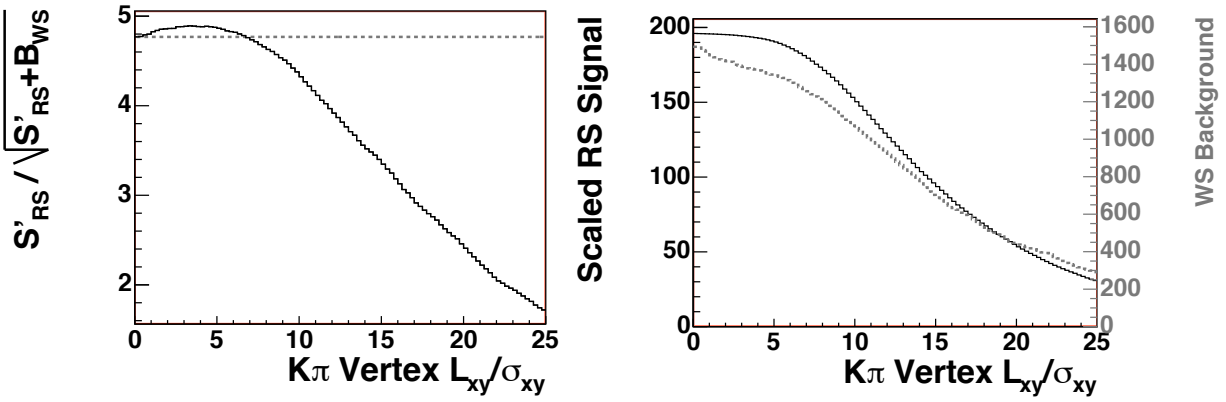

Figure 15: The left plot is the estimated signal significance as a function of the cut value, requiring the $K\pi$ vertex L_{xy}/σ_{xy} to be greater than the value. The dashed line shows the significance without any cuts on this variable. The right plot shows the scaled RS signal (solid black line) and WS background (dashed grey line) when applying the cut.

values.

The yield technique was developed, to produce a method that would converge to numbers that were stable even with perturbations in the initial fit settings. The key is that the $K\pi$ distribution has only two sources of events that form a narrow peak: signal, and correctly assigned D^0s with a fake tag. The other backgrounds (besides the fake tag) have broad distributions which will contribute to a linear background in a fit. The yield of events in the $K\pi$ signal fit can then be plotted as a function of the mass difference. For the mass difference, the signal events will be in a narrow peak. The fake tag D^0s will be spread out, in a shape similar to the background function (equation 2) mentioned in section 4.1. A fit to this yield distribution will give the number of signal events.

Two dimensional histograms of $K\pi$ mass versus mass difference are made, for RS and WS events. (Figure 16 is an example of the WS histogram.) The opposite assignment cut and the minimum cuts are used. Slices in mass difference are taken, each slice being a 1-D histogram of the $K\pi$ distribution. Each slice is separately fit with a variable width gaussian (signal) and a linear background. An example of the $K\pi$ slice fits is given in appendix B. The shape of the signal is fixed. The amplitude of the signal and the linear parameters are allowed to vary. The "log-likelihood" fit option is turned on, so bins with zero events will be used.

The number of signal events for each slice is then plotted as a function of mass difference, as shown in figure 17. The error bars on the points are taken from the uncertainty on each $K\pi$ slice's signal fit. The mass difference yield plot is then fit, with a variable width gaussian and the background distribution described in section 4.1. The ROOT fit uses the standard "chi-squared" calculation. The RS data has all fit parameters floating. The WS data has the signal shape for the mass difference yield fixed from the RS fit parameters. (The WS

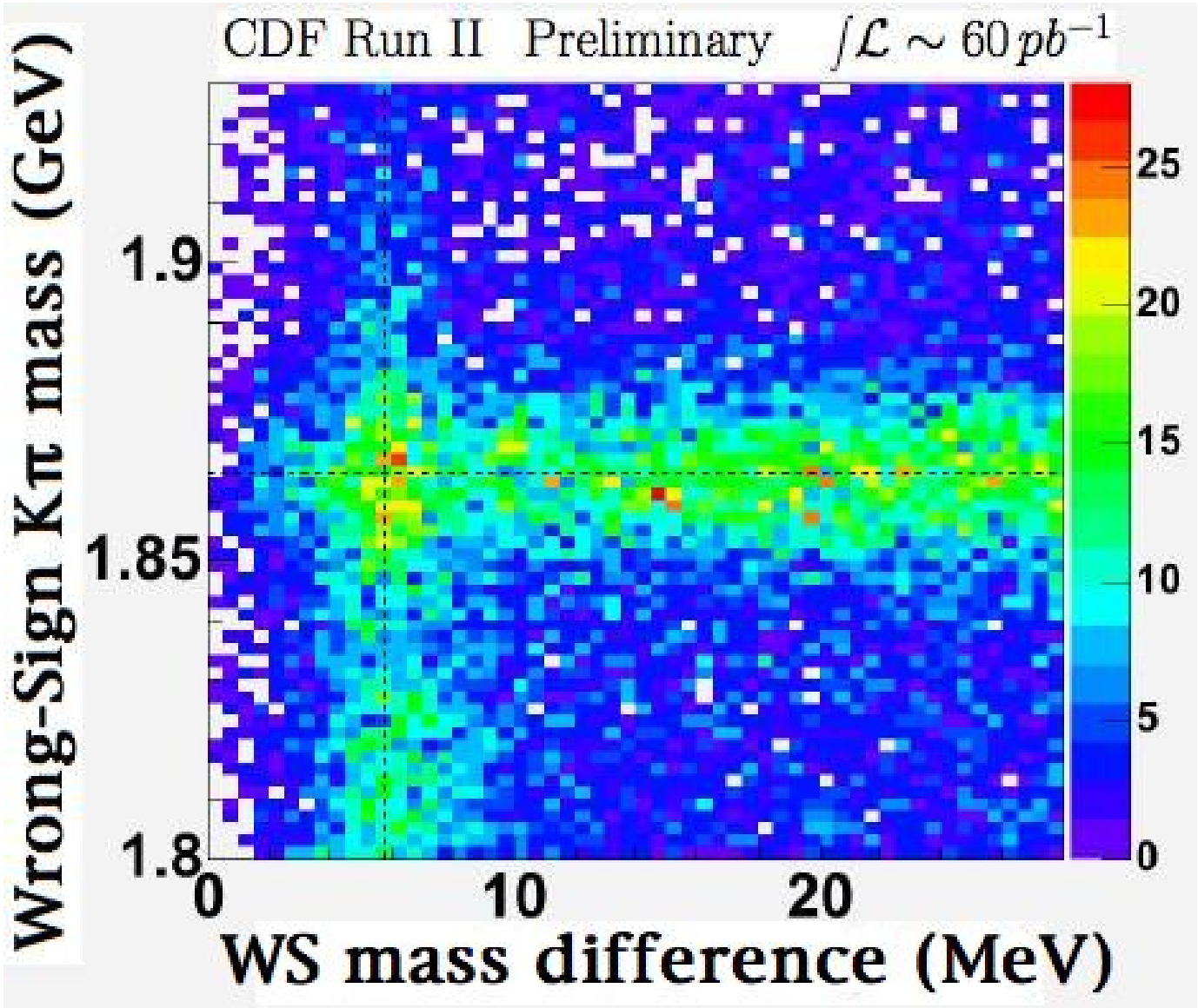

Figure 16: Events that survived the minimum cuts and the opposite assignment cut. PDG values for the D^0 and D^* are shown by the dashed lines. The $K\pi$ axis is in 2 MeV bins, the mass difference ($m_{K\pi\pi^*} - m_{K\pi} - m_\pi$) axis is 0.5 MeV bins.

signal amplitude and all background parameters are floating.)

4.5 Cut Optimization Using the D^* Yield Technique

After using the opposite mass assignment cut and the yield technique, fake D^*s are the background that will have the greatest effect on the WS signal. The yield technique was used to see if there are any ROOT variables that will reduce the background. The objective is to improve the signal significance. The WS signal is estimated by scaling the RS D^* signal. The amount of background is taken from the WS yield mass difference distribution. The WS $K\pi$ slices are fit normally (including the signal region). The WS signal region of the D^* mass difference is blinded. A study showed that the background fit is stable (within errors) even if the signal region is not used. The mass difference background is extrapolated into the signal region, to get the background level.

The opposite assignment cut is used for both RS and WS distributions, but the D^0 vertex L_{xy}/σ_{xy} cut is not yet used. A script produces plots for each ROOT ntuple variable, where 50 bins are used to scan possible cut values. Most of variables available in the ROOT ntuple do not improve the significance when they are used in a cut. Figure 18 is an example, using the p_T of the D^0 candidate. No choice of cut value would improve the estimated signal significance, compared to not cutting with this variable.

After looking at the plots, three cuts were chosen: the number of silicon hits for the π^* tagging track ≥ 3 (figure 19), D^* vertex $|L_{xy}/\sigma_{xy}| \leq 8$ (figure 20), and D^* vertex quality measure (two dimensions) $\chi^2_{xy} \leq 10$ (figure 21). The first cut improves the quality of the π^* track, making it less likely to be a wrongly reconstructed track. The second requires that the D^* vertex is not too far away from the primary vertex, since the D^* decays strongly. The last cut requires the vertex fit to be of reasonable quality. The improvements are modest, as no cuts were found that drastically improved the significance. The last two cuts had broad plateaus of the same signal significance, instead of a peak value. For these variables, a value safely in the plateau (a loose cut) was chosen.

A few ROOT variables were found to be correlated with the selected cuts. Without the new "optimum" cuts, these extra variables could improve the significance. Figure 22 gives an example, with the absolute impact parameter. The left plot shows a marginal improvement in the estimated signal significance could be made by cutting on $|IP|$. The right plot shows what happens after applying the four optimal cuts (including the D^0 vertex L_{xy}/σ_{xy} cut), cutting on $|IP|$ will no longer improve the situation. By using the optimum cuts, none of the extra variables are effective. Since they became redundant, the choice was made not to cut on the extra variables.

4.6 Optimized ROOT Cuts

Besides the opposite mass assignment cut, the following ROOT cuts are applied to the hbot0h data:

- D^0 vertex L_{xy}/σ_{xy} (pLxyD/pELxyD) ≥ 4.

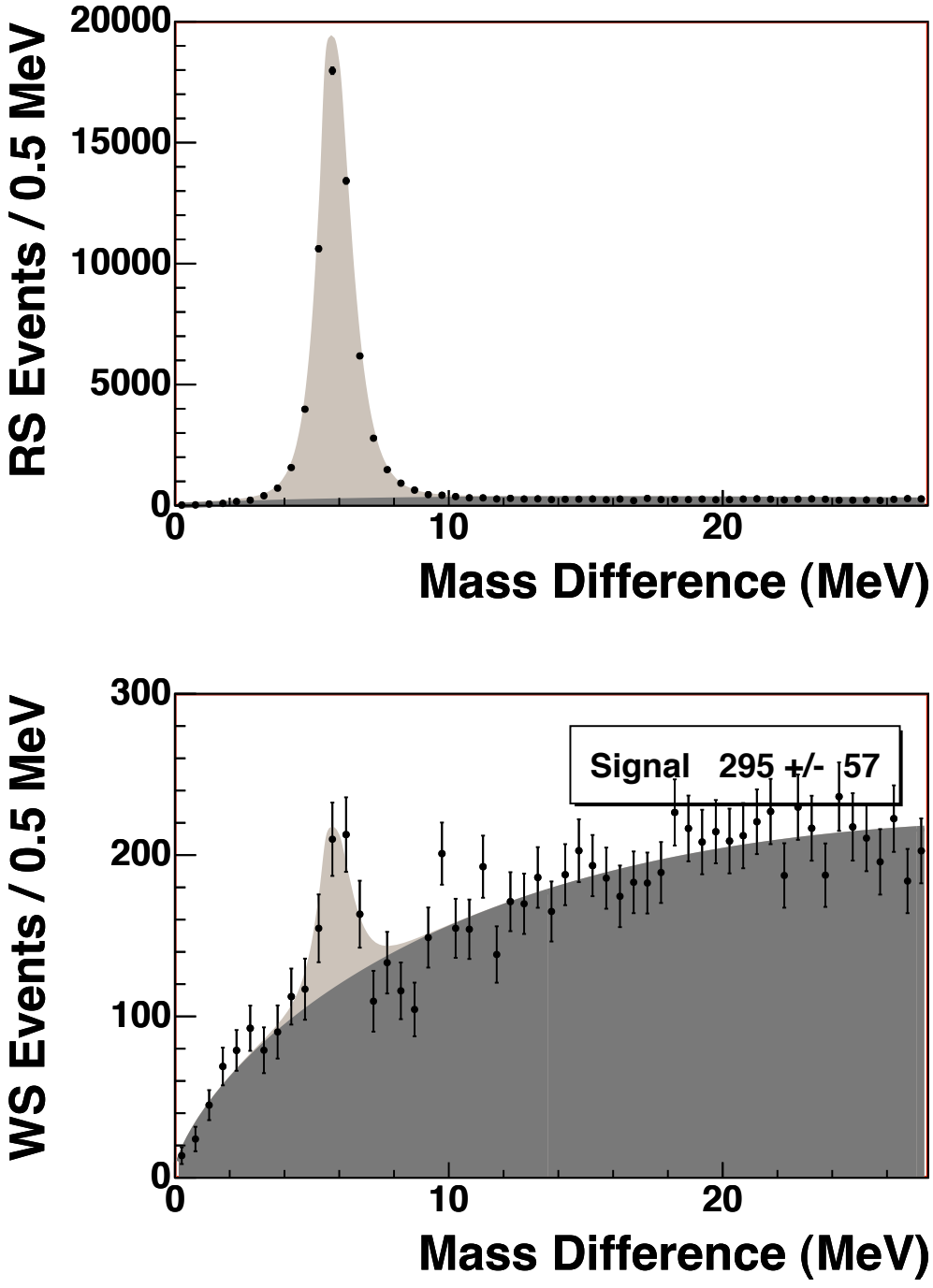

Figure 17: The number of events per bin are obtained from the signal fit of the $K\pi$ slices, with the error bars taken from the signal uncertainty of each slice . Light grey is the signal fit, dark grey is the background. The opposite assignment mass cut and the minimum cuts are used.

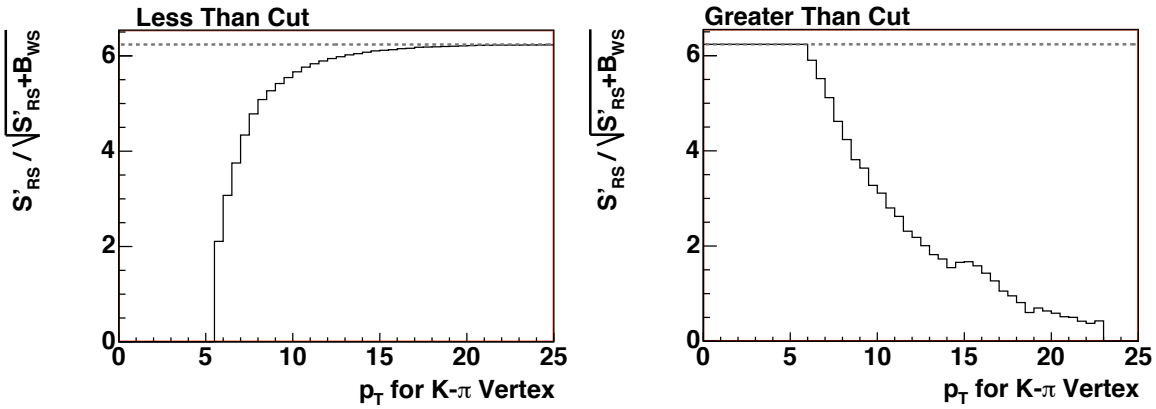

Figure 18: The left plot is the estimated signal significance as a function of the cut value, requiring the p_T of the $K\pi$ candidate to be less than the value. The right plot is for a cut requiring greater than the value. The dashed line shows the significance without any cuts on this variable. The minimum cuts require a minimum p_T, so the distribution does not go down to zero.

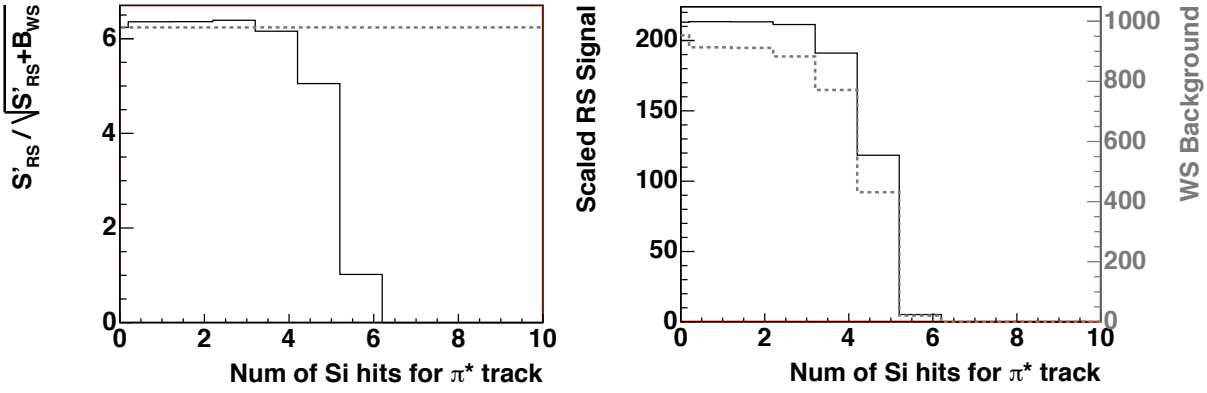

Figure 19: The left plot is the estimated signal significance as a function of the cut value, requiring N or more silicon hits on the $\pi*$ track. The dashed line shows the significance without any cuts on this variable. The right plot shows the scaled RS signal (solid black line) and WS background (dashed grey line) when applying the cut.

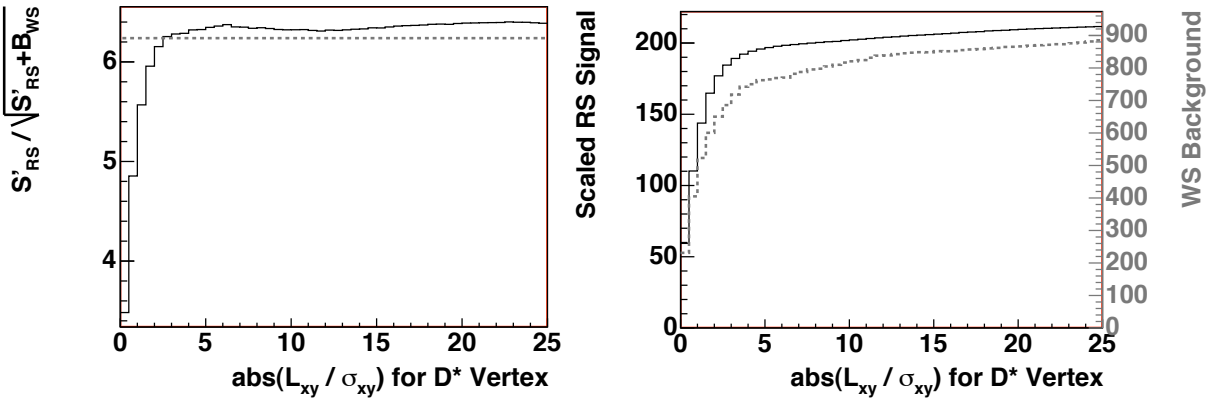

Figure 20: The left plot is the estimated signal significance as a function of the cut value, requiring $D*$ vertex $|L_{xy}/\sigma_{xy}|$ to be less than the value. The dashed line shows the significance without any cuts on this variable. The right plot shows the scaled RS signal (solid black line) and WS background (dashed grey line) when applying the cut.

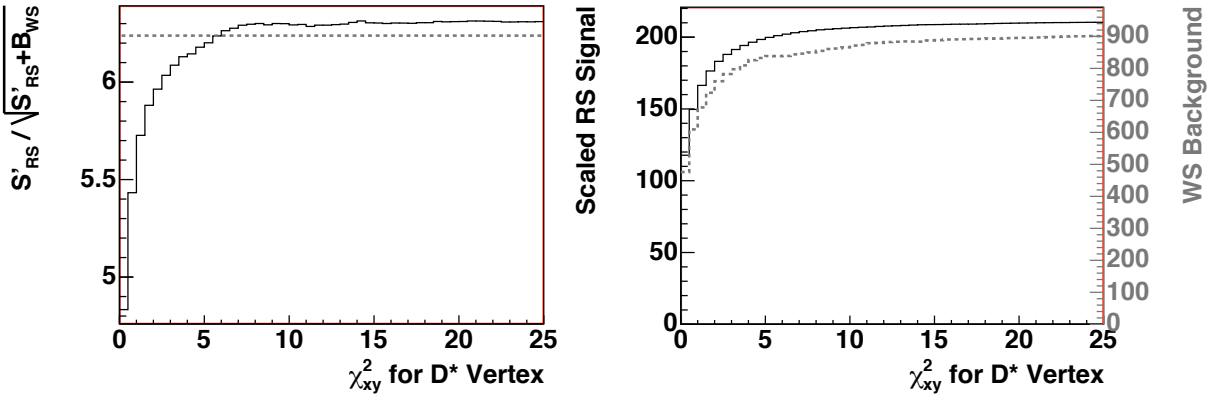

Figure 21: The left plot is the estimated signal significance as a function of the cut value, requiring the $D*$ vertex fit χ^2_{xy} to be less than the value. The dashed line shows the significance without any cuts on this variable. The right plot shows the scaled RS signal (solid black line) and WS background (dashed grey line) when applying the cut.

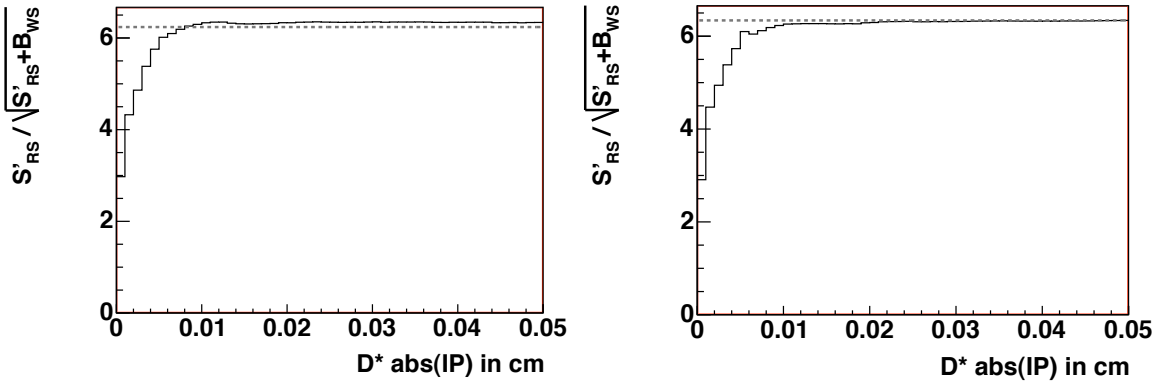

Figure 22: The plots are the estimated signal significance as a function of the cut value, requiring the absolute value of the $D*$ vertex impact parameter to be less than some value. The dashed line shows the significance without any cuts on this variable. The left plot is with opposite assignment and minimum cuts. The right plot is after applying the additional set of ROOT cuts.

- Number of silicon hits for the $\pi*$ tagging track (pNhPIS) ≥ 3
- D^* vertex $|L_{xy}/\sigma_{xy}|$ (abs(pLxyDS/pELxyDS)) ≤ 8.
- D^* vertex 2-D chisq χ_{xy} (pChixy) $\leq$10.

After applying the optimized list of cuts, the optimization procedure was repeated. This scan was to check if new optimum cut values could be found, or if other variables became effective. For the hbot0h data and this set of cuts, no additional improvement was possible.

The study showed that the significance should improve by a small but noticable amount. The yield technique was used on RS and WS data to get figure 23. The numbers are shown in table 6. Taking the significance as signal divided by the uncertainty (from the yield technique), the ROOT cuts have improved the significance. This gives confidence that we can optimize the cuts on the xbhd0d data without looking at the WS signal region.

Cut Selection	# of RS D^*	# of WS D^*	WS Significance	Ratio of WS / RS
minimum	59547 $\pm$ 319	295 $\pm$ 57	5.15	0.50 $\pm$ 0.10 %
optimized	53148 $\pm$ 302	254 $\pm$ 47	5.36	0.48 $\pm$ 0.09 %

Table 6: Yield Results

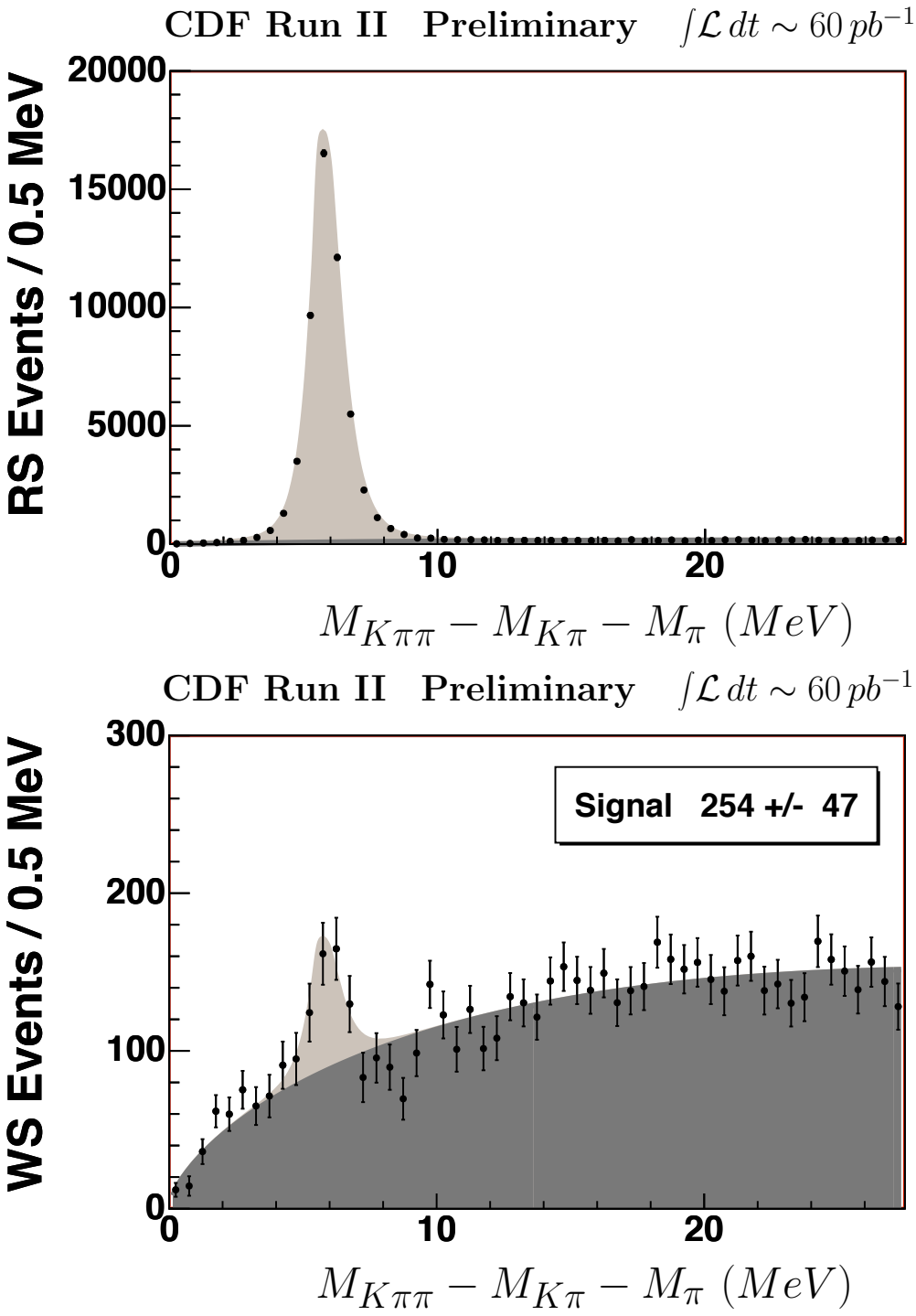

Figure 23: The number of events per bin are obtained from the signal fit of the $K\pi$ slices, with the error bars taken from the signal uncertainty of each slice. Light grey is the signal fit, dark grey is the background. The opposite mass assignment cut and the cuts listed in section 4.6 are applied.

5 Time Integrated Ratio

The work in the previous chapters laid the ground work to get the time-integrated ratio of WS to RS D^*s. The first part of the chapter describes the xbhd0d data set, which will replace the hbot0h set. After that will be a description of the procedures used, with more detail being given to methods that are new or modified from the previous chapters. This will include a study of systematic uncertainties. Finally, predictions for the ratio will be given.

The WS D^* signal was blinded, to avoid bias for the ratio during optimization. The results when the procedure is unblinded will be described in chapter 7.

5.1 Analysis Executable Changes

Most of the requirements that were imposed, at the time the ntuples were made, have remained the same as described in chapter 2. The changes are detailed below.

At the time of the analysis, the "B Decays and Direct CP Violation" subgroup had these recommendations on the web page:

> We recommend analizing (sic) this data with release 5.3.4, apply KAL track refitting with ProcessName PROD_PHYSICS_CDF, PassName 16, keeping ISL, SVX stereo. Keeping L00 hits improves the impact parameter distribution, but the MC may not reproduce it well. For COT covariance rescaling, phantom-layers, B-field calibration use the prescription described in CDFnote 6905. Consult the BPAK pages or the offline operations pages for more detailed instructions.

This section uses CDF analysis code release 5.3.4 to process the data that was written to tape. L00 hits were included.

Although Event-By-Event Vertexing was available, we chose not to use it. That code was still in its early stages, with incomplete verification. EbEV would require running silicon-alone tracking, which increases total processing time by 2-3 times. For future work, this code could be included when making the ROOT ntuples, if there is a clear advantage for using it.

5.1.1 Cuts for the Ntuple Construction

The B-Group made recommendations for the COT and silicon hit requirements for tracking. The D^0 tracks have slightly tighter requirements than the soft pion used for the D^* tag. All tracks were required to have at least 3 silicon hits. The tracks associated with the D^0 were require to have 3 axial and 3 stereo COT track segments, with a minimum of 5 hits per segment. The minimum p_T (with respect to the beamline) is 2 GeV. The tracks that will be used as the D^* tag were require to have 3 axial and 2 stereo COT track segments, with a minimum p_T of 0.3 GeV.

5.1.2 dE/dX Particle Identification

dE/dX is defined as the energy loss per unit length in a media. For CDF II, it refers to the ionization energy loss as particles pass through the COT. For a drift chamber with fixed

gas properties, dE/dX only depends on $\beta\gamma$. Combined with the momentum measurement, dE/dX can be used to distinguish particles of different mass.

The details of how dE/dX is done are too complicated for this note, but are described in other papers[24, 25]. The COT was designed for tracking, and will not have the separation power of detectors optimized for dE/dX. What will be discussed here is what is observed and how it will be used in this analysis.

After the dE/dX information is corrected for local variations, a prediction can be made for a specific $\beta\gamma$. This analysis will be using the dE/dX variable Z. , which is expressed as $Z = log(dedx_{measured}/dedx_{predicted})$. The advantage is that the Z variable has a gaussian distribution, while the difference $dedx_{measured} - dedx_{predicted}$ is log-norm distributed.

Figure 24 shows the Z distribution for CF D^0s. For a correct hypothesis, the Z variable is a unit gaussian centered at zero. For a pion hypothesis, a real kaon will have a Z gaussian distribution centered at -1.6 with a width of 1.25. For a kaon hypothesis, a real pion will be centered at 1.3 with a width of 0.9. These are obtained from data, at the time the ntuple was created. (More recent improvements in the code and calibrations may improve the particle ID separation.)

5.2 Data Set XBHD0D

The original hbot0h sample covered data through the January 2003 shutdown. The xbhd0d sample adds data up to the August 2004 shutdown (which included the fall 2003 shutdown). The b-hadronic compressed set was created with code version 5.1.0 and the latest calibrations. It started later than the hbot0h set, because the L00 detector was not declared "okay" until June 26, 2002.

Table 7 gives some information about the xbhd0d and hbot0h samples. The online trigger adjustments changed the events per integrated luminosity. The D^0 yield improved over time. The D^0 mass resolution improved for xbhd0d, compared to hbot0h.

Run Range	Date	# of Events	# of Files	Int. Lum.	D^0 / pb
147165 - 156600	Jun 02- Jan 03	43 million	6,535	87.5 / pb	1740
158800 - 168900	Feb 03 - Sep 03	96 million	20,004	128.3	2420
174950 - 186600	Nov 03 - Aug 04	131 million	15,582	211.0	2640
138808 - 156487	Feb 02 - Jan 03	43 million	2991	$\sim$ 60 / pb	1420

Table 7: The first three lines are the xbhd0d data, divided by the two long shutdown periods in 2003. The last line is information for the older hbot0h data set.

5.2.1 "Good" Runs

After data is written to tape, the shift crew mark bits for the run, to state which detector systems were operating good enough for use in analysis. The BPAK group has a good run

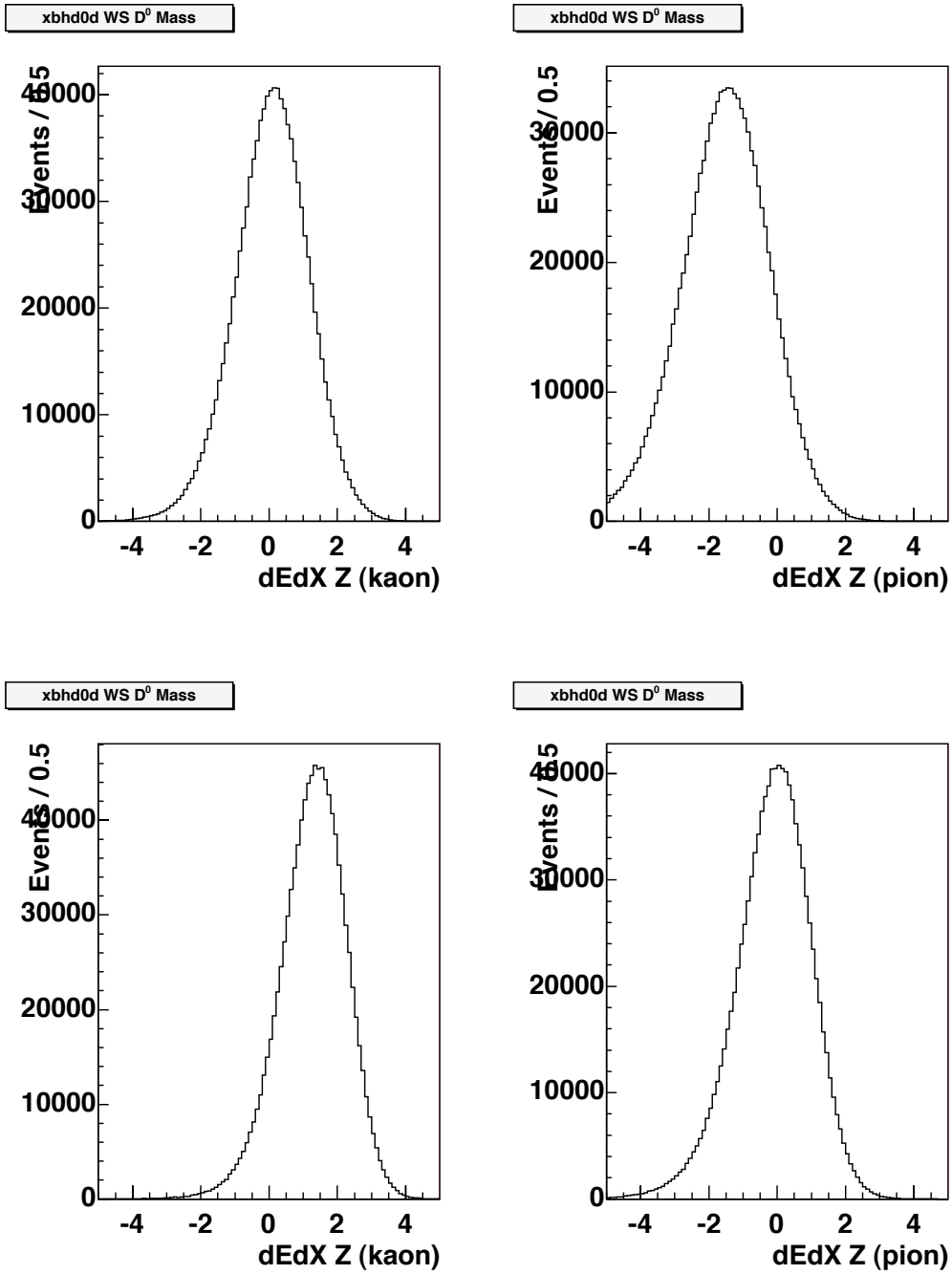

Figure 24: Events that have a good RS D^0 mass and good mass difference were selected, to get a sample that is mostly CF D^*. The Z variable, described in the text, is shown for the kaon hypothesis (left column) and pion hypothesis (right column). The top row is for the D^0 kaon track, and the middle row is the D^0 pion track. A correct hypothesis (upper left and lower right) will be a unit gaussian centered at zero.

list (generated by Matt Herndon) where the detector was considered good for all B analyses. The list is available at http://www-cdf.fnal.gov/internal/physics/bottom/bpak/basics.html.

The ROOT ntuples made for this analysis (as described in last section's table 7) did not limit runs to be on the good run list. Some of the "bad" runs had problems with the calorimeter or muon systems, which we do not use. Others had COT or silicon problems, which should be excluded.

We decided to exclude the "bad" run data from our final results (although it was used in cut optimization). The increase in the statistical error is small, despite losing about a sixth of the signal. This issue may be revisited in the future. The RS D^* signal-to-noise was the same for both good and bad runs. Our tests showed at most a modest decrease in tracking and dE/dX efficiency. However, the effort to convincingly prove that the data is good enough is more than the potential gains, at this time. Refer to Appendix A for more details.

5.3 Blinded WS Signal Yield Technique

For this data set, we decided to blind the WS mass difference yield signal during cut optimization. Although there is no obvious bias in the cut selection, this seemed the safest course.

The yield technique, described in section 4.4 is unchanged for the RS distributions. The WS $K\pi$ slices are not blinded. The mass difference yield plot is filled, but the WS signal region is erased. The background is fit using the yield sidebands. The bins in the signal region are then filled, using the extrapolated background fit and adding RS D^*s scaled by 0.36 %. The scale value is based on the PDG value for the WS/RS ratio . The WS signal is estimated by the scaled RS signal. The uncertainty for each bin is corrected to include the amount of background in the original WS $K\pi$ slices.

The WS signal uncertainty can be observed directly from the fit. A check using the hbot0h data shows that the uncertainty from the blinded method was very close to the normal fit. The differences were due to the choice of the RS scaling factor used to make the WS signal estimate.

5.4 Cut Optimization of the Ntuple Variables

The cut optimization is very close to the procedure described in section 4.5, which uses the blinded yield technique. The largest difference is adjusting the yield bin uncertainties to include the amount of background in the WS $K\pi$ slices. This allows the significance to be taken as the signal uncertainty from fitting the (blinded) WS yield plot. The previous calculated significance only included the background from D^0s with unassociated pions.

As a note, all of the optimized cuts reduce the significance of the RS signal. That is due to small background under a huge RS signal. The optimization is to improve the WS signal to background. The WS signal dominates the time-integrated ratio statistical uncertainty.

5.4.1 Opposite Assignment Mass Cut and dE/dX

The WS background coming from mis-assigned CF D^*s can be reduced by two cuts: the opposite assignment mass cut, and using dE/dX for particle identification. Other cuts would not see a difference when the D^0 kaon and pion assignments are swapped.

As mentioned in section 5.1.2, we will be using Z, the normalized dE/dX variable. The cut variable that we decided to use will be a difference of the sum of the squares of the Z variable for the tracks, comparing RS and WS hypothesis. For example, the square of the Z variable for the first track, assuming it is a kaon, is $Z^2_{K,1}$, while a pion hypothesis for the second track will be $Z^2_{\pi,2}$. The right-sign hypothesis would be the sum of these two squares. The wrong-sign hypothesis would have the track indices switched. The cut variable would be $(Z^2_{K,1} + Z^2_{\pi,2}) - (Z^2_{\pi,1} + Z^2_{K,2})$. A RS D^0 should have a negative value, since the WS sum of squares will be larger than the RS sum of squares.

For illustration purposes, figure 25 shows the cut variable distribution for CF D^0s. (The sample has background contamination, but is mostly signal.) As expected, the variable is mostly negative. Approximately 85% of the CF D^0s have a negative value, leaving a 15 % tail with positive values. A WS D^0 is expected to have a similar distribution, but mirrored around zero (positive and negative distributions reversed).

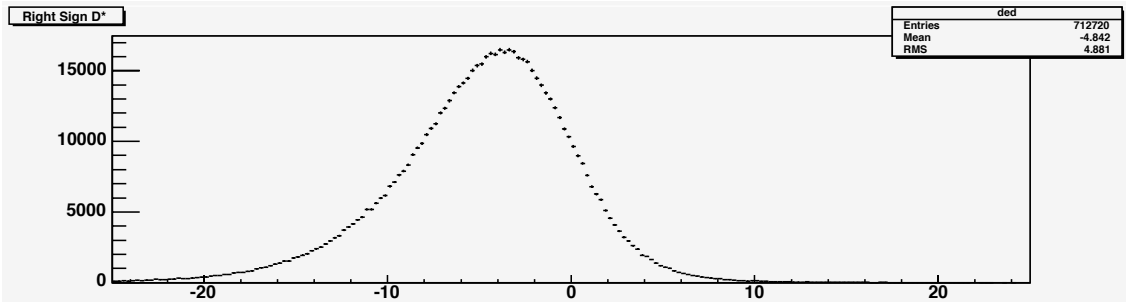

Figure 25: Events that have a good RS D^0 mass and good mass difference were selected, to get a sample that is mostly signal. The horizontal axis is the dE/dX cut variable, as described in the text. An average, RS D^0s have negative values, while WS D^0s would have positive values.

Since both OAM and dE/dX cuts attack the same background, it is easier to simultaneously optimize the cuts, rather than separately. The dE/dX cut variable is required to be less than (greater than) a given cut value, for the RS (WS) distributions. The opposite assignment mass cut is then chosen, with the blinded yield technique used to find the WS yield significance. The OAM cut value is varied, to find an optimum for the given dE/dX cut value. As an example, figure 26 shows the WS yield significance as a function of the OAM cut, with the dE/dX cut set at zero. The dE/dX cut is then changed, and the procedure repeated.

Table 8 summarizes the results of the cut optimization. While there is some overlap between the two cuts, using both OAM and dE/dX cuts is stronger than either of them

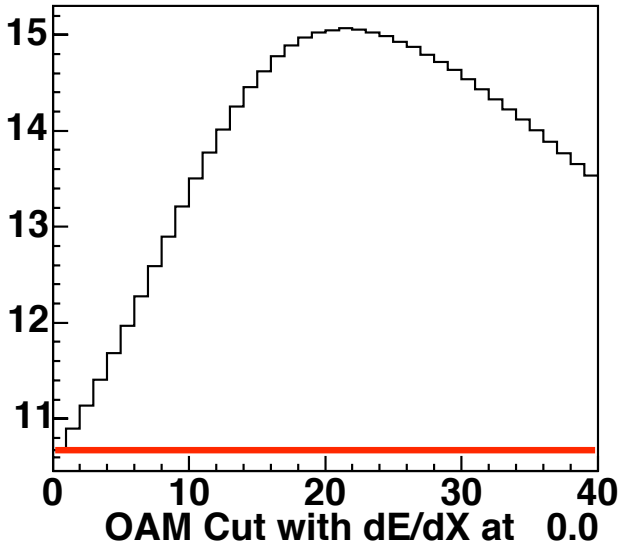

Figure 26: This is the WS yield significance as a function of the OAM cut (in MeV), with the dE/dX cut set at zero. A OAM cut of zero is the same as not applying the cut.

dE/dX Cut Value	Max Significance	OAM Cut Value
-3.0	14.1	19
-2.5	14.5	19
-2.0	14.7	20
-1.5	14.9	20
-1.0	15.0	20
-0.5	15.1	22
0	15.1	22
+0.5	15.0	22
+1.0	14.9	23
+1.5	14.8	23
+2.0	14.7	25
+2.5	14.6	25
No dE/dX	13.0	28 MeV

Table 8: The blinded yield technique is used to get the WS signal significance for dE/dX and OAM cut values. The dE/dX cut is fixed at a value, while the OAM cut is scanned (in steps of 1 MeV) to find value with the highest significance. The dE/dX cut is then changed by half a unit, and the procedure repeated.

alone. The OAM cut value will be set at 20 MeV, and the dE/dX cut at 0. These are convenient, round numbers that are very close to the maximum significance. An advantage of having the dE/dX cut at zero, is that an event that passes the RS cut will fail the WS cut, and vice versa. Any other cut value will have events that could pass both the RS and WS dE/dX cuts, or fail both cuts.

5.4.2 Other Ntuple Cuts

After the dE/dX and OAM cuts were set, other variables in the ntuple were tried. Figures 27, 28, 29, 30, and 31 show the plots used to make the cut optimization. For each of those figures, the left plots only have the optimized dE/dX and OAM cuts applied. The red line shows the significance without additional cuts. The curve shows the significance when that particular cut is used. The maximum significance printed on those plots are not the cut values chosen, but were printed to assist the choice of cut values. The cut values were adjusted to avoid being near a large change in significance, if possible. Besides the opposite mass assignment and dE/dX cuts, the following additional cuts are applied to the xbhd0d data:

- D^0 vertex $L_{xy}/\sigma_{xy} \geq 5$.
- D^* vertex $|L_{xy}/\sigma_{xy}| \leq 15$.
- D^* vertex 2-D chisq $\chi^2_{xy} \leq 12$.
- π^* tagging track absolute miss distance $|d_0| \leq 0.08$ cm
- π^* tagging track dE/dX $Z \leq 2.25$

For those same figures, the right plots shows the significance when these additional cuts are applied, except for the cut variable being scanned. The WS signal significance from applying these additional cuts is higher than using any single cut (without the others). These significance numbers are different than the numbers listed in table 8, because the previous section included runs that were outside the Good Run selection list. The plots for this optimization were double-checked with only events from the Good Run list. The optimum cut values were unchanged, but the significance changed.

Many other cut variables were tried, such as the number of silicon hits or the p_T of the tracks. They failed to improve the expected significance.

5.5 Misassigned D^0 Background in WS $K\pi$ Fits

The wrongly reconstructed CF D^*s, where the kaon and pion assignments are swapped, need to be accounted for as background in the WS $K\pi$ fits. The fitter has trouble when using a combination of linear and wide gaussian backgrounds, as it tends to confuse those two distributions, when simultaneously fitting a narrow gaussian signal, a broad gaussian background, and a linear background. Without constraints, the fitter will choose parameters

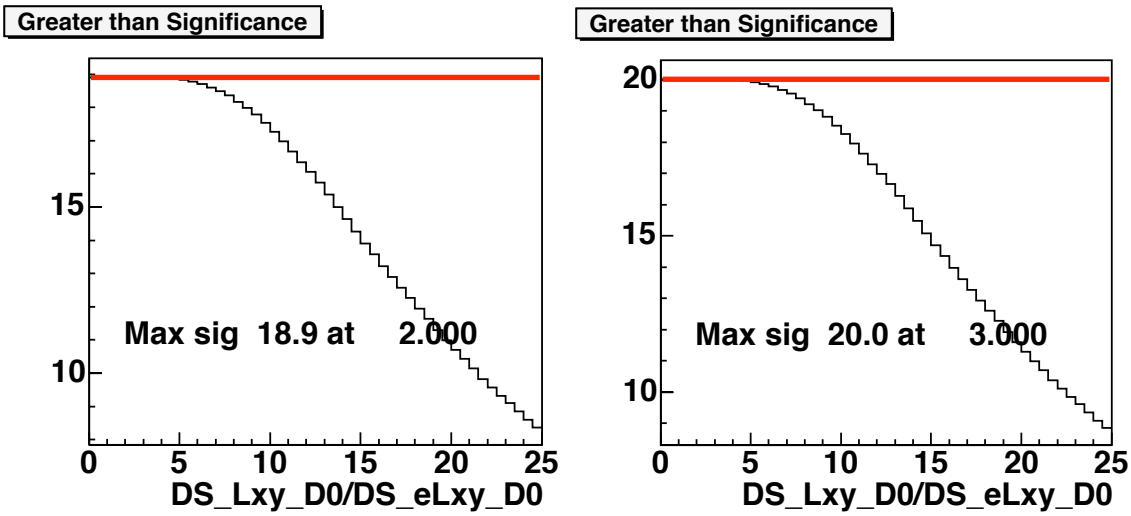

Figure 27: The left plot is the estimated signal significance as a function of the cut value, requiring the $K\pi$ vertex L_{xy}/σ_{xy} to be greater than the value. The red line shows the significance without any cuts on this variable. The right plot shows the optimization when all of the new cuts are applied, except the for the cut on L_{xy}/σ_{xy}.

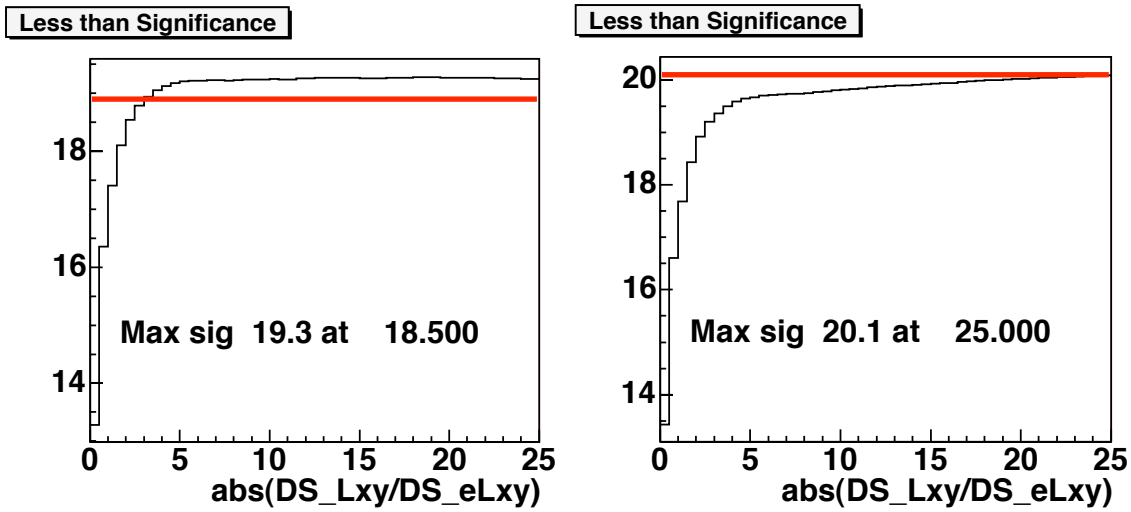

Figure 28: The left plot is the estimated signal significance as a function of the cut value, requiring the D^* Vertex $|L_{xy}/\sigma_{xy}|$ to be less than the value. The red line shows the significance without any cuts on this variable. The right plot shows the optimization when all of the new cuts are applied, except the for the cut on $|L_{xy}/\sigma_{xy}|$.

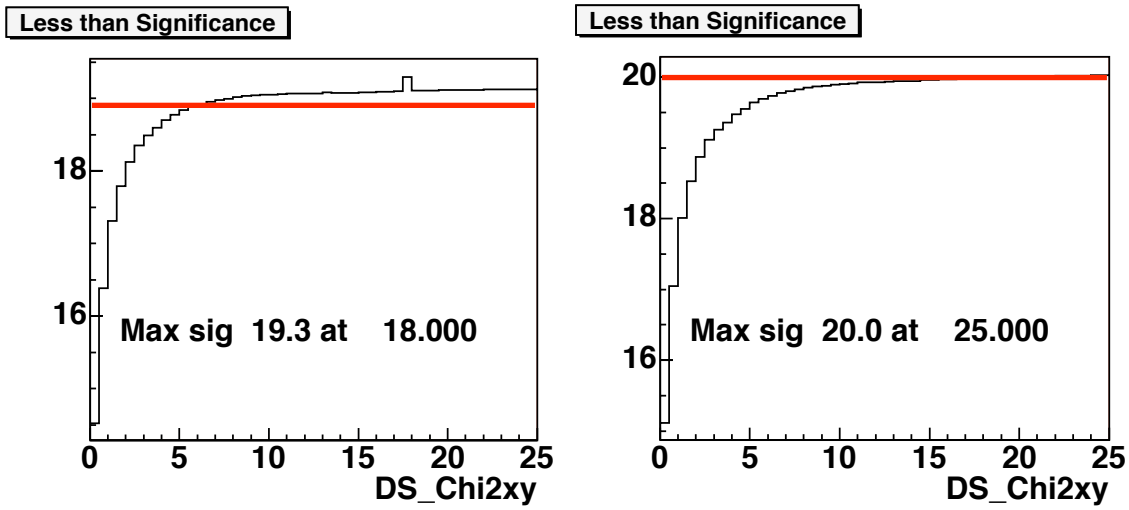

Figure 29: The left plot is the estimated signal significance as a function of the cut value, requiring the D^* Vertex χ^2_{xy} to be less than the value. The red line shows the significance without any cuts on this variable. The right plot shows the optimization when all of the new cuts are applied, except the for the cut on D^* Vertex χ^2_{xy}.

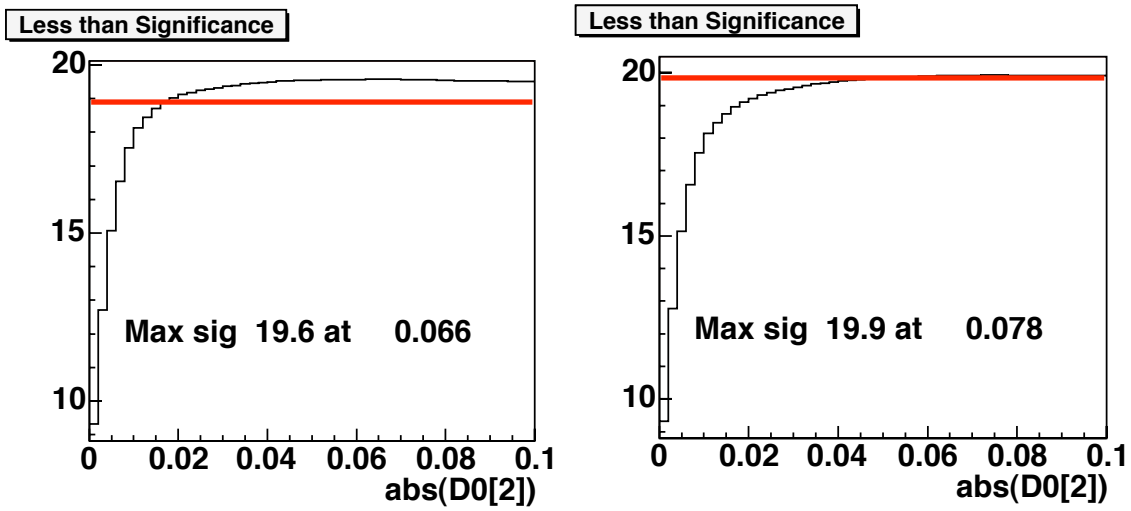

Figure 30: The left plot is the estimated signal significance as a function of the cut value, requiring the π^* track $|d_0|$ to be less than the value. The red line shows the significance without any cuts on this variable. The right plot shows the optimization when all of the new cuts are applied, except the for the cut on π^* track $|d_0|$.

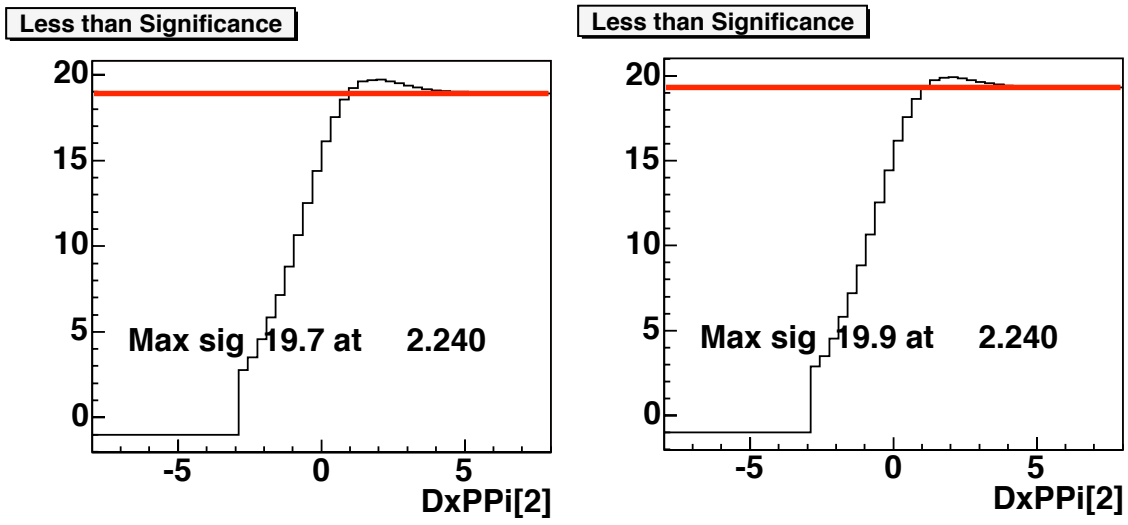

Figure 31: The left plot is the estimated signal significance as a function of the cut value, requiring the π^* track dE/dX variable (assuming a pion hypothesis) to be less than the value. The dashed line shows the significance without any cuts on this variable. The right plot shows the optimization when all of the new cuts are applied, except the for the cut on π^* track dE/dX variable.

that neglect one of the background shapes, putting all those background events in the other shape.

The WS $K\pi$ fit will be modified to include a broad gaussian background, which will be constrained to match the expected mis-assigned CF D^* background in the WS plot. To get that estimate, several numbers will need to be known from data or models. For the following discussion, all of the following numbers apply only to RS D^*s, not WS D^*s. (Any mention of wrong-sign are the efficiency for CF D^*s to show up as background in the WS mass plots). If we start with N_{D^*}, the total number of CF D^*s, then the amplitude of the signal in the RS yield plot (S_{RS}) will be

$$S_{RS} = N_{D^*}\,\epsilon_{RS}^{dE/dX}\,\epsilon_{RS}^{oamc}\,\epsilon_{cuts}, \tag{4}$$

where $\epsilon_{RS}^{dE/dX}$ is the fraction of CF D^*s that survive the RS dE/dX cut, ϵ_{RS}^{oamc} is the fraction of events that survive the opposite assignment mass cut applied to the WS $K\pi$ distribution (to get good RS signal), and ϵ_{cuts} are the fraction of events that survive all other cuts. The amount of mis-assigned CF D^*s in the WS plot (B_{MRS}) will be

$$B_{MRS} = N_{D^*}\,\epsilon_{WS}^{dE/dX}\,\epsilon_{WS}^{oamc}\,\epsilon_{cuts}, \tag{5}$$

where $\epsilon_{WS}^{dE/dX}$ is the fraction of CF D^* that pass the WS dE/dX cut (or the fraction of mis-assigned CF D^* that will survive to the WS plot), and ϵ_{WS}^{oamc} is the fraction of events that

pass the opposite assignment mass cut applied to the RS $K\pi$ distribution (to get a good WS signal).

From the data, we can get the RS D^* yield. The yield can be measured before and after applying the dE/dX cut, so those efficiencies are known. What are not known from data are the (WS) OAM cut efficiencies, and the distributions of the mis-assigned CF D^* in the WS $K\pi$ and mass difference plots.

5.5.1 OAM Cut Efficiency From Data

To get the Opposite Assignment Mass cut efficiencies ϵ_{RS}^{oamc} and ϵ_{WS}^{oamc}, we will use D^0s from data. Figure 32 shows the plots that were used. D^0s from data were plotted for RS and WS mass before the OAM cut is applied. A good RS D^* mass difference was required, but the D^0s include both real D^*s and D^0s with a fake tag. The events that are in the top plot are interpreted as WS and used for the bottom plot. The blue area (CF D^0s) is the same in both plots, when the under- and over-flow bins are included in the bottom plot. The red areas (DCS D^0s) are the same. The green area is the linear background, which is fit separately for both plots. The narrow signal and the broad gaussian shapes have the same shape parameters for both fits. The fits were repeated several times, to get the same numbers and fit shapes for both plots.

Once the shapes are known for signal (narrow variable width gaussian) and mis-assigned background (wide gaussian), those functions are used to get the fraction of events more than 20 MeV from the D^0 mass. The signal shape was used to get $\epsilon_{WS}^{oamc} = 2.46/pm0.05\%$. The wide background shape was used to get $\epsilon_{RS}^{oamc} = 77.9 \pm 0.3\%$. The ratio of those two terms is $\epsilon_{WS}^{oamc}/\epsilon_{RS}^{oamc} = 3.16 \pm 0.07\%$

As a check, figure 33 was made. The good RS D* requirement was dropped, which will allow a lot of D^0s with a fake tag into both plots. With these plots, the efficiency numbers are 2.44, 77.6, and 3.15 %, all consistent with the first set of plots.

5.5.2 Misassigned RS D^0 Model

A toy Monte Carlo in ROOT can be used to model the mass change of the D^0 (and the change in mass difference for the D^*), when the kaon and pion assignments are swapped. This model was originally used to get the OAM cut efficiencies, until it was determined that data could be used to get better numbers. The model will still be needed, to get the distribution of MRS background as a function of the WS mass difference.

The variables involved in the model are:

- Momentum of the D^* in the lab frame
- Cosine of the angle of the π^* track in the D^* rest frame, with respect to the D^* momentum vector
- Cosine of the angle of the K track in the D^0 rest frame, with respect to the D^0 momentum vector

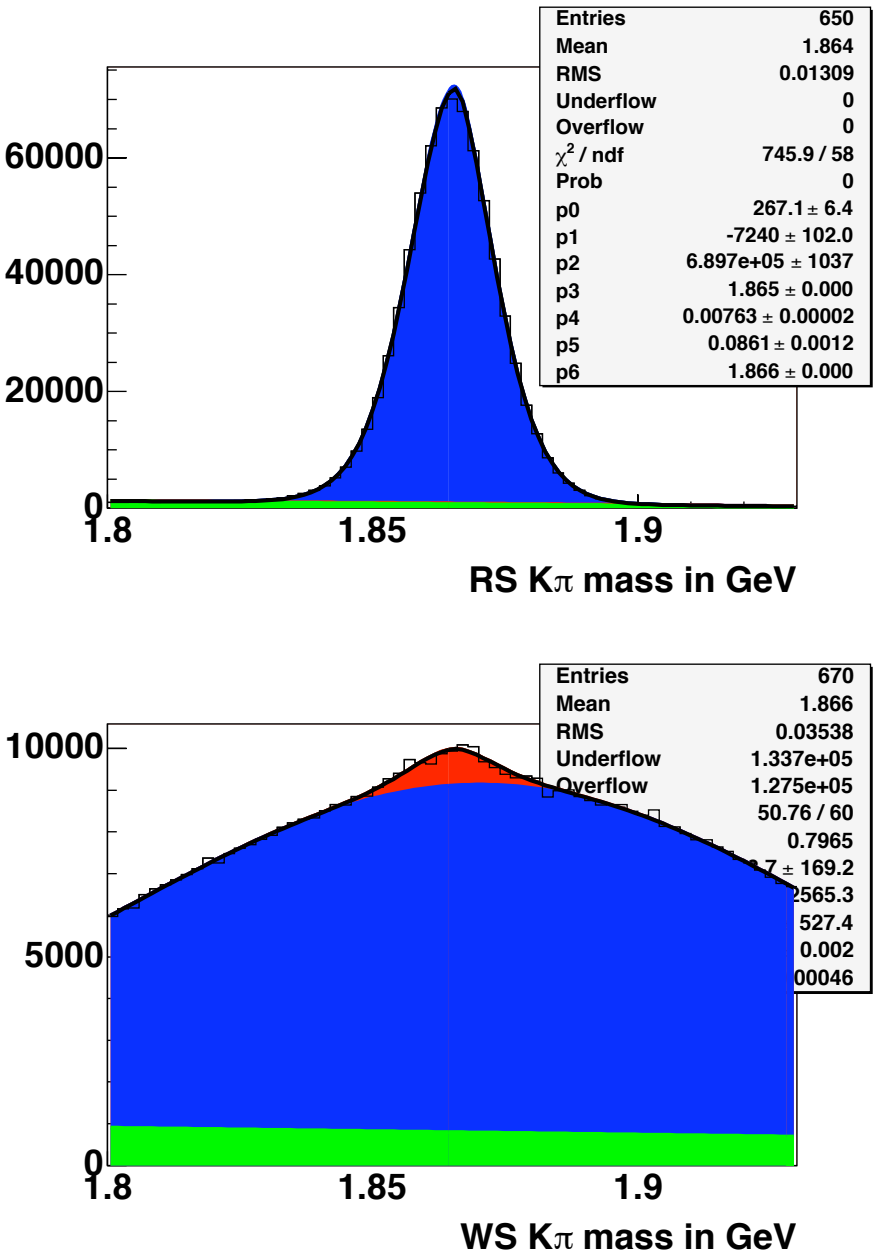

Figure 32: RS (top) and WS (bottom) mass plots for D^0s from data, before the OAM cut is applied. A good RS D* mass difference was required. The events that are in the top plot are interpreted as WS and used for the bottom plot. The blue area (CF D^0s) is the same in both plots, when the under- and over-flow bins are included in the bottom plot. The red areas (DCS D^0s) are the same. The green area is the linear background, which is fit separately for both plots. The narrow signal and the broad gaussian shapes have the same shape parameters for both fits. The D^0s include both real D^*s and D^0s with a fake tag.

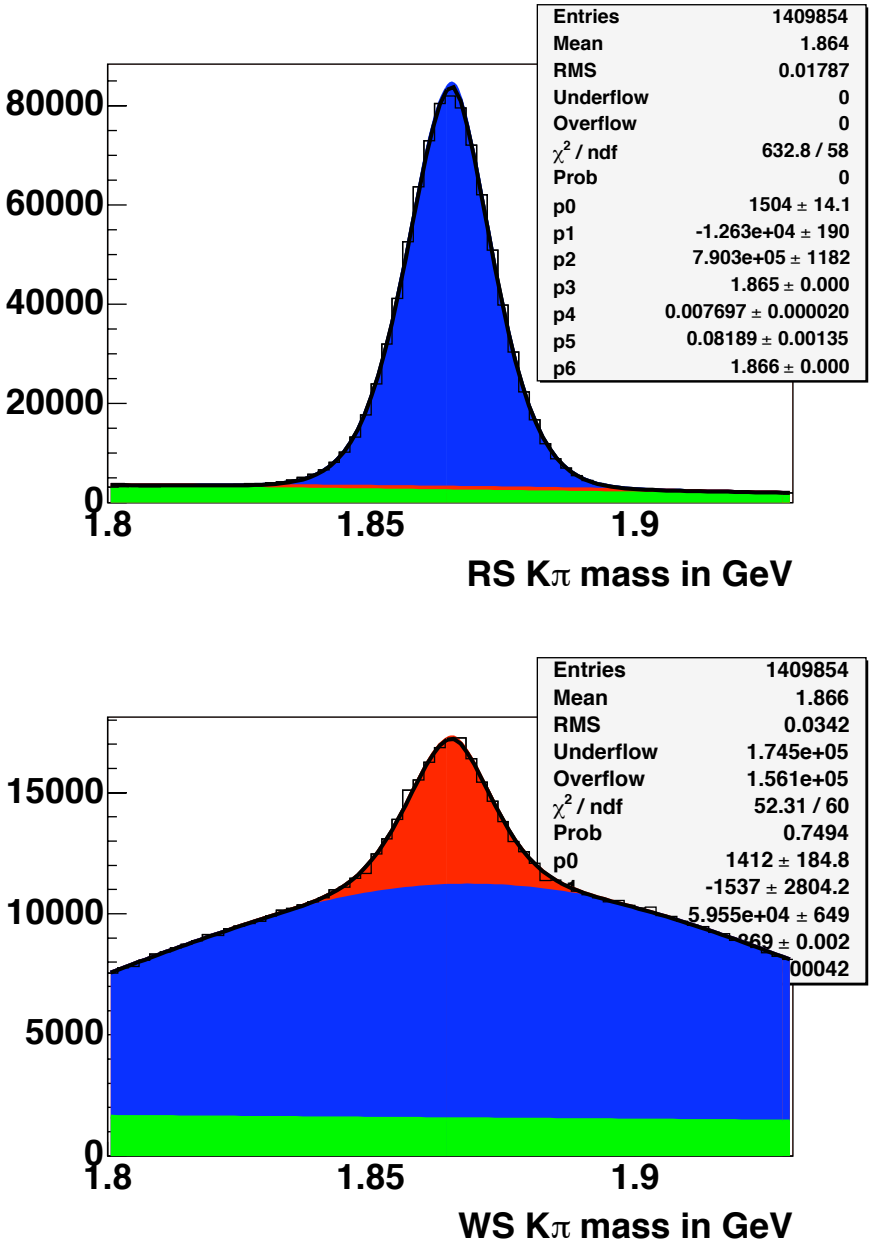

Figure 33: RS (top) and WS (bottom) mass plots for D^0s from data, before the OAM cut is applied. The events that are in the top plot are interpreted as WS and used for the bottom plot. The blue area (CF D^0s) is the same in both plots, when the under- and over-flow bins are included in the bottom plot. The red areas (DCS D^0s) are the same. The green area is the linear background, which is fit separately for both plots. The narrow signal and the broad gaussian shapes have the same shape parameters for both fits. The D^0s include both real D^*s and D^0s with a fake tag.

- Masses assigned to the D^* and D^0 particles. These will have a distribution, instead of a single value, to simulate the errors due to detector resolution.

With that information, the kaon and pion momentum are known in the rest frame of the D^0. The kaon and pion assignments are then swapped. The tracks are boosted to the lab frame, and the new (wrongly constructed) D^0 and D^* masses are calculated.

The simulation uses the RS D^0 mass and D^* mass difference distributions, fit from real data. A simple parameterization of the p_T distribution is used, as well as the mass resolution (as a function of p_T). The decay distributions are generated as spherically symmetric. Software loops vary the variable values. For each set of variable values, it is weighted to reflect the assumed distributions and phase space. Both the RS and WS masses must lie in the range from 1.7 to 2.0 GeV, as this is a requirement for the real data.

The first attempt at using this model failed to match real data, specifically the WS background distribution. The primary cause is the minimum track miss distance cut $d0$ that is used in the trigger, as mentioned in chapter 2. This cut is at 120 microns, which is comparable to the proper decay length $c\tau$ for a real D^0. The trigger cut removes events where the kaon and pion are travelling close to the direction of the D^0, which are also the events that have the largest mass shift when the kaon and pion are misassigned. Adding this cut to the model reproduced the WS broad background seen in data.

The (opposite assignement) mass cut is applied to the RS and WS distributions separately. The cut removes events within 20 MeV of the correct D^0 mass (1.8645 GeV). Figure 34 shows the RS and WS distributions for simulated events that survive the OAM cut, cutting on the RS $K\pi$ mass. Similar plots are available for before the OAM cut was applied, and for cutting on the WS $K\pi$ mass.

The shapes of the distributions from the simulation should reflect the data, but the total number of events is not meant to simulate the actual number of CF D^* in real data. We do want the relative number of events between the RS and WS plots to be accurate. The same number of simulated events are present before the two opposite assignment mass cuts are tried (independently of each other). The simulation generates the expected number of events in the RS D^* yield plot (N_{RS}^{sim}) and the expected number of events in the WS D^* yield plot (N_{WS}^{sim}). The important points are:

- $$\epsilon_{WS}^{oamc}/\epsilon_{RS}^{oamc} = N_{WS}^{sim}/N_{RS}^{sim} \tag{6}$$

  To set a scale, the ratio from the simulation is about 2.7 % .

- Using the WS $K\pi$ plot of figure 34, a gaussian fit gives a width of 73.5 MeV centered at 1.873 GeV. This fit will be used as the shape for misassigned RS background, when we fit real WS data. The amplitude of the shape takes into account that only 58% of the distribution lies between 1.8 and 1.93 GeV.

- The WS mass difference histogram of figure 34 will be used for the misassigned RS D^* background distribution. The variable $n_{mrs}^{sim}(i)$ will be the number of events in bin i

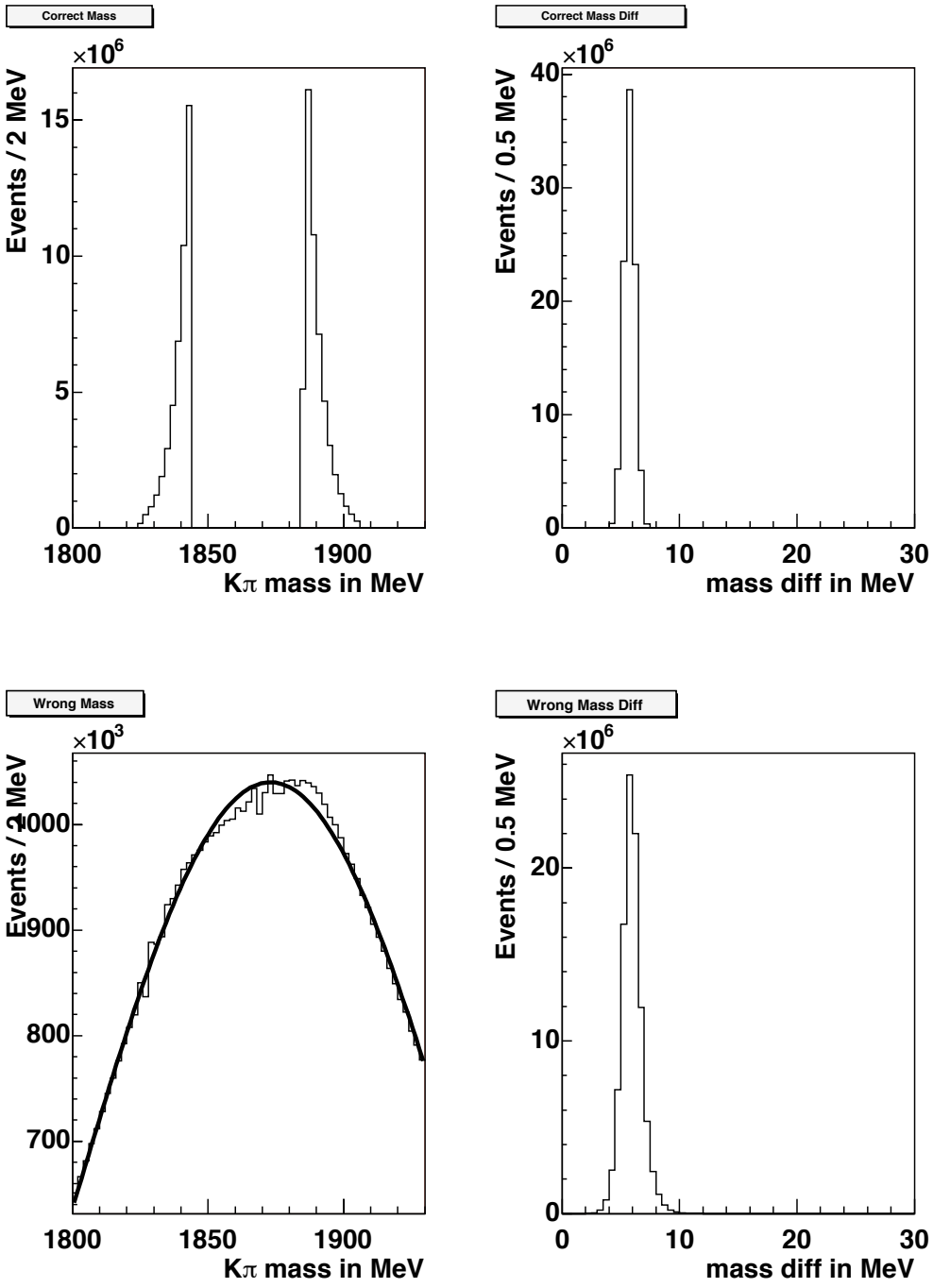

Figure 34: RS (top) and WS (bottom) mass plots for the model, with the OAM cut removing RS D^0s. The left plots are $K\pi$ mass, the right plots are mass difference $(D^* - K\pi - \pi)$. The normalization requires the set of plots made before the OAM cut is applied.

of that histogram. The background shape is wider than the RS signal mass difference peak, but most of the background is still concentrated near the WS signal region. If we wanted to normalize that distribution to a unit area, $n^{sim}_{mrs}(i)$ would be divided by the total number of events in that histogram (N^{sim}_{WS}).

5.5.3 Adjusting WS Data Fit

The WS $K\pi$ slices for the hbot0h data were fit using a narrow gaussian ($\sim$ 10 MeV) and a linear background. For the xbhd0d data, we will add a wide gaussian ($\sim$ 75 MeV) to that fit, to account for the influence of misassigned RS D^*s. The magnitude of that gaussian will be fixed before the WS fit, from information available due to the model and real data.

Equation 4 can be rewritten as

$$N_{D^*} = S_{RS} \,/\, (\epsilon^{dE/dX}_{RS}\, \epsilon^{oamc}_{WS}\, \epsilon_{cuts}) \tag{7}$$

Combining that with equation 5 produces

$$B_{MRS} = S_{RS}\, (\epsilon^{dE/dX}_{WS}/\epsilon^{dE/dX}_{RS})\, (\epsilon^{oamc}_{WS}/\epsilon^{oamc}_{RS}) \tag{8}$$

We will need to know how much misassigned background to add to each slice. For slice (bin) i, that amount is

$$b_{MRS}(i) = B_{MRS}\, n^{sim}_{mrs}(i)/N^{sim}_{WS} \tag{9}$$

Combined with equation 9, the final equation becomes

$$b_{MRS}(i) = S_{RS}\, (\epsilon^{dE/dX}_{WS}/\epsilon^{dE/dX}_{RS})\, (\epsilon^{oamc}_{WS}/\epsilon^{oamc}_{RS})\, n^{sim}_{mrs}(i)/N^{sim}_{WS} \tag{10}$$

The model gives the last term ($n^{sim}_{mrs}(i)/N^{sim}_{WS}$), the distribution of MRS events for each slice. The dE/dX fractions were obtained by getting the RS yield with and without the cut. The dE/dX cut value of zero is such that $\epsilon^{dE/dX}_{WS} = 1 - \epsilon^{dE/dX}_{RS}$. From the fits, we have $\epsilon^{dE/dX}_{WS} = 16.5$ %, and $\epsilon^{dE/dX}_{RS} = 83.5$ %.

The amount of background depends on 3 numbers:

- The number of CF D^* in the RS yield plot. This is based on the signal fit of the RS yield plot, and is 495172 ± 976 events.
- The efficiency for CF D^*s to survive the opposite assignment mass cut, to make it to the RS and WS mass plots. This is based on data, with $\epsilon^{oamc}_{WS}/\epsilon^{oamc}_{RS} = 3.16 \pm 0.07\%$. The fit shape widths were varied within errors to get the uncertainty in the efficiencies.
- The efficiency of the dE/dX cut. This is done by getting the RS yield with and without the cut, with $\epsilon^{dE/dX}_{WS}/\epsilon^{dE/dX}_{RS} = 19.8 \pm 0.3\%$. The uncertainty is given by the fits of the RS yields.

Based on the current estimates and efficiencies, the correction is 3098 ± 109 events, for all WS $K\pi$ slices. Figure 35 illustrates the difference including mis-assigned RS background will have on a slice fits (in the D^* signal region).

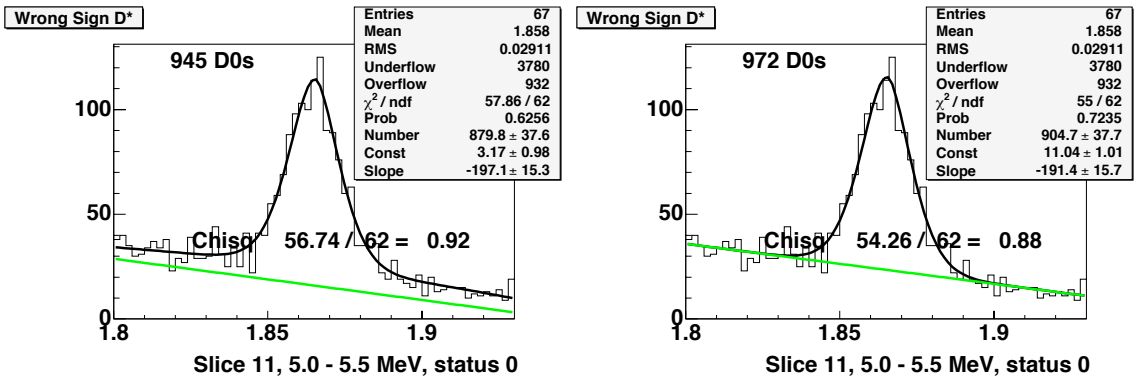

Figure 35: For this particular WS $K\pi$ slice, the left shows the fit which included mis-assigned CF background. The right plot is the signal shape and a linear background. The green line for both plots is the linear background only.

5.6 Checks of the xbhd0d Data

The xbhd0d data appears to have similar behavior as the hbot0h sample that was originally being used. The scatter plot showing the events with RS and WS interpretations, is shown in figure 36. This has similar features to the hbot0h data in figure 6. The scatter plot showing the WS $K\pi$ mass versus mass difference, is shown in figure 37. This has similar features to the hbot0h data in figure 16

Figure 38 shows the fit pulls for the yield plots, as a function of mass difference slice. The WS plot does not show any obvious features. The RS has oscillations in the signal region, as the simple fit function doesn't perfectly model the data. This has been observed in other analyses, for high statistic samples. The effect on the RS yield will be negligible. For the mass difference range from 4-8 MeV, the fit overestimates the data by 1167 events. If we assume that this difference is all signal (instead of a combination of signal and background), it would cause the WS/RS ratio to change by 0.009×10^{-3}, which is negligible compared to the statistical error on the ratio. If the mass difference region is extended to 2-12 MeV, the fit underestimates the data by 667 events.

Figure 39 shows the distribution of those fit pulls.

5.7 Systematic Uncertainties

For this analysis, most of the systematic errors on the RS yield or the WS yield will not affect the ratio of WS to RS. This is because both CF and DCS D^* decays are kinematically identical. They will have the same decay products and mass resolution. Most cuts will have the same efficiency for both RS and WS, which will cancel out when taken as a ratio.

The following sections are using the PDG value for the DCS/CF ratio of 3.6×10^{-3}. When the WS signal is unblinded, the systematics will need to be recomputed using the measured ratio.

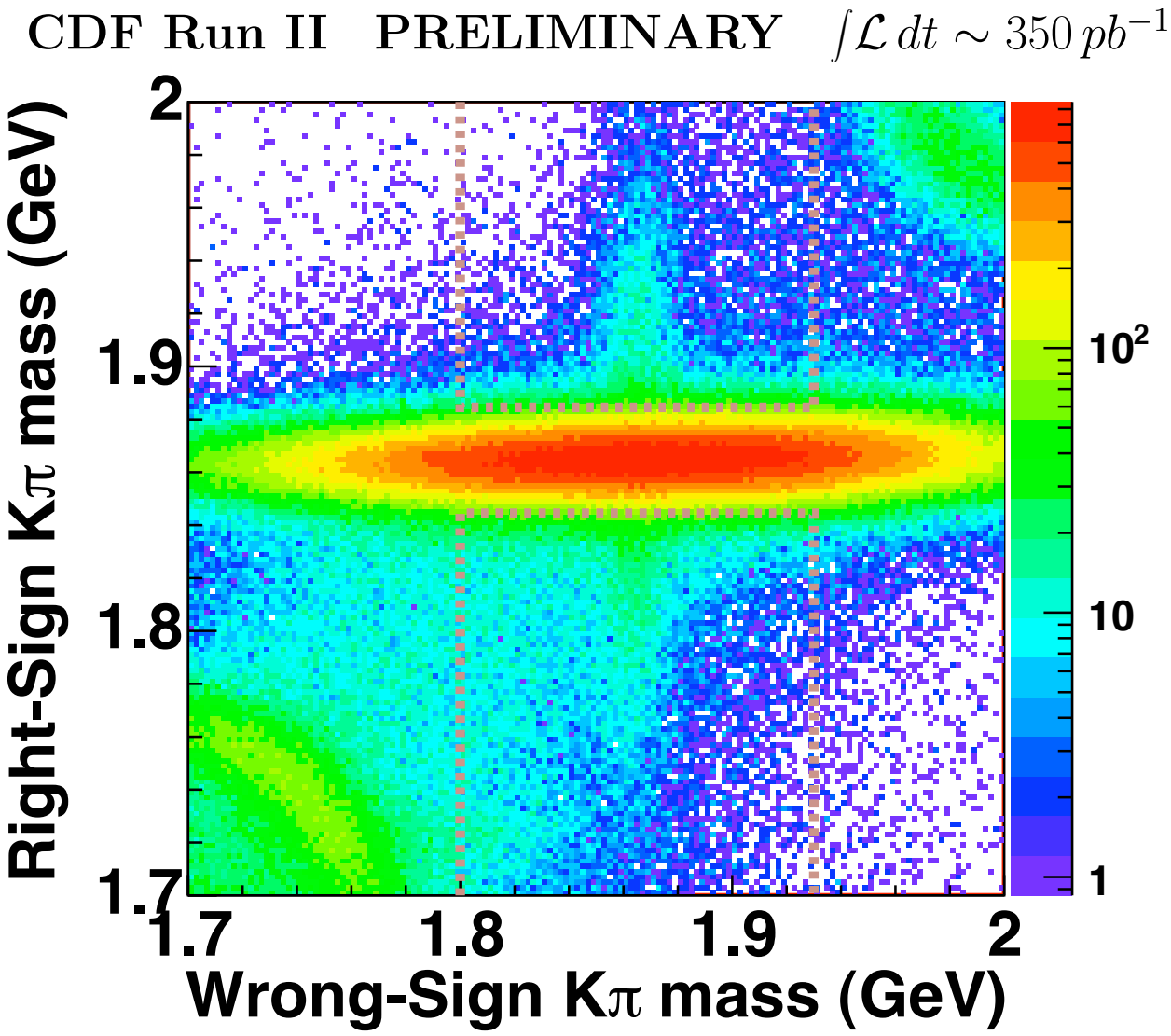

Figure 36: Candidates are plotted with both RS and WS interpretations. A cut requiring a good (WS) D* tag is used to reduce background. The bins are 2 MeV wide, along each axis. The brown regions show the events used for the WS fit, with the RS OAM cut excluding the center region.

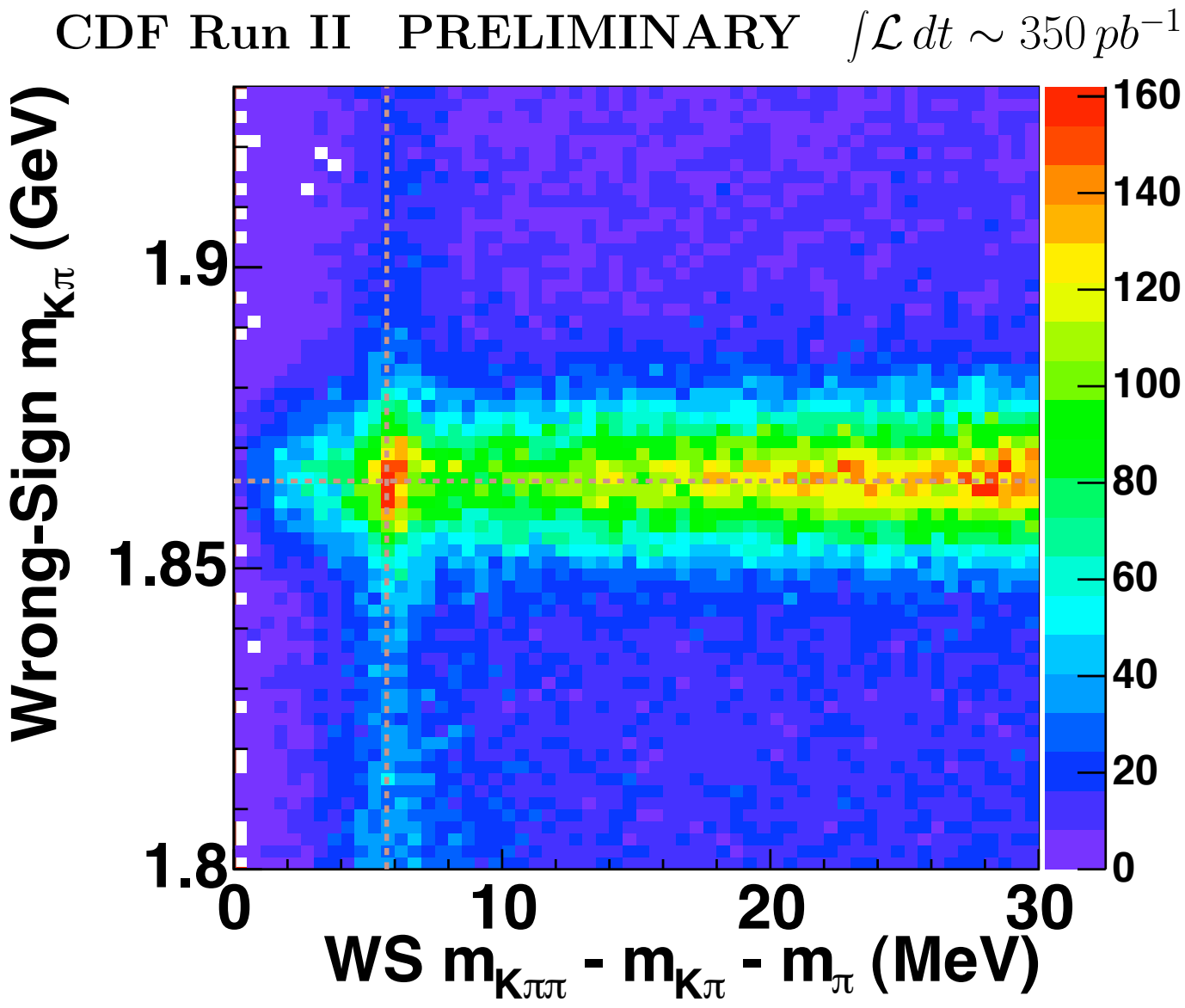

Figure 37: Events that survived the minimum cuts and the opposite assignment cut. PDG values for the D^0 and D^* are shown by the dashed lines. The $K\pi$ axis is in 2 MeV bins, the mass difference $(m_{K\pi\pi^*} - m_{K\pi} - m_{\pi})$ axis is 0.5 MeV bins.

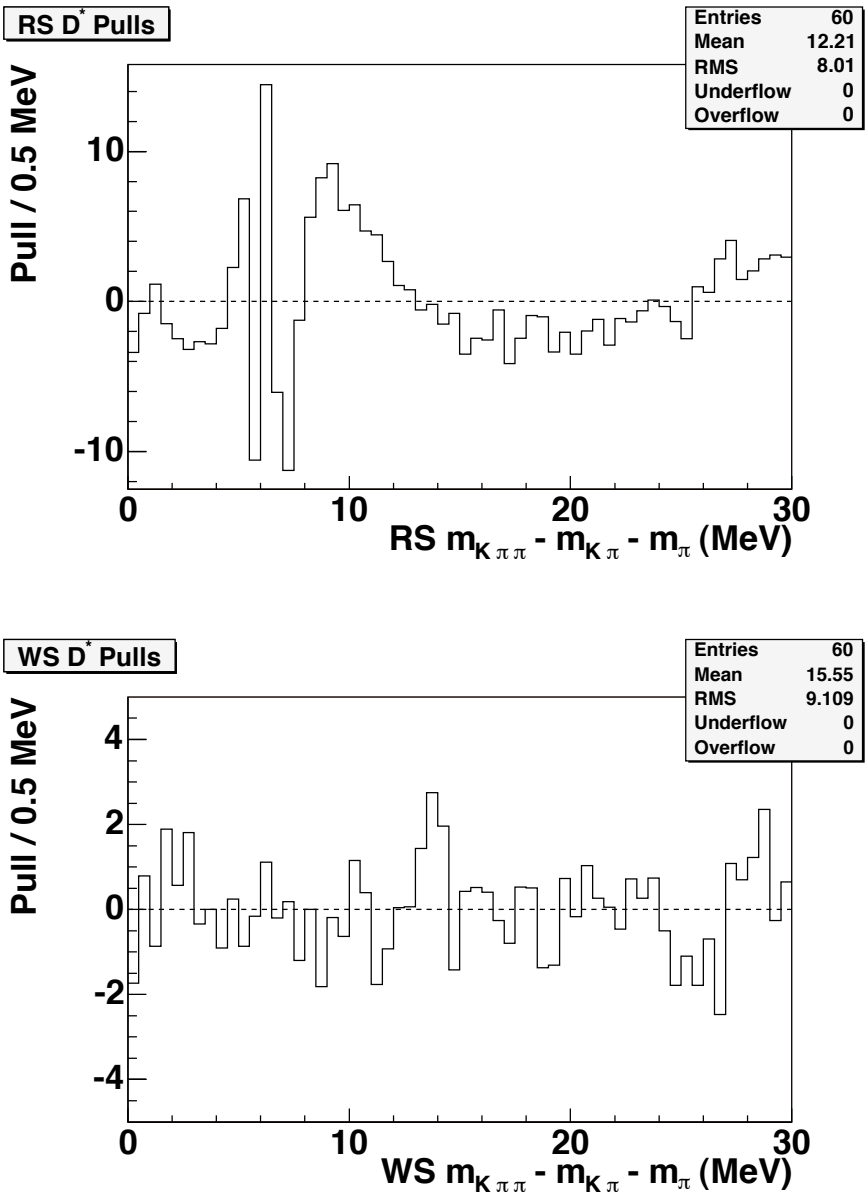

Figure 38: The pulls, comparing the yield histogram to the fit function, is plotted for RS (top) and unblinded WS (bottom).

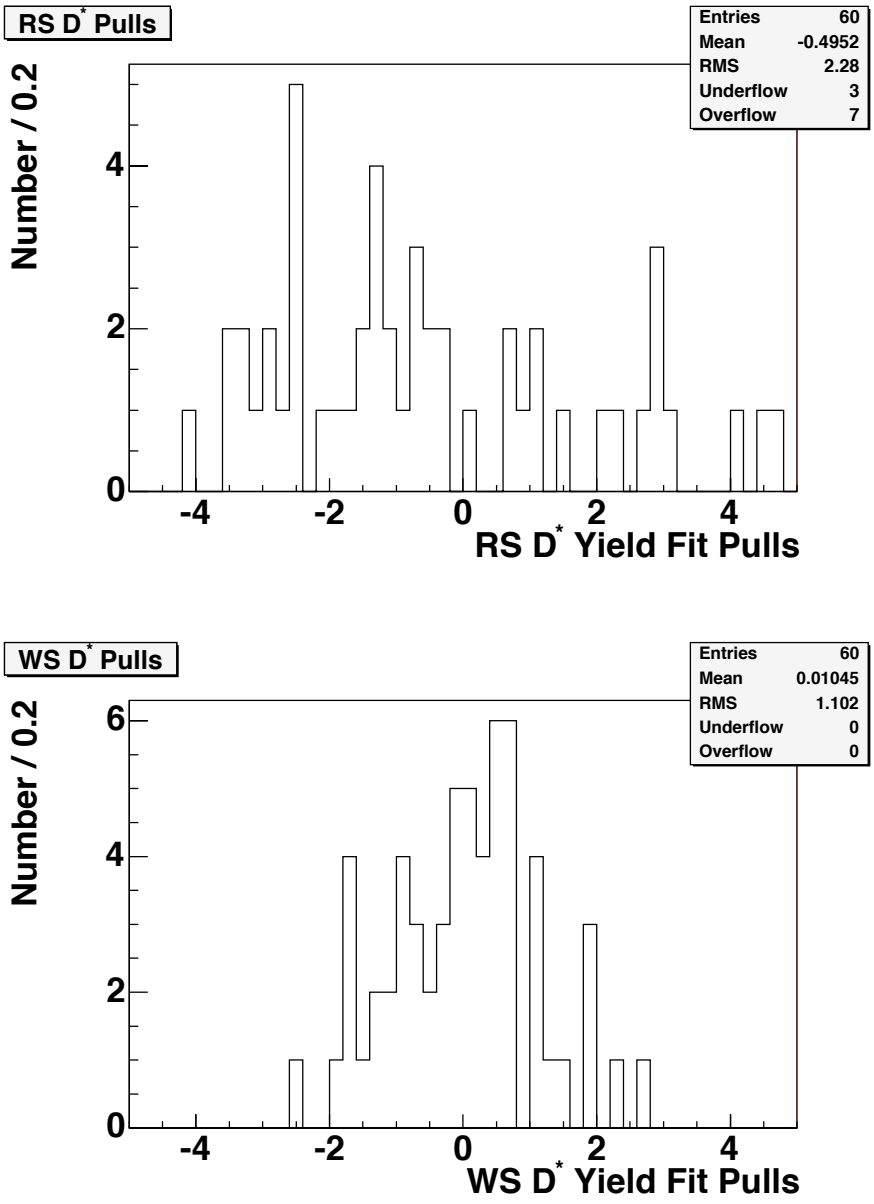

Figure 39: The distribution of the fit pulls for the RS (top) and WS (bottom) yield plots.

5.7.1 $K\pi$ Background

We fit the $K\pi$ slices assuming a linear background. Figure 40 shows the χ^2/dof distribution for the WS $K\pi$ slices. The slice fits appear to work very well.

To get a systematic error due to this choice of the background shape, we tried alternative backgrounds. The first is a quadratic background, requiring that the background be flat or decreasing, as a function of increasing $K\pi$ mass. The second alternative is to extend the fit region from an upper limit of 1.93 GeV out to 2.0 GeV. This region includes background from $D^0 \to \pi\pi$. We use a model to get a fixed shape to describe this background. The toy model used to get the mis-assigned CF background shape was modified, to start with $D^0 \to \pi\pi$ to get the shape of these events in the $K\pi$ plots. The amplitude of this shape is a parameter of the fit, which is allowed to float for each slice. The alternatives have fit qualities (based on χ^2/dof) which are indistinguishable from the normal linear background fit. Figure 41 gives an example of how the fit of the same distribution can change for the different background shapes.

We did an unblinded fit of the WS yield, but did not look directly at the results. The WS signal for an alternative was compared to our normal fit, and only observed the change in WS/RS ratio divided by the ratio. This kept the procedure blind, as we never saw the actual ratio value. The largest change in the WS/RS ratio due to changing the $K\pi$ background is $\Delta R/R = -2.25\%$, when comparing the quadratic background to the normal linear background. This will be chosen as the systematic error. To be conservative, the error will be symmetric around zero. With an assumed ratio of 3.6×10^{-3}, the error becomes $\pm 0.08 \times 10^{-3}$.

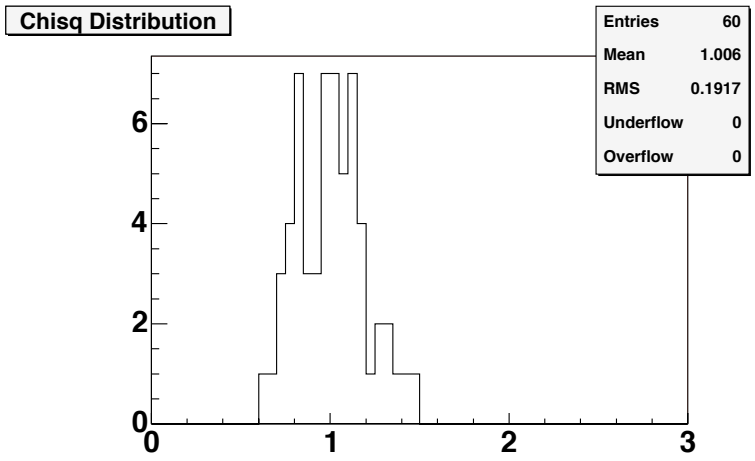

Figure 40: The χ^2/dof for all 60 WS $K\pi$ slices. The fits used signal, linear background, and a fixed amount of mis-assigned RS background, as described in the main text. The mean value is 1.0.

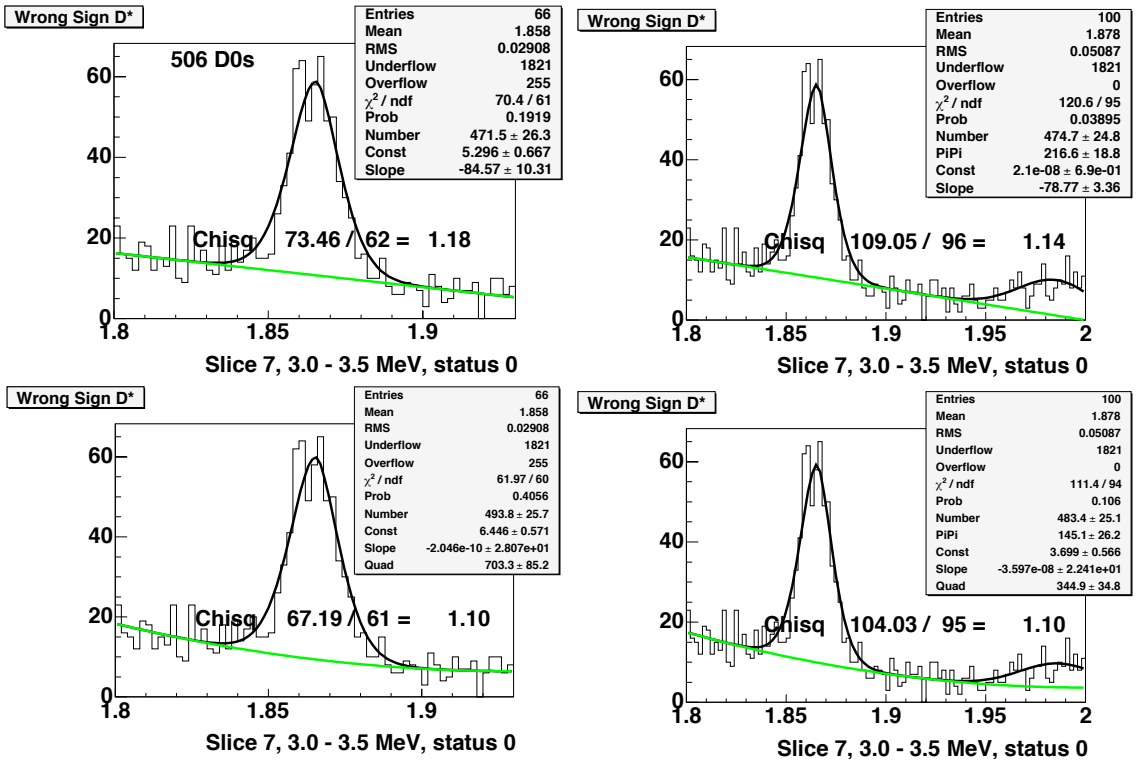

Figure 41: For this particular WS $K\pi$ slice, the background shape was modified between linear (top row) and quadratic (bottom row). The fit range upper limit is 1.93 GeV (left column) and 2.0 GeV (right column).

5.7.2 Misassigned RS D^* Background

The correction of the WS $K\pi$ slice fits, to include mis-assigned CF background, is described in section 5.5. We need to estimate the uncertainty of this correction, and the effect that it would have on the WS/RS ratio.

Based on the current estimates and efficiencies, the correction is 3098 ± 109 events, for all WS $K\pi$ slices. Next, we would need to know how this amount of background would affect the WS signal. A model was made of the $K\pi$ mass distributions, and of the mass difference yield distributions. Those distributions were fit with and without the mis-assigned CF background being part of the model, but the signal and overall amount of background being constant. The fits were then repeated, with the MRS correction deliberately under and overestimated by 10%. Figure 42 shows the results of 200 trials of this toy model. Not correcting for mis-assigned CF background would cause the WS signal to shift by 3.2 ± 0.1 events per 100 background events not accounted for.

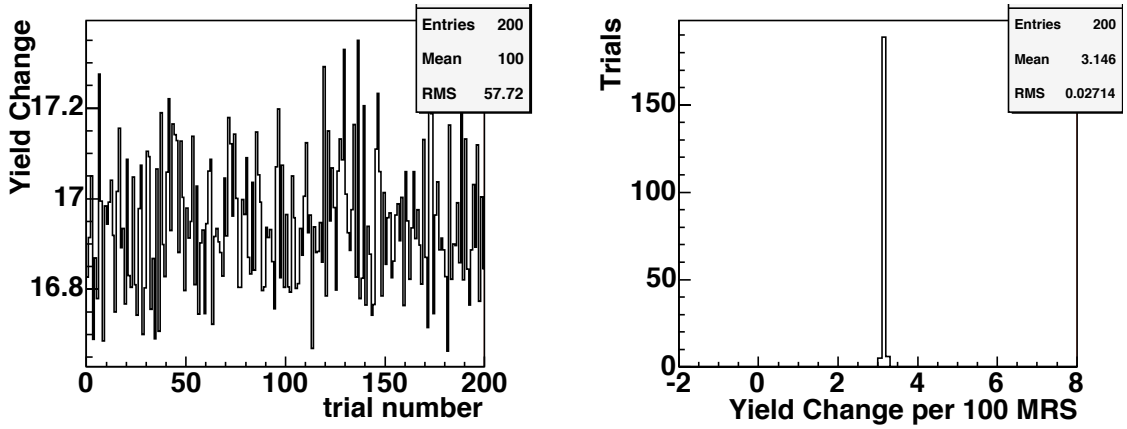

Figure 42: The toy model described in the text models the WS mass and mass difference distributions. With the exact amount of mis-assigned CF background known, the WS slices were deliberately fit with 90% and 110% of the MRS background. For this particular model, we used 2693 MRS events. The left plot shows the difference in WS yield for those two fits, for each trial. The right plot shows the distribution of the yield change between the two fits per 100 MRS events (approximately 17 events, divided by 20% of 2693 mis-assigned CF events).

Working through the math, including the mis-assigned CF background in the fit changes the WS signal of the fit by 99 events, with the uncertainty on the signal correction being 4.7 % of the correction, or 4.7 WS signal events. For the blinded analysis and 1780 WS signal events, this gives a systematic for the WS/RS ratio of $\pm 0.01 \times 10^{-3}$.

5.7.3 D^* Mass Difference Background

The mass difference background shape, due to correctly reconstucted D^0s with a random pion, is given by equation 2. The parameters of that equation are obtained by fitting the yield plots. To get a systematic error due to the differences between the background shape and the actual distribution, we originally varied the equation parameters within the fit error ellipse. That procedure is described in the following text. Ultimately, we decided to try alternate background functions to determine this systematic error. That description is in section 6.2.

Figure 43 shows the result when the yield plots are refit, fixing the background parameters to values along the error ellipse. We used the maximum RS and WS yield changes to get the uncertainty in the ratio of $\pm 0.07 \times 10^{-3}$.

5.7.4 D^* Mass Difference Fitter Bias

During the blinded analysis, we suspected a systematic due to a fitter bias for the yield plots. The rest of this section shows the investigation at the time. This was found to be a feature of ROOT and the toy MC. We do not expect real data to have this bias. That explanation will be in unblinded section 6.1.

When alternative $K\pi$ backgrounds were tried, we looked at the blinded WS yield plots, as shown in figure 44. The WS signal fit after blinding was consistently higher than the number of WS events that were added to the blinded region. Using the four fits shown in the figure, the WS fit overestimates the signal by 4.0 to 4.6 %.

This was checked with the mass distribution model that was used for MRS background. The mass difference distribution was modeled with the fit function and parameters that were used to fit the blinded WS yield plot. WS mass difference distributions were filled randomly by ROOT, using that fit shape as the template. Each of those model distributions was refit. Figure 45 has the results of 400 trials. On average, the WS signal was overestimated by $1.5 \pm 0.2\%$. The final unblinded WS result will be decreased to account for this overestimate. (The blinded results being high by 4.5 % is within the statistical spread of values.)

This translates to a ratio systematic uncertainty of $\pm 0.01 \times 10^{-3}$ (assuming the ratio is 3.6×10^{-3}). The amount of the correction, roughly (1780 events $\times 1.5\%$) 27 events, is still smaller (0.05×10^{-3}) than the statistical and systematic errors.

To be safe, we also checked the RS fit. Figure 46 has the results of 400 trials. The change is less than a tenth of a percent. This is not surprising, as the RS yield plot has very little background compared to signal.

5.7.5 Charge Asymmetry and Kaon Interactions

In CDF note 6391[23], they measure the charge asymmetry in the detector. This will result in a difference in the efficiency of finding the charged pions used to tag the D^*. On page 26, they quote the charge asymmetry as being $A = \frac{N_+ - N_-}{N_+ + N_-} = -1$ % (within errors). So

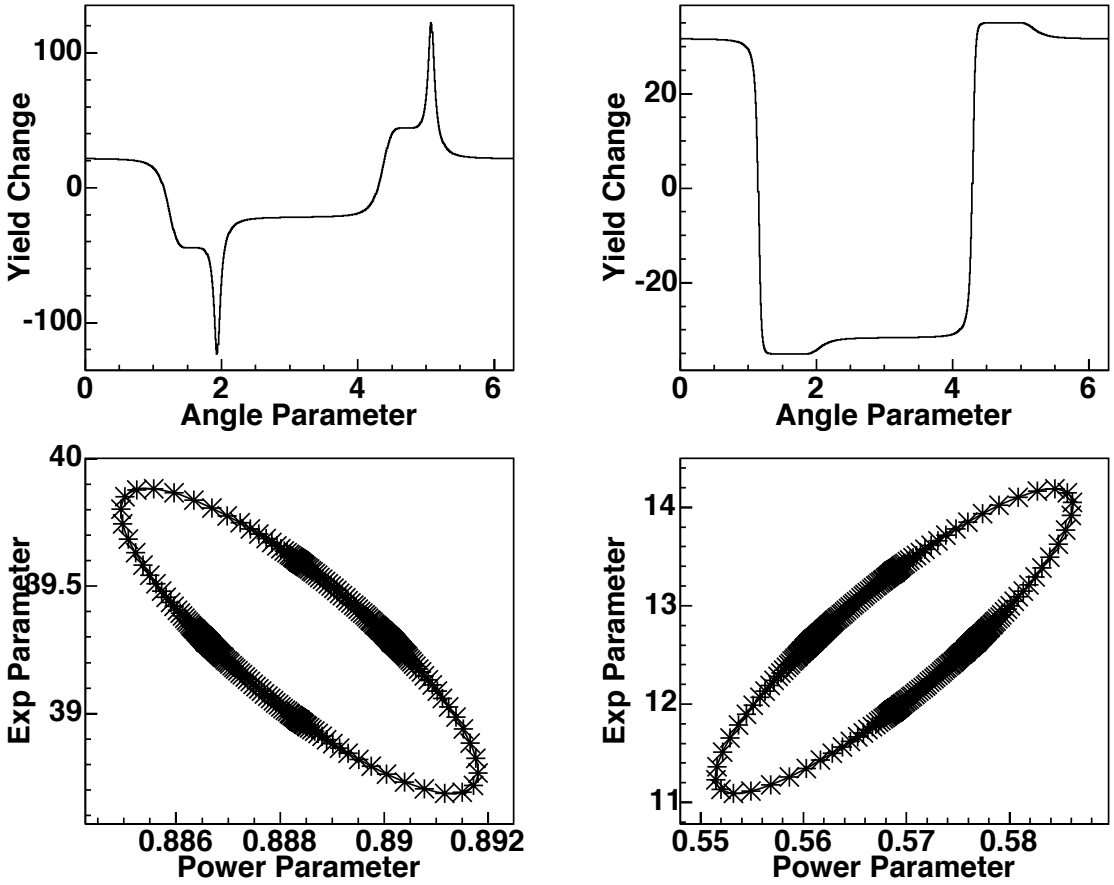

Figure 43: The parameters B and C from equation 2 were varied around the error ellipse, given by the fit covariant matrix. These parameters control the shape of the distribution. Those two parameters were fixed at specific values, and the yield plots were refit, with the signal and background amplitudes determined by the fit. The left column is for RS, right column is for WS. The top plots show the change in signal yield (from the original fit value) for the new background shape. The bottom plots show the changes in the background parameters that were used to get the error ellipse.

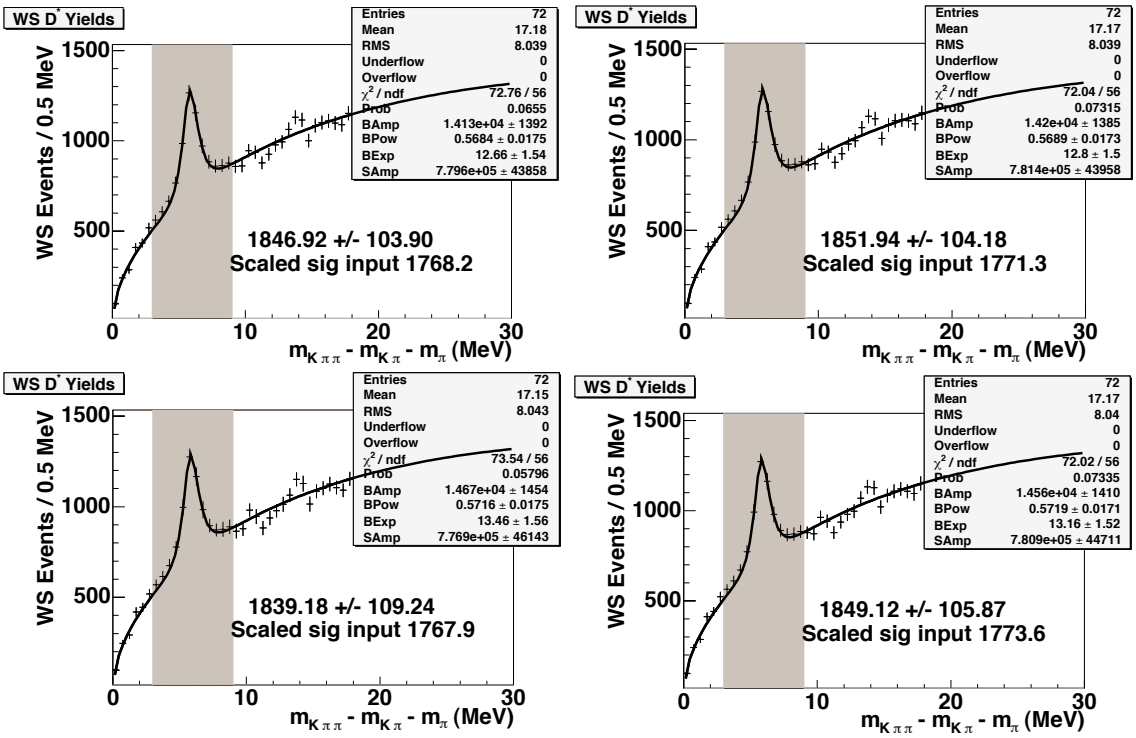

Figure 44: The background shapes were modified between linear (top row) and quadratic (bottom row). The fit range upper limit is 1.93 GeV (left column) and 2.0 GeV (right column). The WS signal fit after blinding was consistently higher than the number of WS events that were added to the blinded region.

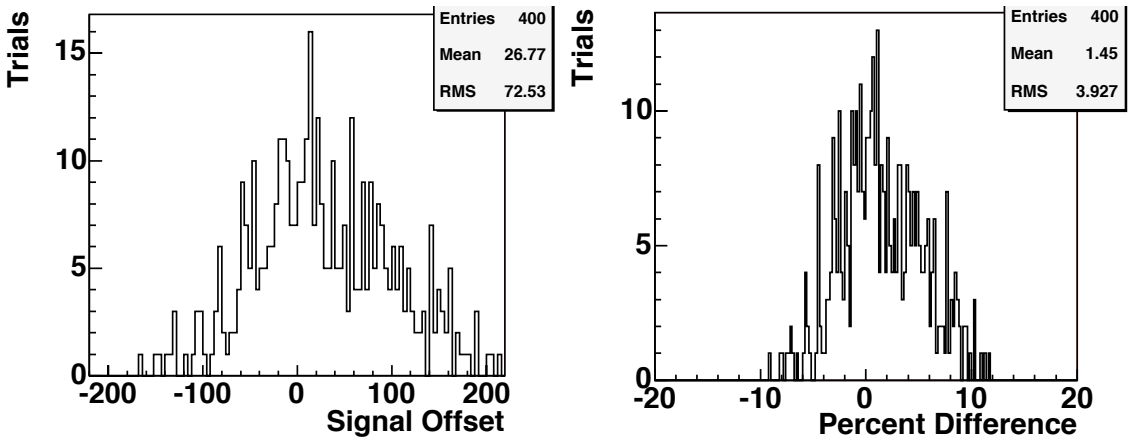

Figure 45: The toy MC was used to get how much the signal fit was different from the amount of signal expected. The function used for the template had 1847 events. The left plot shows the fit results of the 400 trials, the difference in fit signal compared to 1847. The right plot is the percentage change, by dividing the difference by 1847.

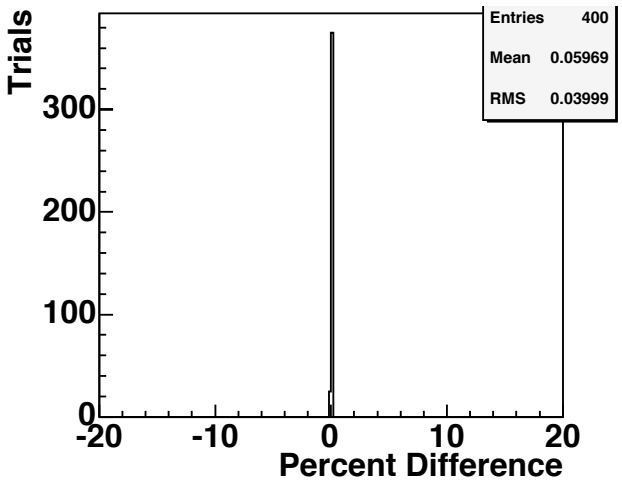

Figure 46: The toy MC was used to get how much the signal fit was different from the amount of signal expected. The function used for the template had 495K signal events. The plot is the percentage change for 400 trials, given by the fit signal minus the expected signal (495K) divided by the expected.

if we started with equal number of positive and negative tracks, we expect to reconstruct $N_- = \frac{1.01}{0.99} N_+$.

Also, the charged kaons have different nuclear interactions. On page 23, the ratio of the efficiencies to reconstruct $K^+\pi^-/K^-\pi^+ = 1.034$.

Our measured WS/RS ratio is

$R = (N_{D*^+,D^0\to K^+\pi^-} + N_{D*^-,\bar{D^0}\to K^-\pi^+})/(N_{D*^+,D^0\to K^-\pi^+} + N_{D*^-,\bar{D^0}\to K^+\pi^-})$

If we assume that we started equal number of mesons and anti-mesons, then we expect to measure

$\Delta R/R = (1.034 + \frac{1.01}{0.99})/(1 + (1.034)(\frac{1.01}{0.99})) - 1 = -0.03\%$

This systematic is negligible compared to the other systematic errors.

5.8 WS Signal Predictions

Figure 47 shows the yield plots, with the WS signal region blinded. The yields are (RS) 495172 ± 976 and (WS) $\sim 1780 \pm 104$. If we add the systematic errors in quadrature, the time-integrated WS/RS ratio is 3.6 (assumed) ± 0.21 (stat.) ± 0.11 (sys.) $\times 10^{-3}$.

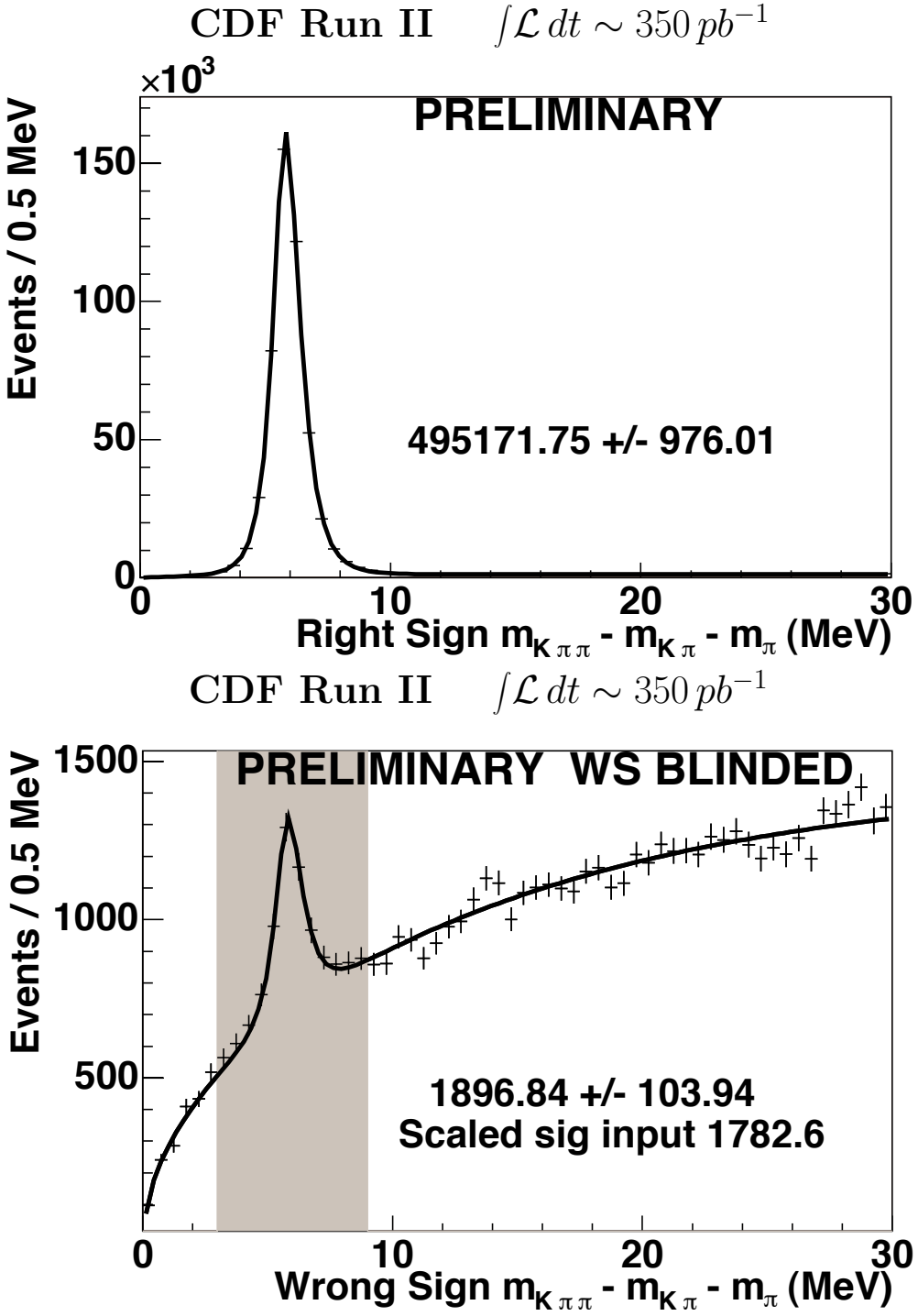

Figure 47: RS (top) and WS (bottom) mass difference yield plots for real data, with the WS signal region (3-9 MeV) blinded.

6 Unblinded Results

The blind analysis was blessed by the B-Physics group at CDF. This allows us to unblind the wrong-sign (WS) signal in the yield plot. Figure 48 shows the yield plots, with the WS signal region unblinded. The yields are (RS) 495172 ± 907 and (WS) $\sim 2005 \pm 104$. With these numbers, the time-integrated WS/RS ratio is 4.05 ± 0.21 (stat.) $\times 10^{-3}$.

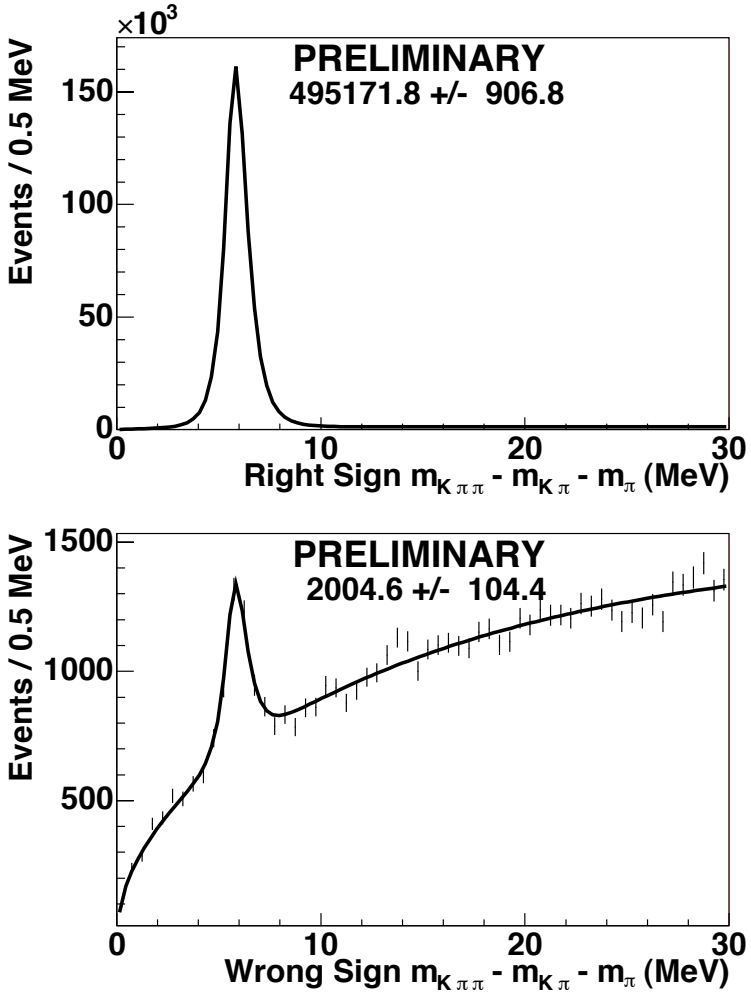

Figure 48: RS (top) and WS (bottom) mass difference yield plots for real data. The WS signal is not blinded.

6.1 Elimination of D^* Mass Difference Fitter Bias

During the blinded analysis, we suspected a systematic due to a fitter bias for the yield plots. That explanation was in section 5.7.4. This was found to be a feature of ROOT and the toy

MC. We do not expect real data to have this bias.

The mass difference distribution was modeled with the fit function and parameters that were used to fit the unblinded WS yield plot. WS mass difference distributions were filled randomly by ROOT with the "FillRandom" TH1 class function, using that fit shape as the template. (This is the recommended function, based on the ROOT example "Histograms with Random Numbers from a Function.) Each of those model distributions was refit. The average difference between the fit signal and the original function was used as the systematic. Figure 49 has the results of 2500 trials. On average, the WS signal was overestimated by $1.9 \pm 0.1\%$, which was an increase from the blinded prediction of 1.5 %.

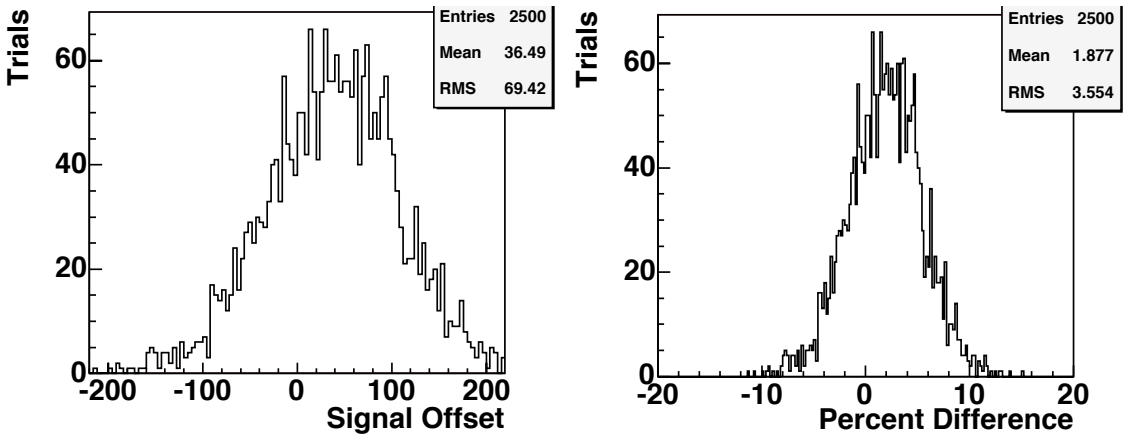

Figure 49: The toy MC was used to get how much the signal fit was different from the amount of signal expected. The function used for the template had 2005 signal events. The left plot shows the fit results of the 2500 trials, the difference in fit signal compared to 2005. The right plot is the percentage change, by dividing the difference by 2005.

During a blessing of the unblinded results, the fitter bias raised concern. Stefano Giagu offered to help investigate the cause. He performed his own toy MC, which used "GetRandom" and used an unbinned likelihood fit. He failed to see a bias. This helped us to discover that FillRandom is making an approximation of the integral of the function, that is not good enough for this precision measurement.

Figure 50 shows the difference between integrating the function by using 60 points (the function at the bin center), versus a more exact integration. The largest difference between the two is in the signal region. A difference of 40 events is on the scale of the fitter bias that we were chasing.

"FillRandom" can use a histogram, instead of a function. Figure 51 shows the toy MC results when using a histogram filled by integrating the function across each bin, versus using the function value at the bin center. The bin-integral model shows no bias. The bin-center shows a bias of 2.6 %. "FillRandom" is using an approximation of the original fit function that is close to the bin-center model. This also explains why the toy model prediction

increased when we went from blinded to unblinded WS. Since the signal increased from $\sim$ 1800 events to $\sim$ 2000 events, the error in the signal region due to imperfect integration should also get larger.

6.2 Unblinded Systematic Errors

The largest change in the WS/RS ratio due to changing the $K\pi$ background is $\Delta R/R = -2.25\%$, when comparing the quadratic background to the normal linear background. This will be chosen as the systematic error. To be conservative, the error will be symmetric around zero. With the ratio of 4.05×10^{-3}, the error becomes $\pm 0.09 \times 10^{-3}$.

The mass difference background shape, due to real D^0s with a random pion, is given by equation 2. The parameters of that equation are obtained by fitting the yield plots. Since the true distribution for the background may differ from the formula being used, we tried two alternate functions for background (where x is the D^* mass minus the D^0 and π mass):

$$Ax^B + C + Dx \tag{11}$$

$$A\,x^B\,exp(-Cx - Dx^2) \tag{12}$$

Figure 52 shows the fit to data using equation 11. The WS signal had 1980 events. Figure 53 shows the fit to data using equation 12. This fit had a signal of 1973 events. We used the larger difference in WS signal (31 events from equation 12) to set the magnitude of this systematic uncertainty. With the ratio of 4.05×10^{-3}, the error becomes $\pm 0.06 \times 10^{-3}$.

We originally varied the equation parameters within the fit error ellipse to get the systematic uncertainty for the mass difference background. Figure 54 shows the result when the yield plots are refit, fixing the background parameters to values along the error ellipse. The maximum RS and WS yield changes (135 and 35 events, respectively) resulted in the previous uncertainty in the ratio of $\pm 0.07 \times 10^{-3}$.

The blinded analysis predicts that the uncertainty on the amount of mis-assigned CF background in the WS plots will have a magnitude of 4.7 (yield signal) events. For the unblinded analysis and 2005 WS signal events, this gives a systematic for the WS/RS ratio of $\pm 0.01 \times 10^{-3}$.

6.3 WS Signal Results

Table 9 summarizes the systematic errors. If we add the systematic errors in quadrature, the time-integrated WS/RS ratio is 4.05 (corrected) ± 0.21 (stat.) ± 0.12 (sys.) $\times 10^{-3}$.

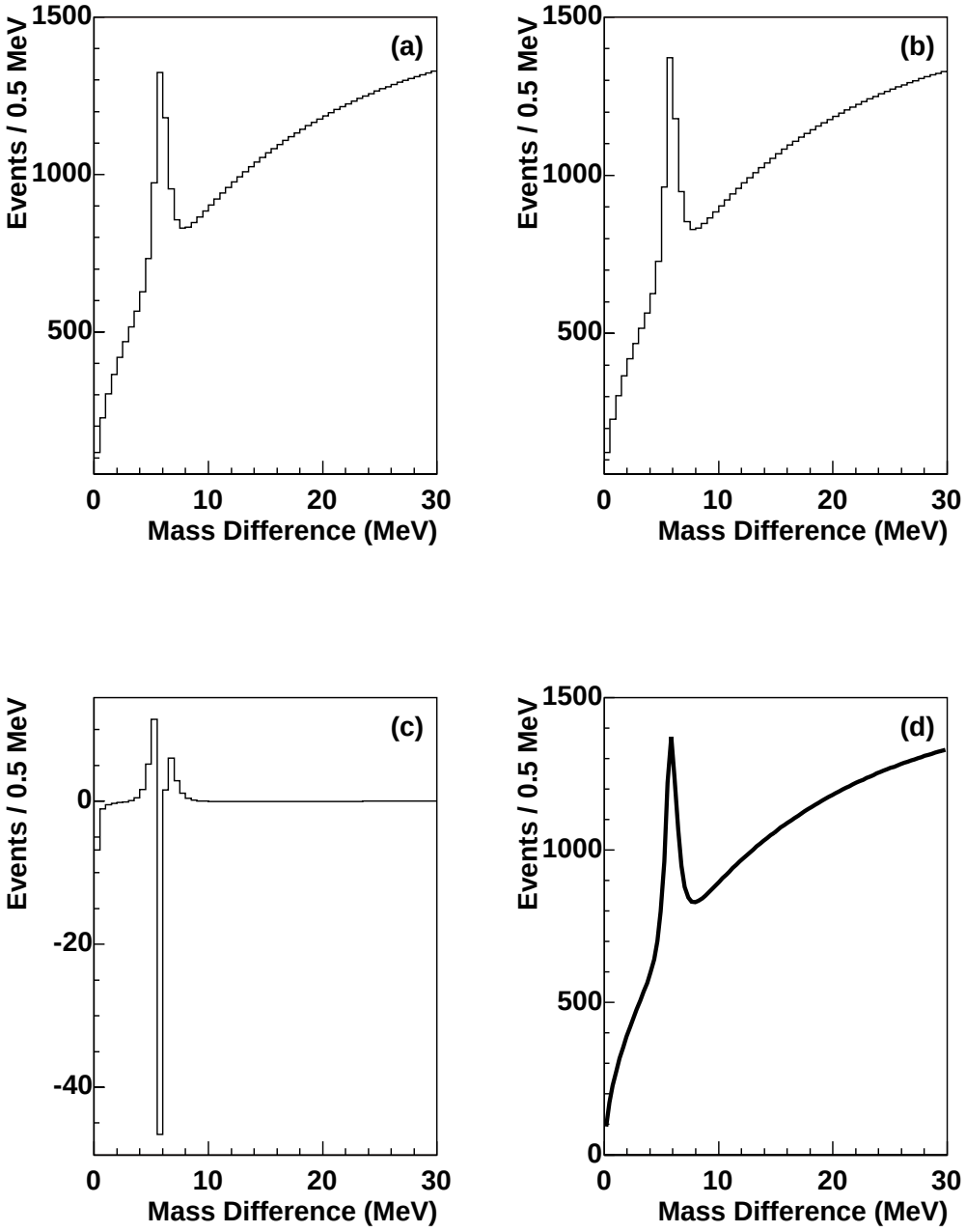

Figure 50: The fit function used for WS data (d) was used to fill histograms that have the same x-axis as the mass difference yield plots. One was filled using the function integrated across each bin (a), the other using the function evaluated at the bin center (b). The difference between the two histograms (c) shows the largest change near the signal region.

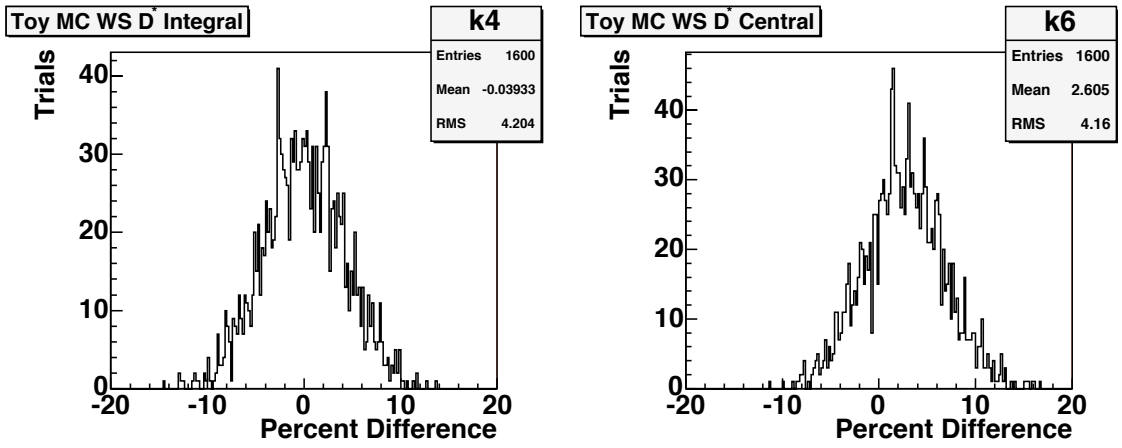

Figure 51: The toy MC was altered to try two templates. One used the function integrated across each bin, with the fitter bias results in the left plot. The other used the function evaluated at the bin center, with the fitter bias results in the right plot.

Systematic	Error ($\times 10^{-3}$)
Kpi Background Shapes	0.09
Mass Difference Background	0.06
Mis-assigned RS Background	0.01
Total	0.11

Table 9: Systematic Errors for Unblinded Data

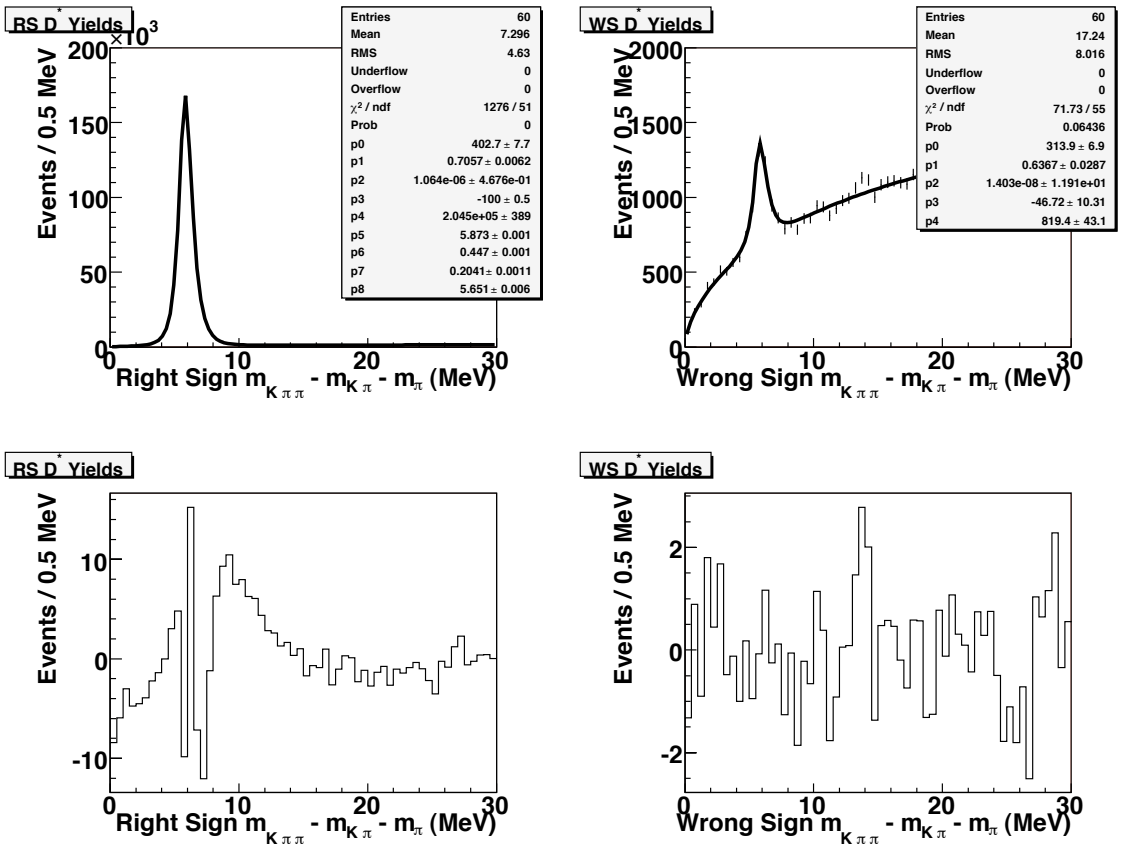

Figure 52: The function for the mass difference background was replaced with equation 11. The left plots are from the RS fits, the right plots are for the WS fits. The top plots are the fits to the mass difference yield plots (unblinded data), while the bottom plots are the pull distributions.

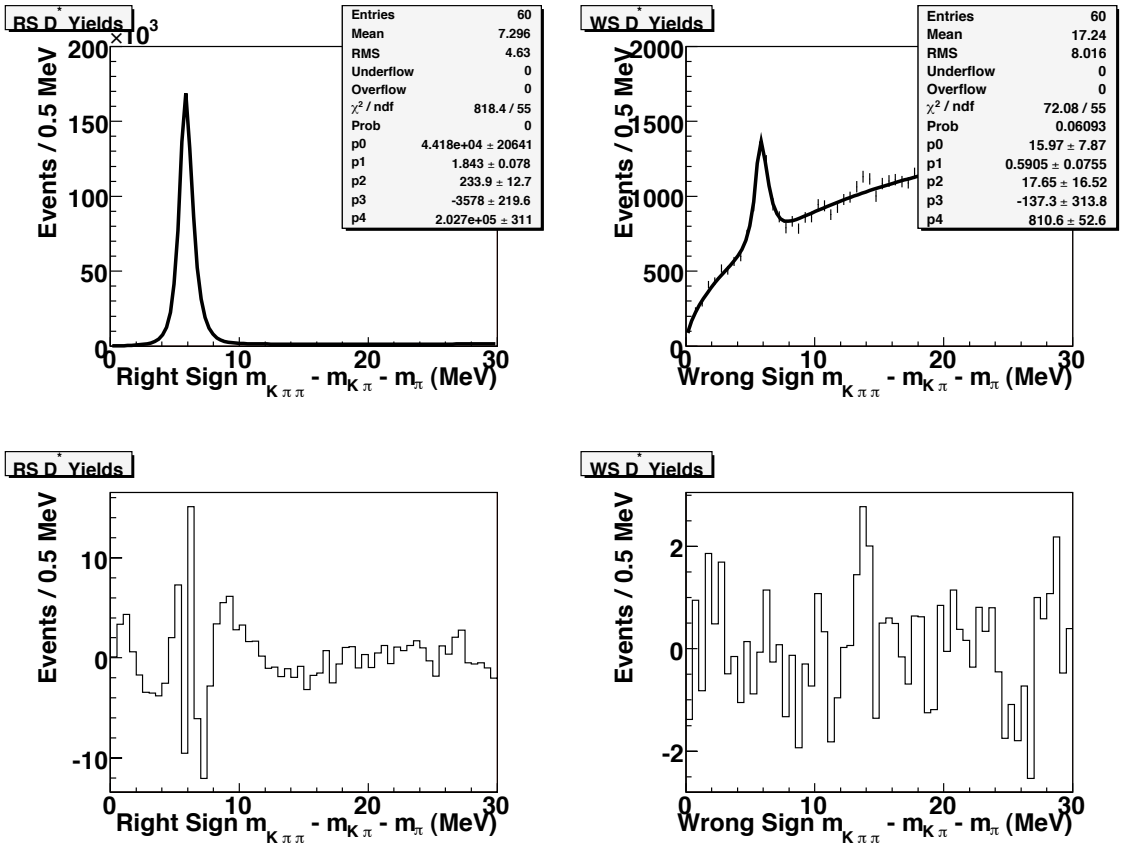

Figure 53: The function for the mass difference background was replaced with equation 12. The left plots are from the RS fits, the right plots are for the WS fits. The top plots are the fits to the mass difference yield plots (unblinded data), while the bottom plots are the pull distributions.

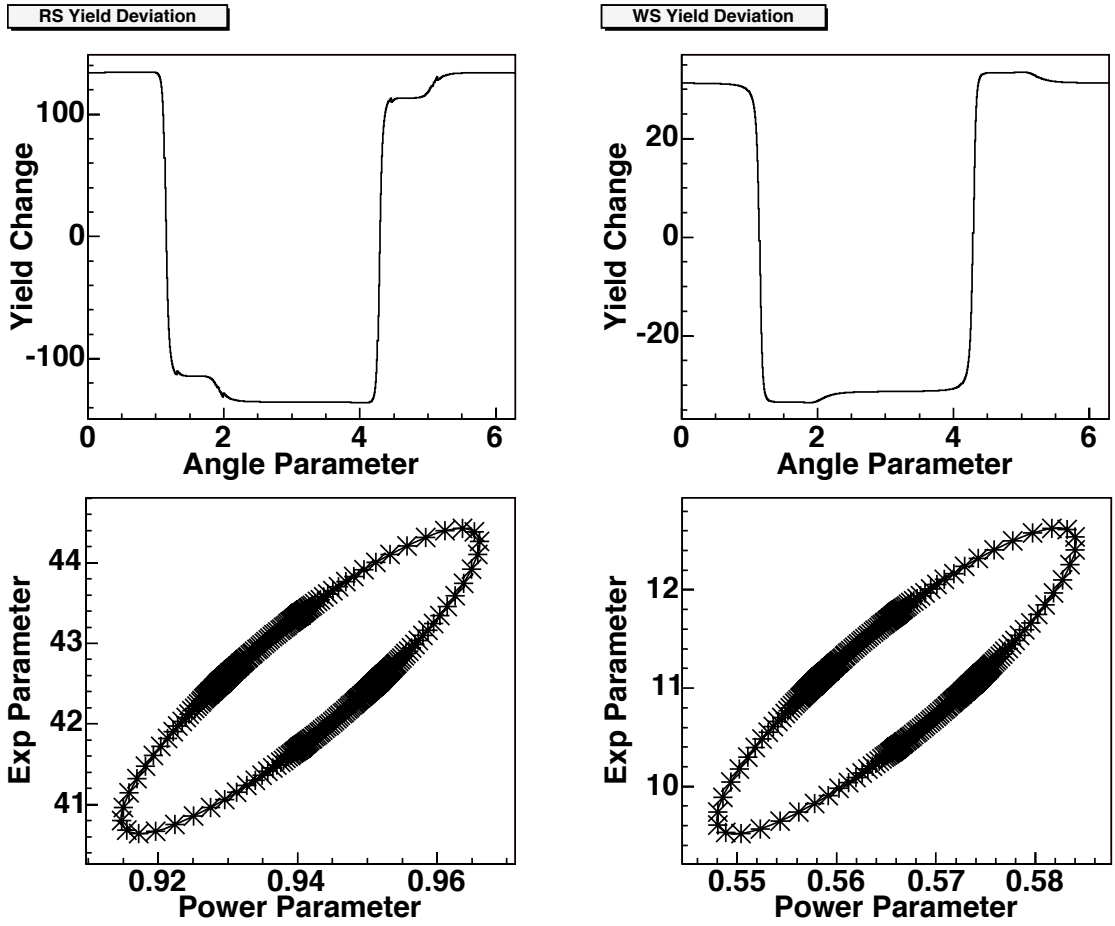

Figure 54: The parameters B and C from equation 2 were varied around the error ellipse, given by the fit covariant matrix. These parameters control the shape of the distribution. Those two parameters were fixed at specific values, and the yield plots were refit, with the signal and background amplitudes determined by the fit. The left column is for RS, right column is for WS. The top plots show the change in signal yield (from the original fit value) for the new background shape. The bottom plots show the changes in the background parameters that were used to get the error ellipse.

7 Conclusion

A set of the CDF data (xbhd0d) has been used to investigate $D^0 - \bar{D}^0$ mixing. The reconstruction uses decays with $D^0 \to K\pi$. An understanding of the backgrounds is necessary to measure the ratio of WS decays to RS decays. The largest background for the WS $K\pi$ mass plot comes from CF D^*s, where the D^0 daughter tracks have their mass assignments swapped. Studies from data and toy Monte-Carlo show that we understand how the RS sample transforms in the WS plot. That background can be mostly removed at a moderate cost to signal, by using an opposite assignment mass cut (selecting on the candidate's RS mass when plotting the WS mass combination).

A combination of techniques were used to find a set of ROOT cuts that would improve the signal to background. A cut optimization method was shown, to be used when the WS D^* signal region is blinded. If we assume that the time-integrated WS/RS ratio is 3.6×10^{-3}, the predicted uncertainties on the ratio are ± 0.21 (stat.) ± 0.11 (sys.) $\times 10^{-3}$.

After the blinded procedure was blessed, we looked at the unblinded results. The RS and WS D^* signals can be cleanly seen, against a background of correctly reconstructed D^0s with fake D^* tags, as seen in figure 55. The yields are (RS) 495172 ± 907 and (WS) 2005 ± 104. The systematic errors are detailed in table 9. With approximately $\int \mathcal{L} \sim 350\, pb^{-1}$, the time-integrated ratio of WS to RS D^0s is 4.05 ± 0.21 (stat.) ± 0.11 (sys.). This measurement is competitive with the current world-best results by Belle[17] and BABAR[18], as shown in table 10 and figure 56.

Figure 57 shows the WS $M_{K\pi}$ with the fit projections. This plot can be useful for comparison with other experiments.

The CDF II data taking continues, which will allow increased statistics for this analysis. The methods of this analysis can also be a foundation for measuring the time-dependent WS/RS ratio.

Experiment (Luminosity)	# of RS D^0	# of WS D^0	Ratio of WS / RS
PDG values[13]	BR (3.80 ± 0.09) %	BR (1.38 ± 0.11) x 10^{-4}	0.362 ± 0.030%
BABAR[18] 57.1 fb^{-1}	120000	430	0.357 $\pm 0.022 \pm 0.027$ %
Belle[17] 90 fb^{-1}	227721± 497	845 ± 40	0.381 $\pm 0.017^{+0.08}_{-0.16}$ %
CDF II (preliminary) $\sim 350 fb^{-1}$	495172 ± 907	2005 ± 104	0.405 $\pm 0.021 \pm 0.011$ %

Table 10: Latest Results of the Time-Integrated WS/RS D^0 Ratio

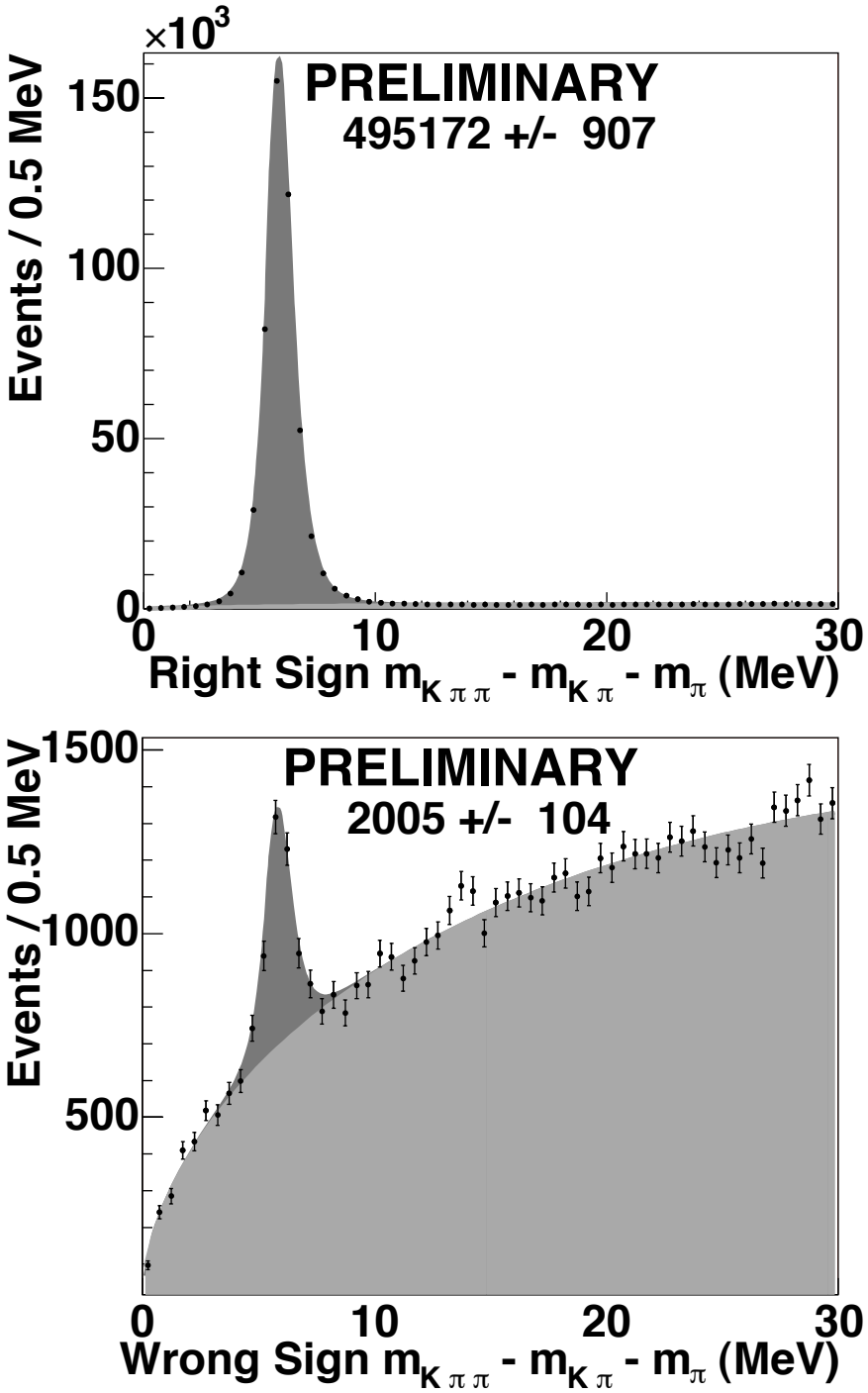

Figure 55: The number of events per bin are obtained from the signal fit of the $K\pi$ slices, with the error bars taken from the signal uncertainty of each slice. Dark grey is the signal fit, light grey is the background.

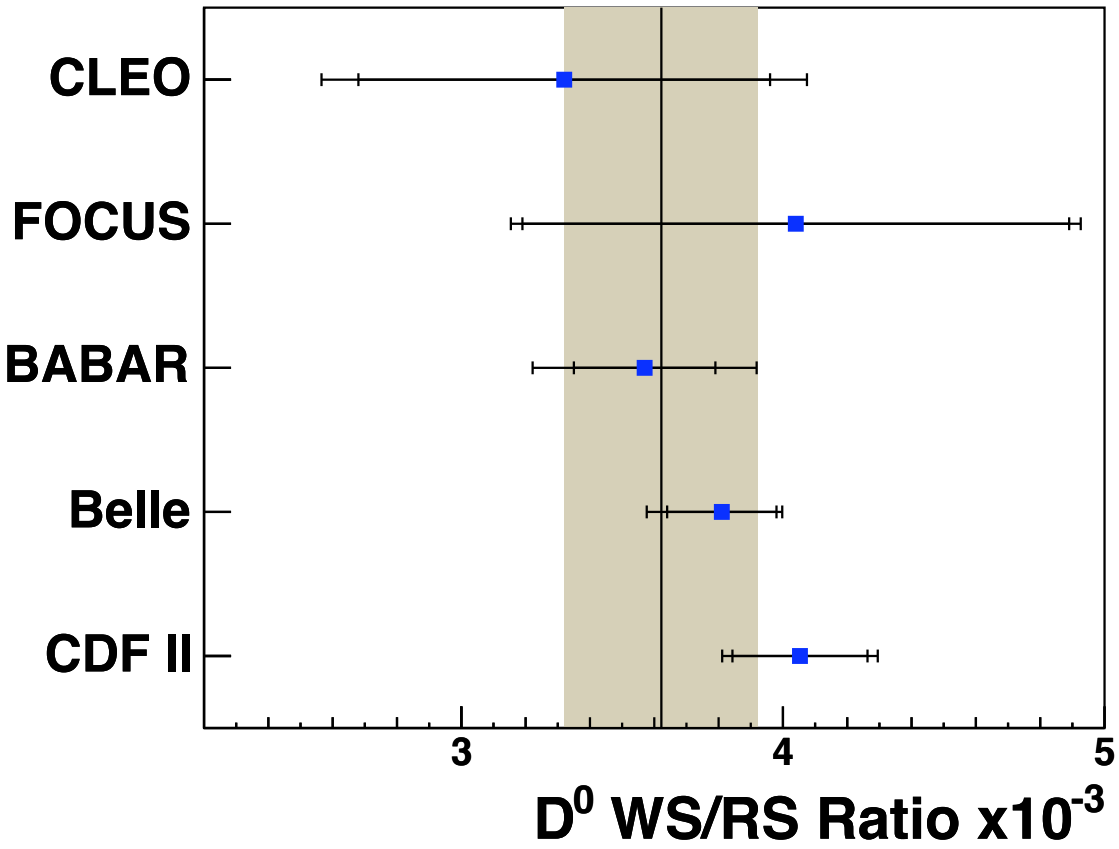

Figure 56: The time-integrated ratio of WS to RS D^0s, by experiment. The inner error bars are statistical, the outer bars are statistical and systematic added in quadrature. The grey region is the current PDG value. The CDF II result has not been added to the world average. The other experiment numbers are from tables 1.

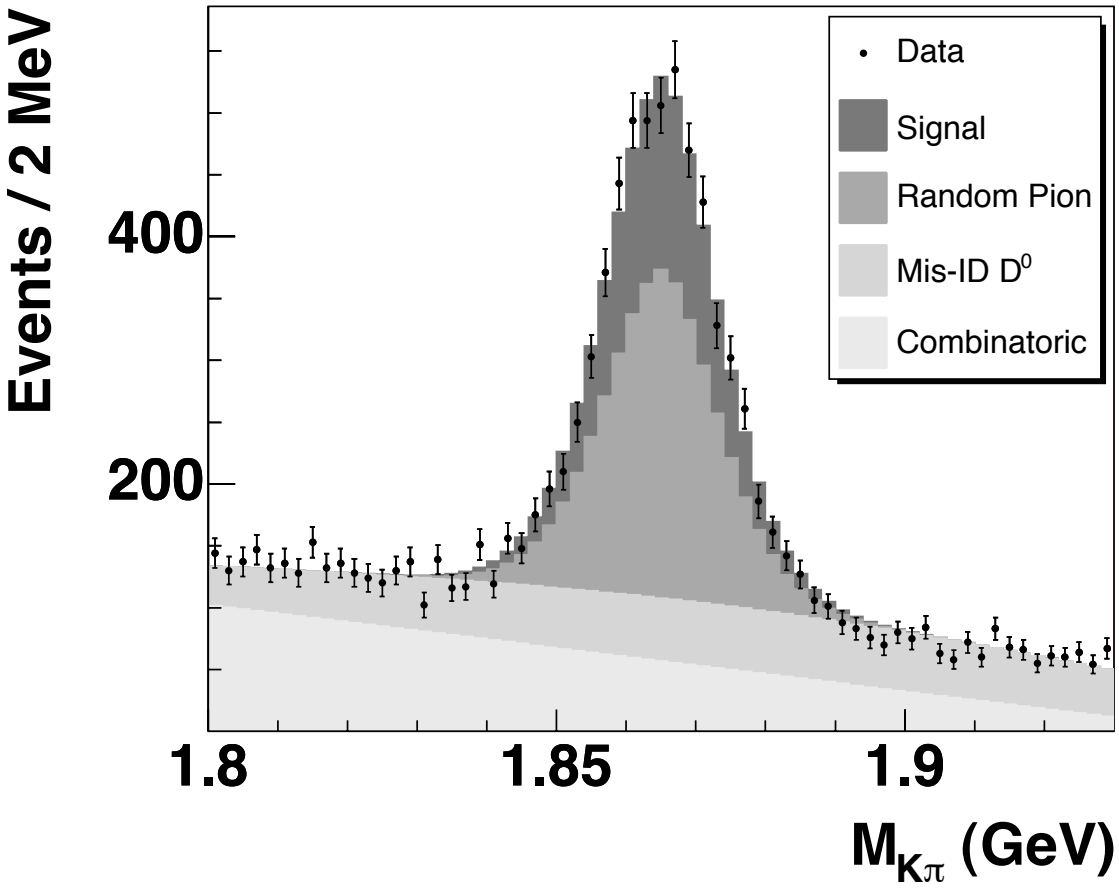

Figure 57: The distribution of WS $m_{K\pi}$ with the D^* mass difference in the range from 5-7 MeV. Superimposed on the data (points with error bars) are the projections from the yield technique fit. The projections are for WS D^0 signal, D^0s with a fake tag (random pion), CF D^*s with the kaon and pion swapped (mis-ID D^0), and other backgrounds where either or both of the high-momentum tracks do not belong to $D^0 \to K\pi$ (combinatoric).

Appendices

A Good and Other Runs

After data is written to tape, the shift crew mark bits for the run, to state which detector systems were operating good enough for use in analysis. The BPAK group has a good run list (generated by Matt Herndon) where the detector was considered good for all B analyses. The ROOT ntuples made for this analysis were not limited runs to be on the good run list.

We made the decision to only use events from the good run list for our final result, as the remainder of the events in the "bad" runs were not checked for data quality. The good runs represent 5/6ths of the events in our ntuples. We found 348 runs in our ntuple which would have contributed to our RS and WS yield plots. (There may be more runs than that, but if they were bad enough to make severe tracking errors, then they would not have survived the ntuple making requirements.) Included in that list are 125 runs from the COT compomised period (run numbers between 179056 and 182843).

Figures 58 and 59 show the WS blinded yield plots, for bad runs. The estimated WS signal to background is similar to good run data. Figure 60 shows the dE/dX cut variable for RS D^0s for the good and bad runs. The COT compromised period shows less dE/dX separation than for good runs, which is expected since the dE/dX calibrations were not computed for this period. What is interesting is that whatever default values were used do provide some particle identification. (If it was random, we would expect the distribution to be centered at zero.) The remainder of the bad runs appear to have good dE/dX particle identification.

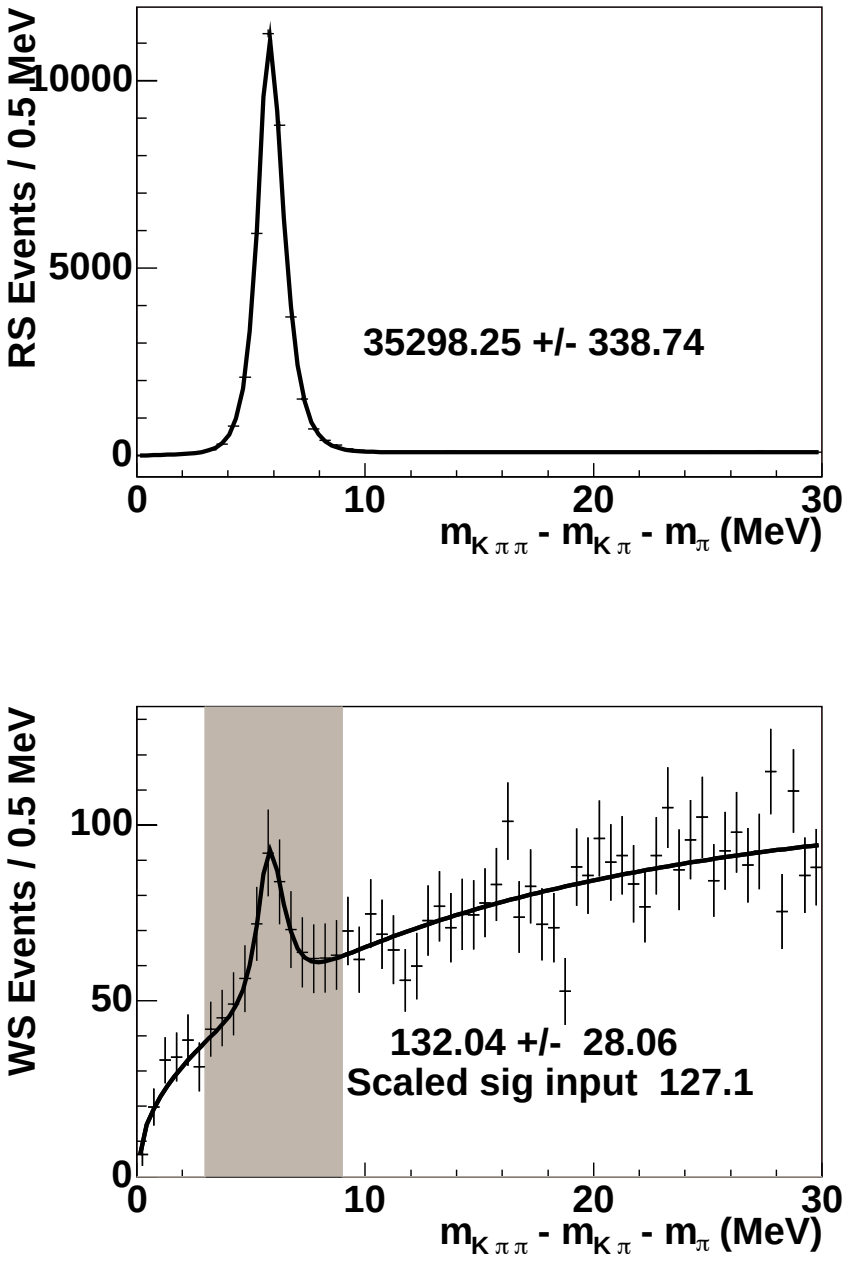

Figure 58: Yield plots for runs not in the Good Run list, excluding the COT compromised period.

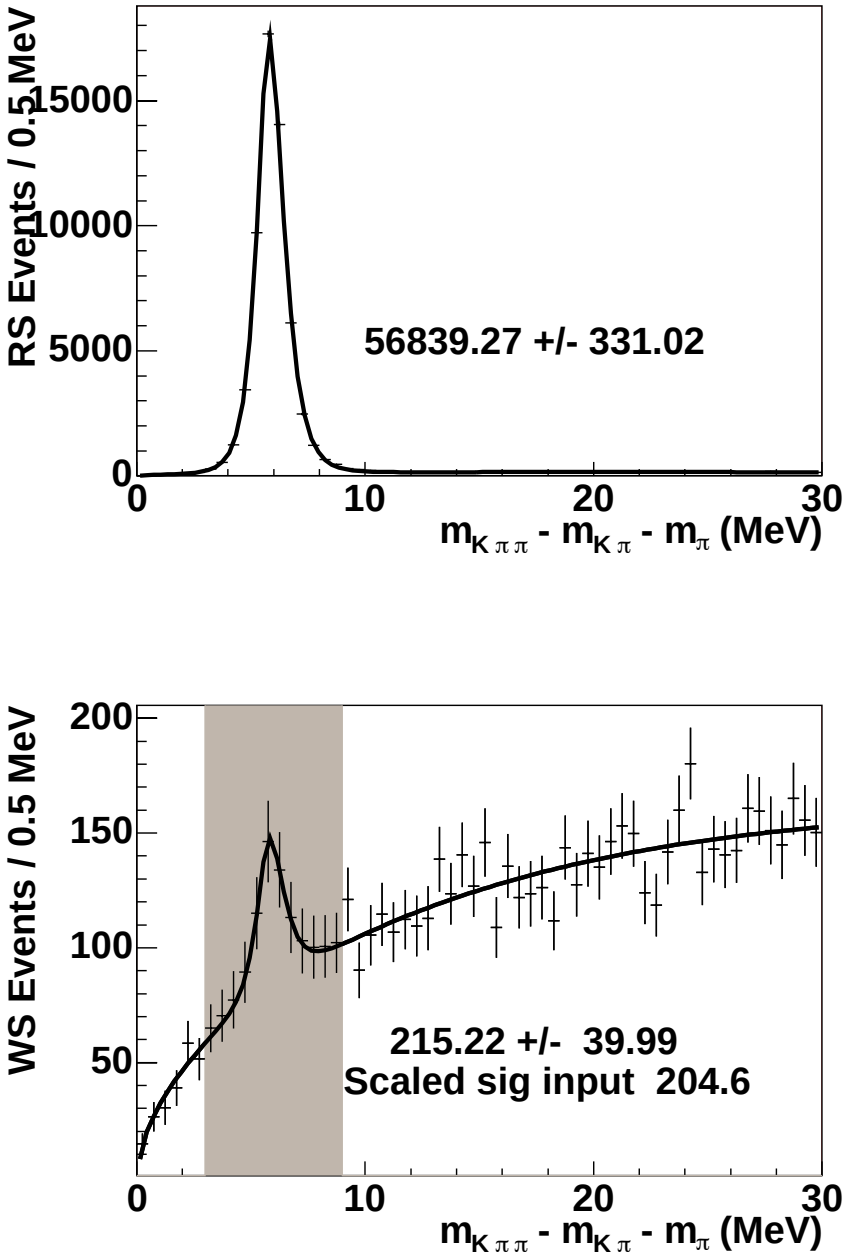

Figure 59: Yield plots for runs during the COT compromised period, run numbers between 179056 and 182843.

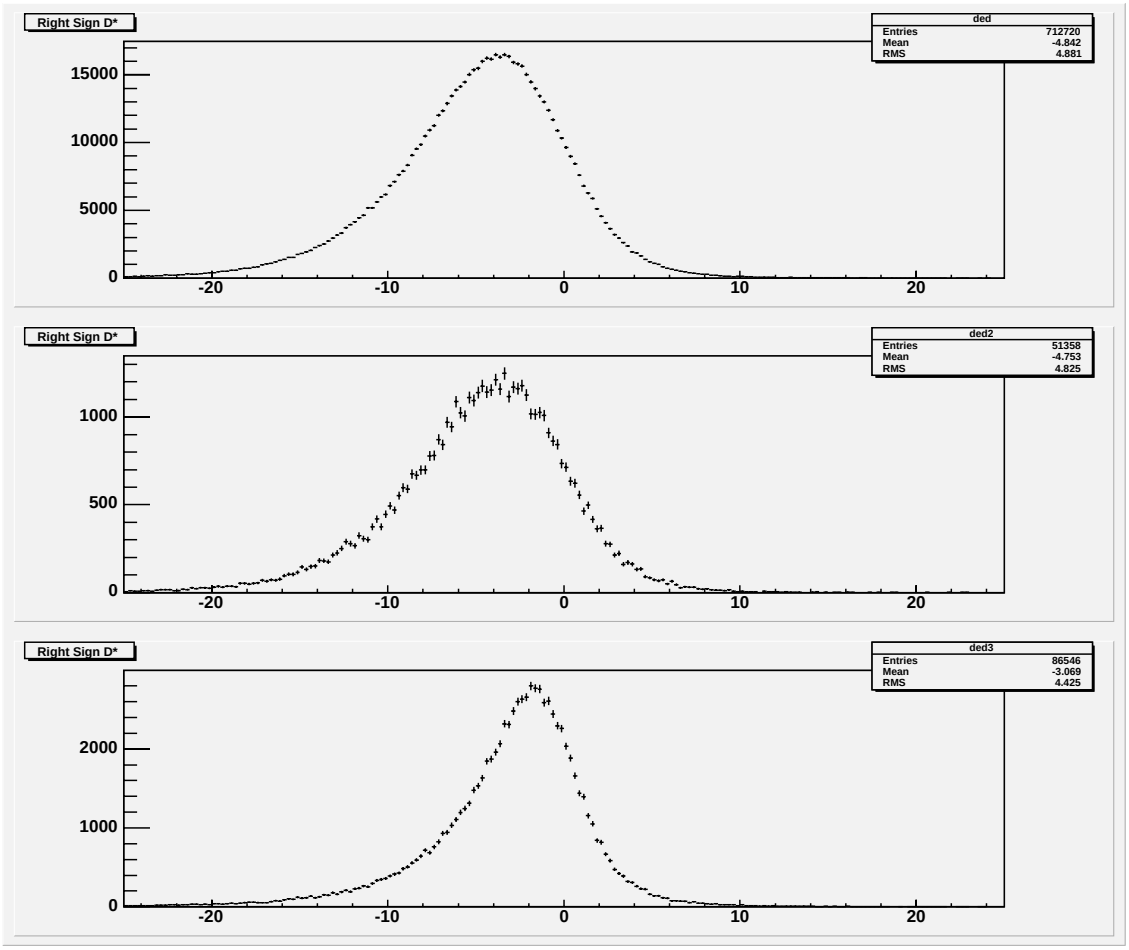

Figure 60: The dE/dX cut variable for RS D^0s, for runs in the good run list (top row), bad runs outside the COT compromised period (middle row), and the COT compromised period (bottom row).

B $K\pi$ Slice Fits

The yield technique was described in section 4.4. The next 8 pages show the slice fits that were used to make figure 55. The first four pages are for the RS $K\pi$ candidates, the last four for the WS candidates. For each plot, the x-axis is the $K\pi$ mass in GeV. The y-axis is the number of events per 2 MeV wide bin. The label at the bottom shows the range of mass difference used in the slice. There are 60 slices, each 0.5 MeV wide in mass difference. Candidates had to pass the minimum cuts, the opposite mass assignment cut, and the optimized cut list (section 5.4).

The signal shape is a variable width gaussian, described in section 4.1. The linear background and the amplitude of the signal shape were allowed to float. The green curve shows this background. For wrong-sign slices, the full fit (black curve) also includes misassigned RS background. The shape of the signal function was fixed, so the fit would still work for slices with low statistics. The shape is not normalized to the "number" parameter, so the yield of D^0s is printed in the corner of each plot. The fixed parameters for the signal shape are:

- $\mu = 1.86489$ GeV (mean value for exponential)
- $\sigma_0 = 7.71928$ MeV (minimum width)
- $B = 0.0833402$ (scale factor for growth of the width)
- $C = 1.8660$ GeV (minimum sigma at this mass value)

The fit uses the "log-likelihood" option. The χ^2 calculated in the statistics box takes the bin error as the square root of the number of events, so bins that fluctuate low will contribute more than bins that fluctuate high. The χ^2 printed on the plot itself uses the square root of the fit function value for that bin.

Appendix B: Right-Sign $K\pi$ Yield Fits

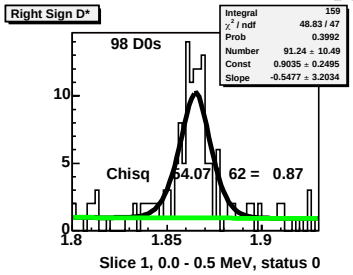

Slice 1, 0.0 - 0.5 MeV, status 0

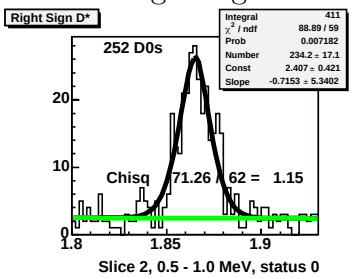

Slice 2, 0.5 - 1.0 MeV, status 0

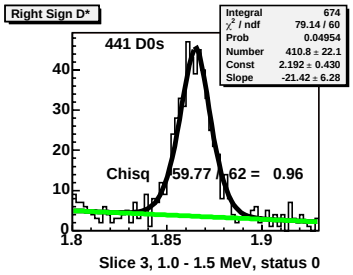

Slice 3, 1.0 - 1.5 MeV, status 0

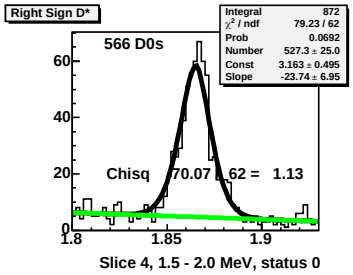

Slice 4, 1.5 - 2.0 MeV, status 0

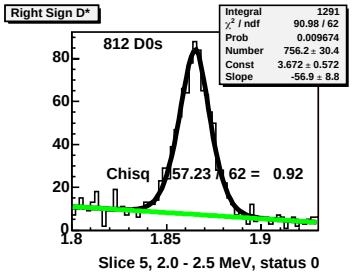

Slice 5, 2.0 - 2.5 MeV, status 0

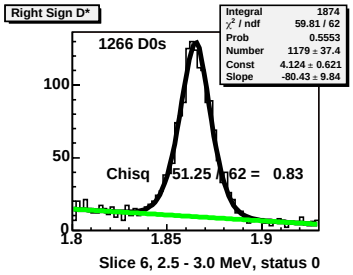

Slice 6, 2.5 - 3.0 MeV, status 0

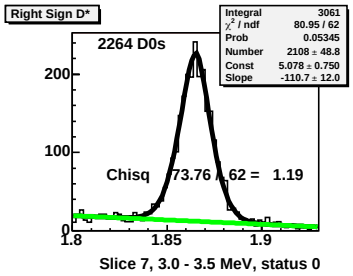

Slice 7, 3.0 - 3.5 MeV, status 0

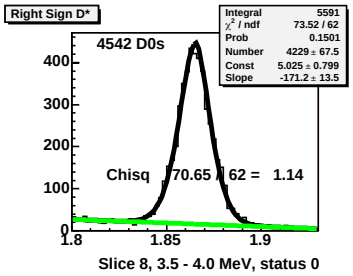

Slice 8, 3.5 - 4.0 MeV, status 0

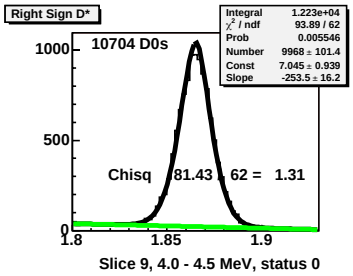

Slice 9, 4.0 - 4.5 MeV, status 0

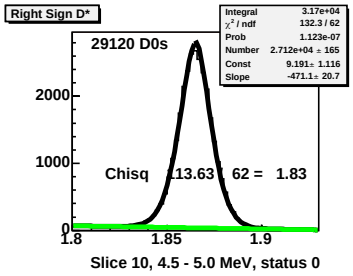

Slice 10, 4.5 - 5.0 MeV, status 0

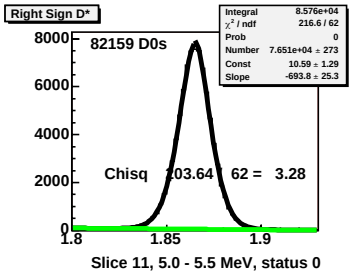

Slice 11, 5.0 - 5.5 MeV, status 0

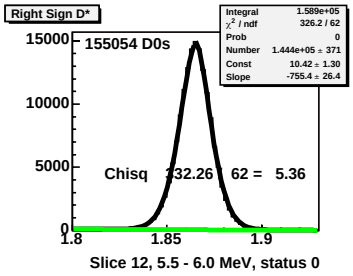

Slice 12, 5.5 - 6.0 MeV, status 0

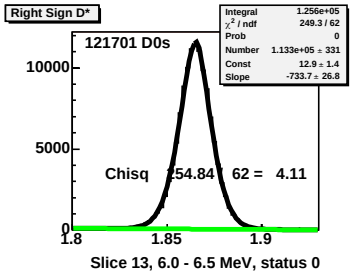

Slice 13, 6.0 - 6.5 MeV, status 0

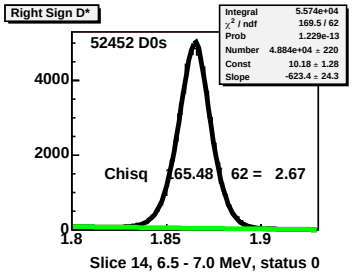

Slice 14, 6.5 - 7.0 MeV, status 0

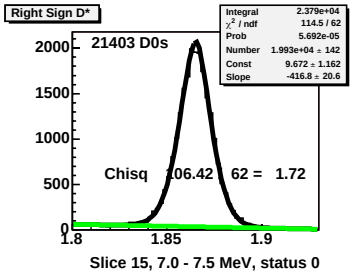

Slice 15, 7.0 - 7.5 MeV, status 0

Appendix B: Right-Sign $K\pi$ Yield Fits

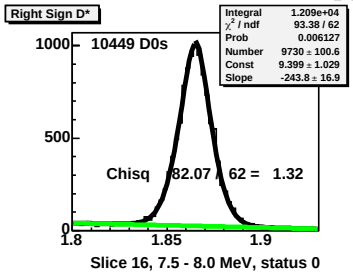

Slice 16, 7.5 - 8.0 MeV, status 0

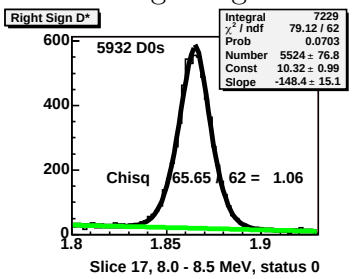

Slice 17, 8.0 - 8.5 MeV, status 0

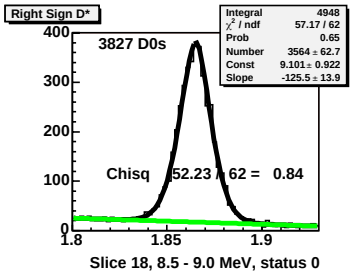

Slice 18, 8.5 - 9.0 MeV, status 0

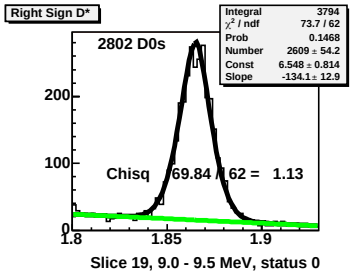

Slice 19, 9.0 - 9.5 MeV, status 0

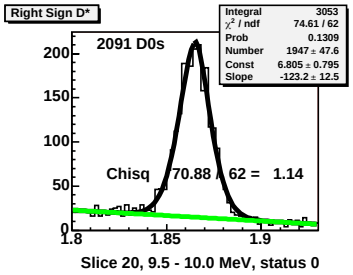

Slice 20, 9.5 - 10.0 MeV, status 0

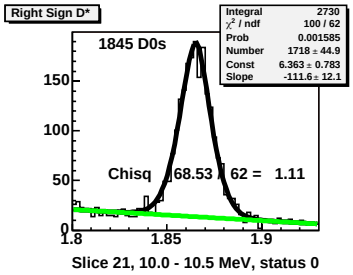

Slice 21, 10.0 - 10.5 MeV, status 0

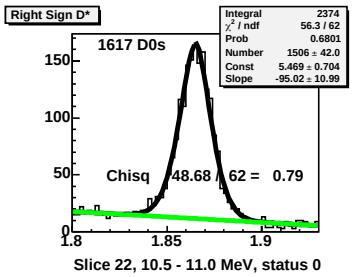

Slice 22, 10.5 - 11.0 MeV, status 0

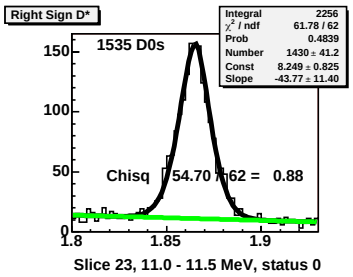

Slice 23, 11.0 - 11.5 MeV, status 0

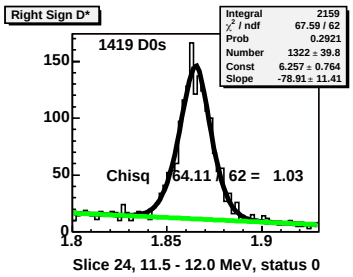

Slice 24, 11.5 - 12.0 MeV, status 0

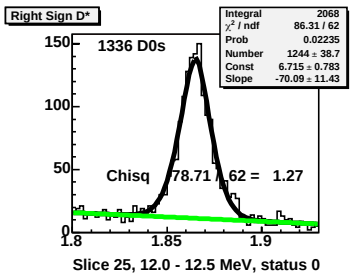

Slice 25, 12.0 - 12.5 MeV, status 0

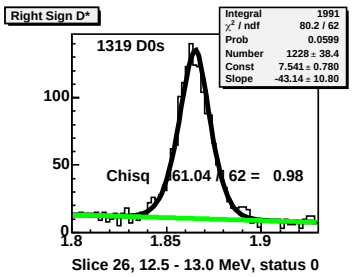

Slice 26, 12.5 - 13.0 MeV, status 0

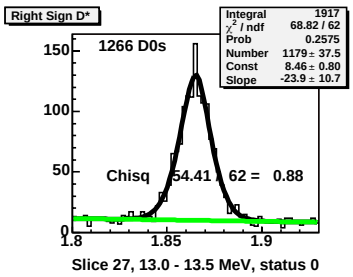

Slice 27, 13.0 - 13.5 MeV, status 0

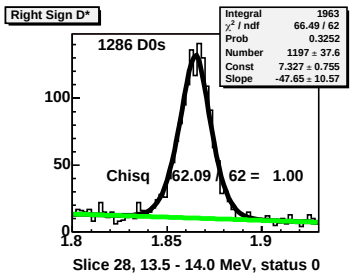

Slice 28, 13.5 - 14.0 MeV, status 0

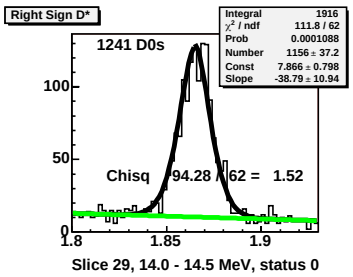

Slice 29, 14.0 - 14.5 MeV, status 0

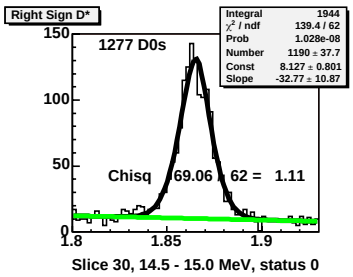

Slice 30, 14.5 - 15.0 MeV, status 0

Appendix B: Right-Sign $K\pi$ Yield Fits

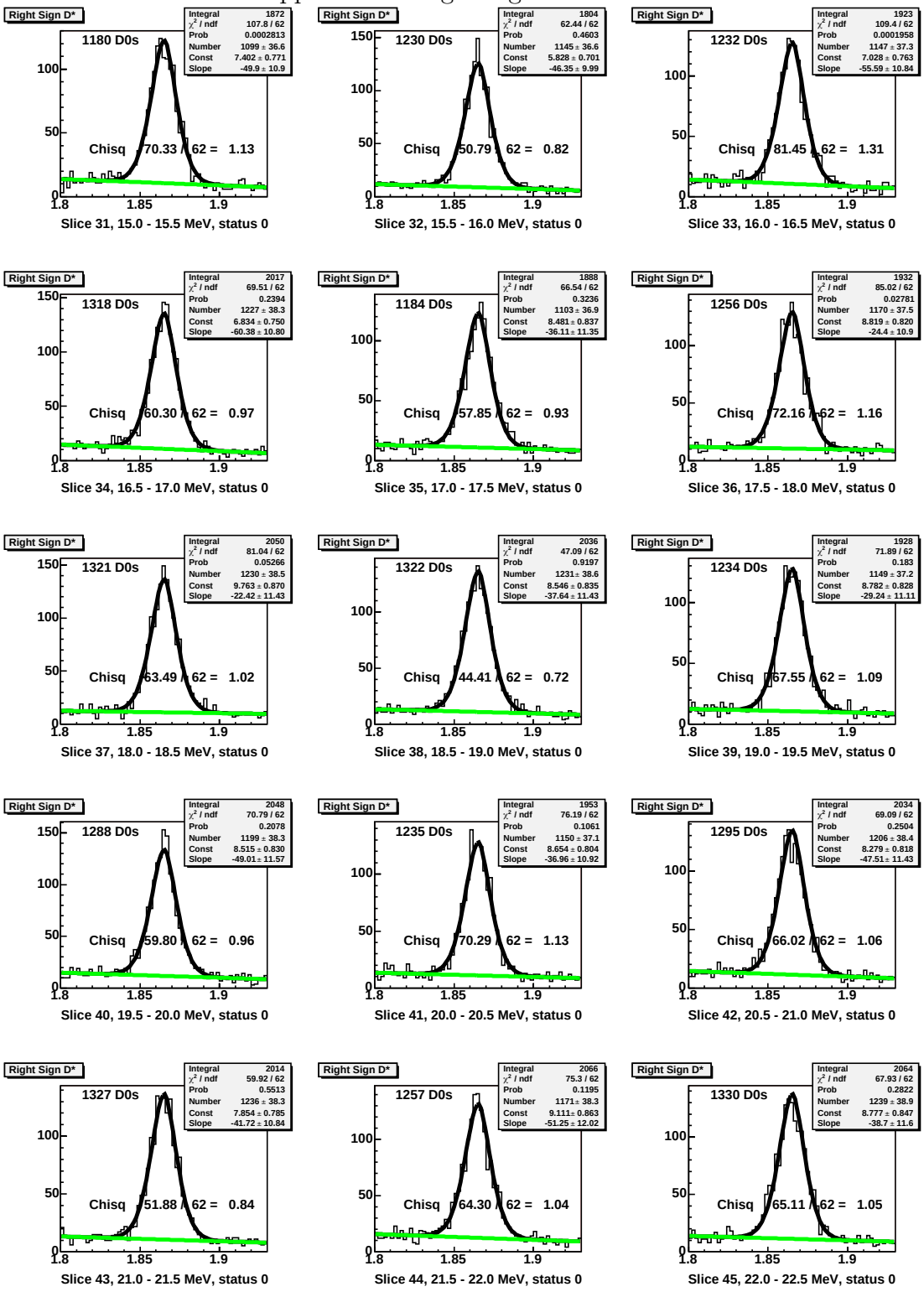

Appendix B: Right-Sign $K\pi$ Yield Fits

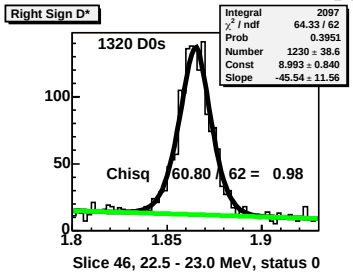

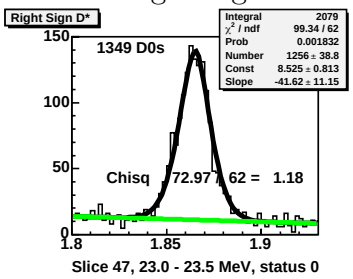

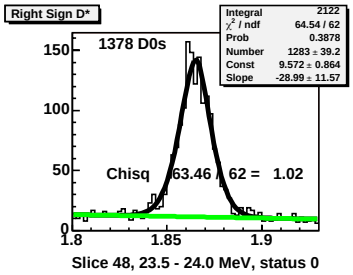

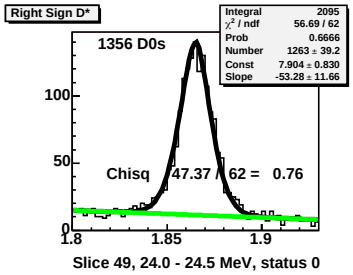

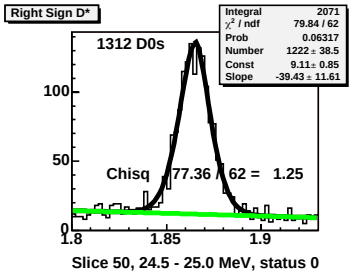

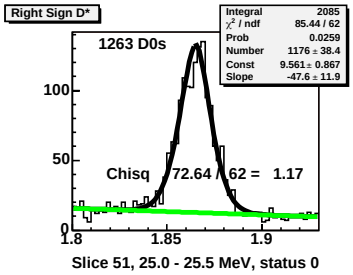

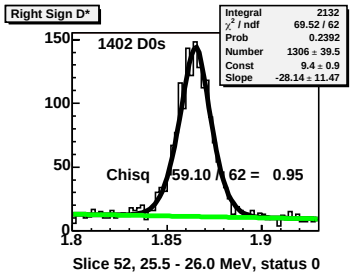

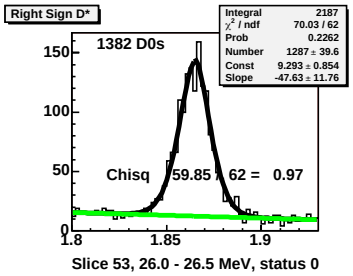

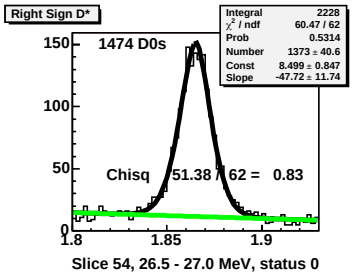

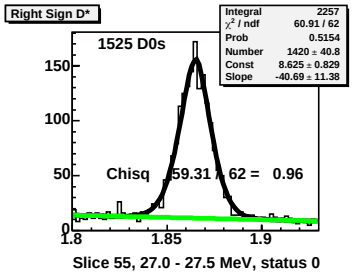

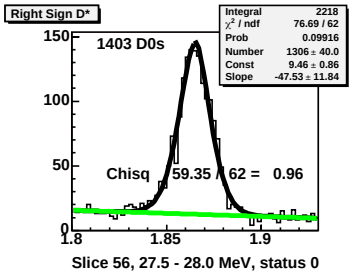

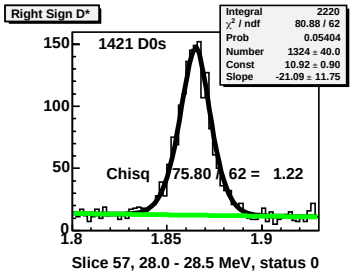

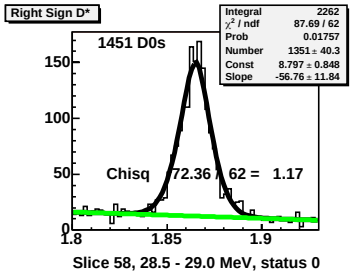

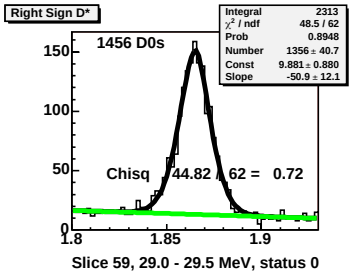

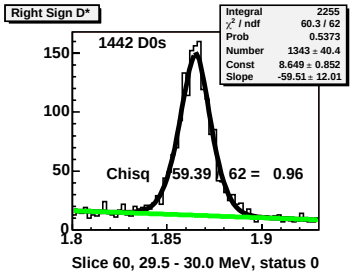

Appendix B: Wrong-Sign $K\pi$ Yield Fits

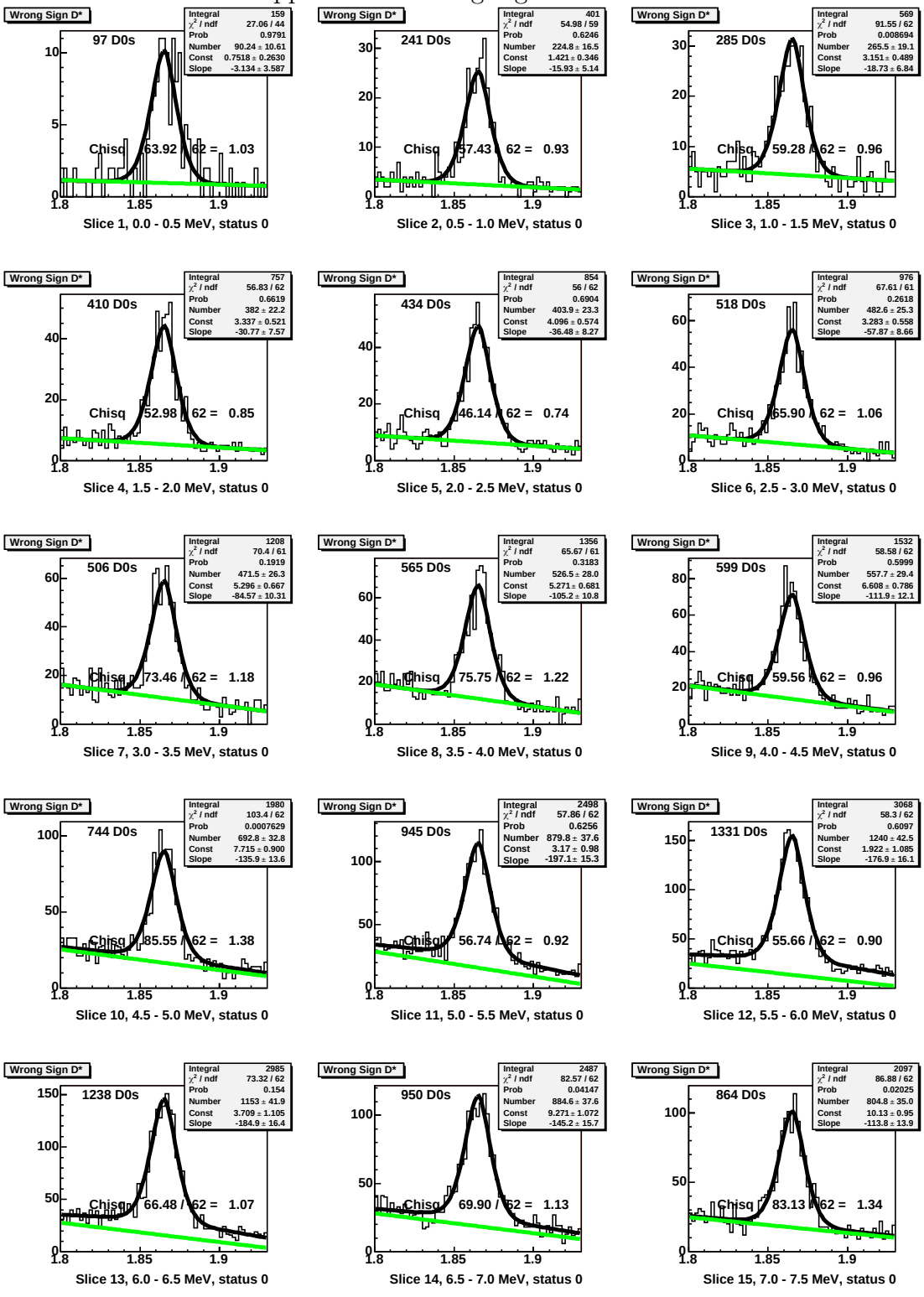

Appendix B: Wrong-Sign $K\pi$ Yield Fits

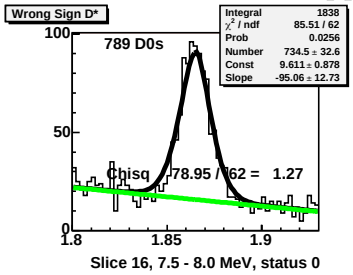

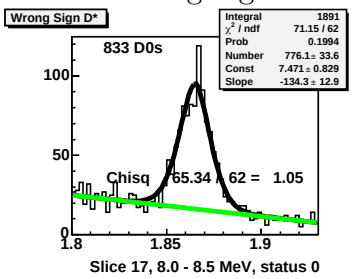

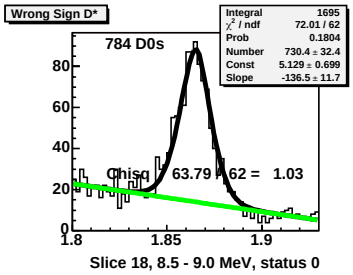

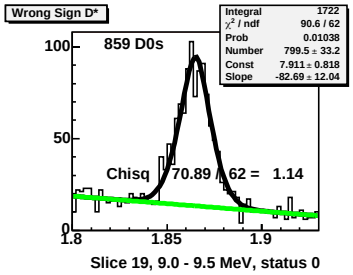

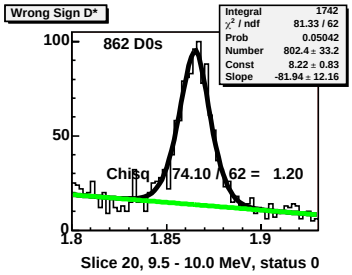

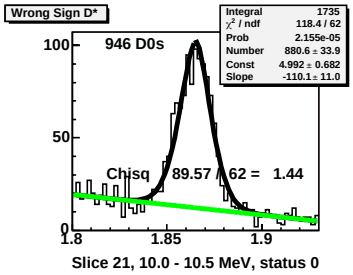

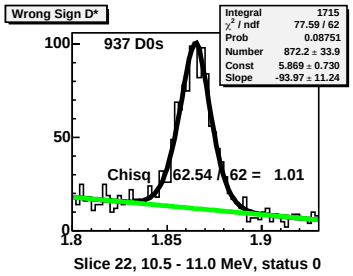

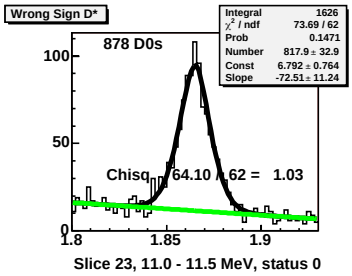

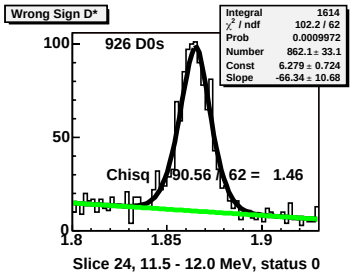

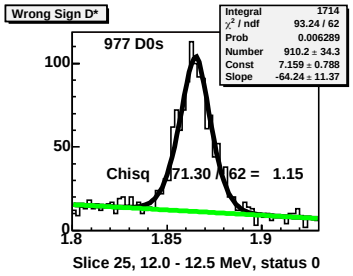

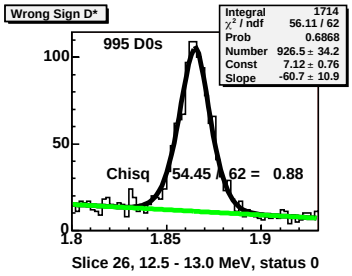

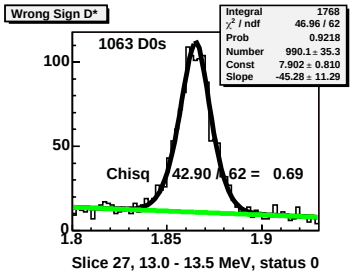

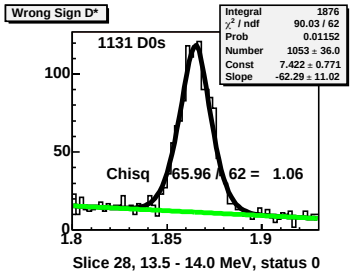

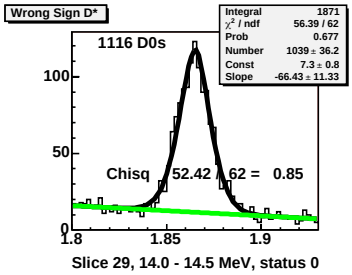

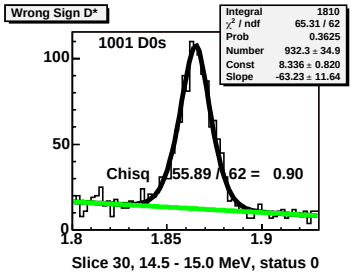

Appendix B: Wrong-Sign $K\pi$ Yield Fits

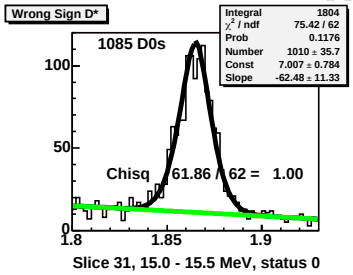

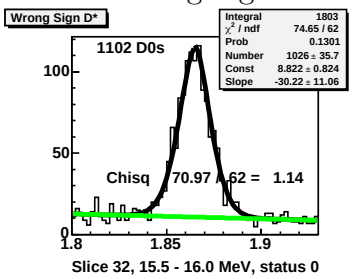

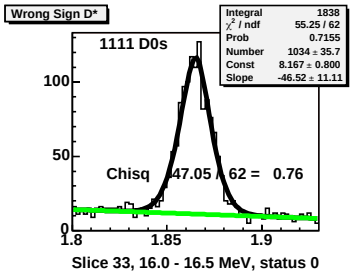

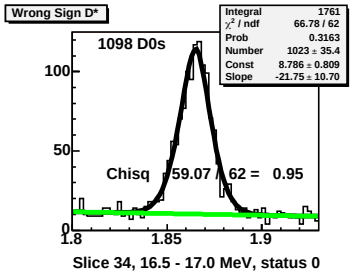

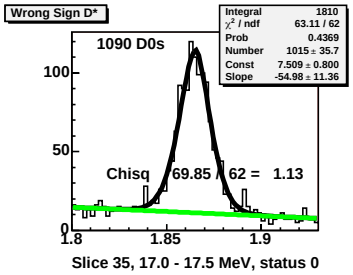

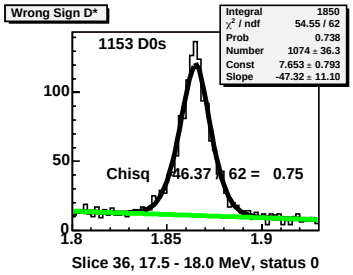

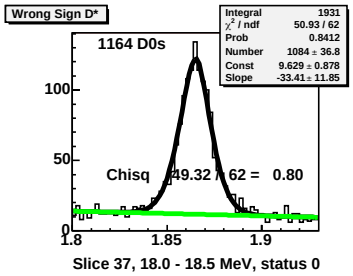

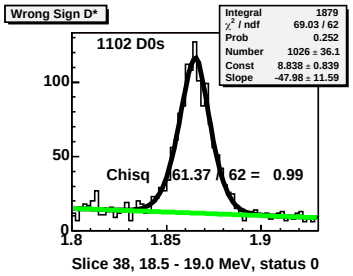

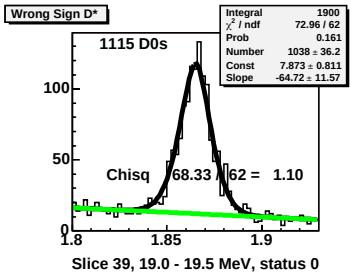

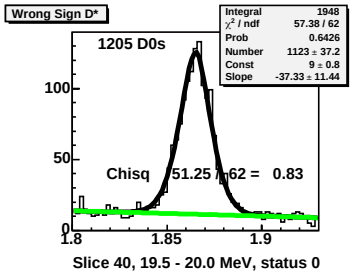

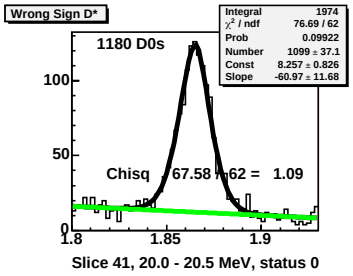

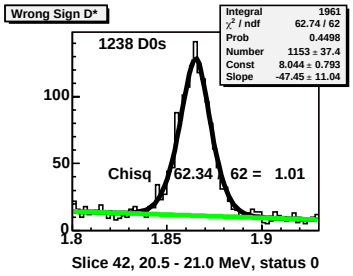

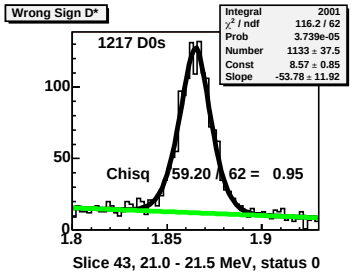

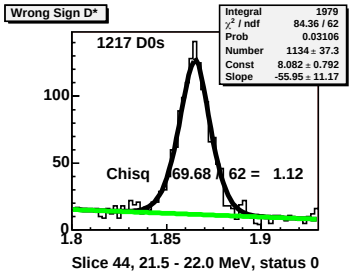

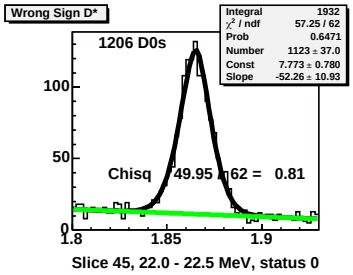

Appendix B: Wrong-Sign $K\pi$ Yield Fits

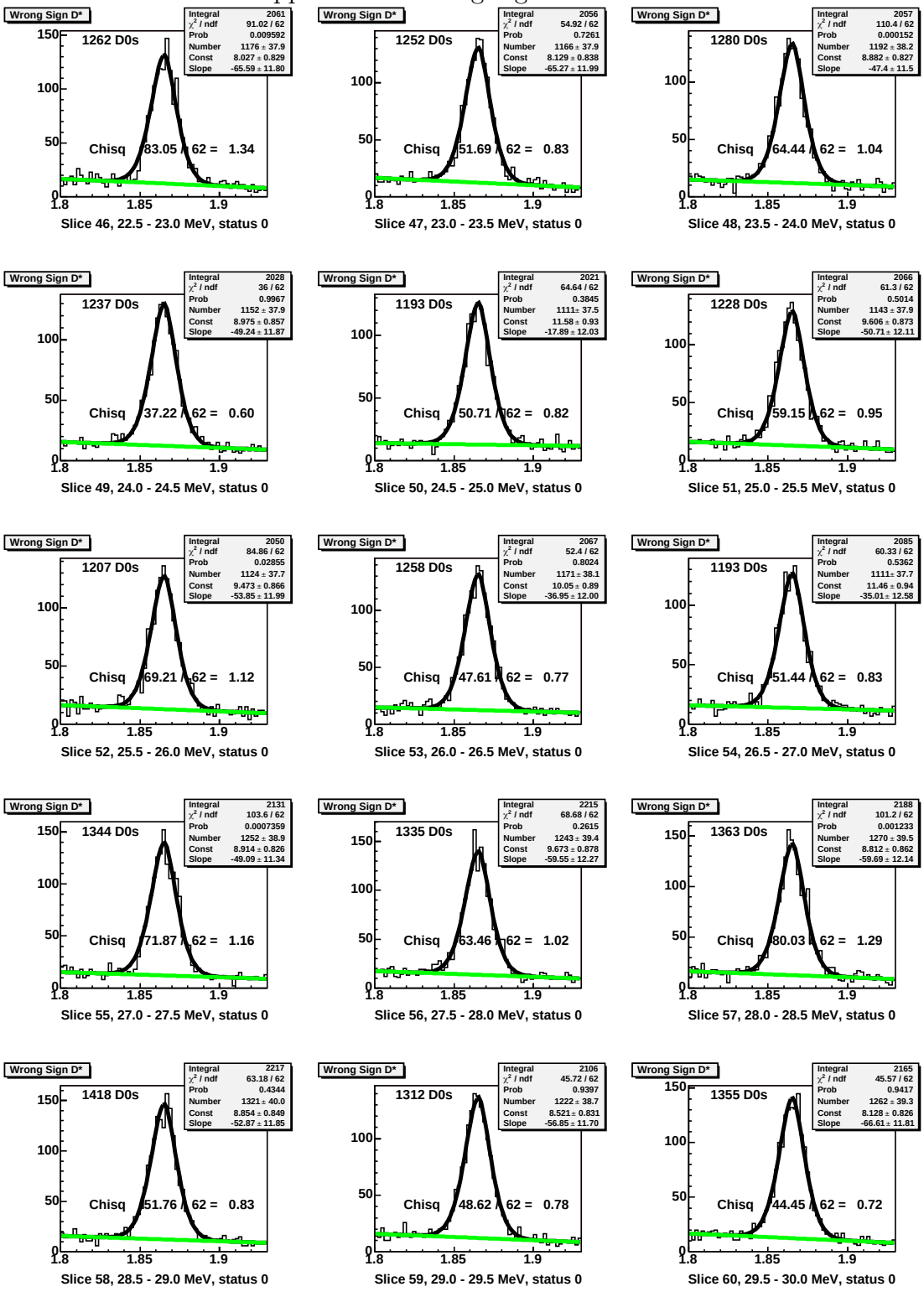

C Version Differences

As the analysis evolves, this CDF note will be modified to include new information. This section presents a history, to allow the authors to keep track of the changes.

C.1 Version 1.5

This version was posted on March 6, 2006. in preparation for the first draft of the measurement of the time-integrated ratio.

- The cut optimization plots had been left off the xbhd0d section. That has been corrected.
- With the paper Godparents, the decision was made to try alternate background functions for the mass difference yield plots, instead of varying the parameters within the fit error ellipse.
- Since CF D^0s make up the signal peak of the RS yield plot, there was a trend to use "RS signal" when "CF decay" should have been used instead. A pass was made over the note, to try to clear up the terminology used when describing the CF decays that were mis-assigned (kaon and pion particle assignments swapped) as WS events.

C.2 Version 1.4.2

This version was posted on my CDF web page on December 7, 2005. Konstantin had suggestions to improve the CDF note, which were implemented. More changes will come after this round of corrections.

- Captions previously used one argument. Two arguments are now used, which will make the figure text a different font size than the normal test.
- Figure 6 caption mentioned brown lines that showed the events that were used to get WS signal, but the figure did not have them. The figure now has dashed brown lines. (The figure underwent revisions, and at some point this mistake crept in.)
- Table 6, which describes our signal and background mass distributions, is outdated. It has been replaced by a figure (12) with cartoon distributions. The entire chapter (3) has been reorganized to better match figure 50, which has the fit projections onto a $K\pi$ distribution.

C.3 Version 1.4.1

This version was posted on October 31, 2005. The blessing of the unblinded results raised questions about the fitter bias. More investigation revealed that this was a feature of ROOT, rather than the data.

- Fitter bias no longer applied to real data. Explanation for the problem is included in the unblinded results chapter.
- Cosmetic changes to plots in the conclusion. Added a plot for the WS mass plot with fit projections.

C.4 Version 1.4

This version was posted on October 17, 2005, with the unblinded results.

- New short chapter, with the unblinded results.
- Conclusion updated

C.5 Version 1.3

This version was posted on October 10, 2005, before the blinded analysis blessing.

- Included dE/dX cut for the pi* track, in the cut list of section 5.4.2.
- Added subsection on the OAM cut efficiency from data, in section 5.5
- Added section 5.6, which has the updated support plots (RS vs WS scatter plot, WS mass vs mass diff) and the pulls for the yield fits
- Fitter bias for the yield plots is taken from the model, and described in slightly more detail

C.6 Version 1.2

This version was posted on September 26, 2005, before the pre-blessing.

- Chapter 5 is brand new. It describes the xbhd0d data set, and how the analysis procedures were modified. Also investigates the systematics.
- Chapter 6, the conclusion, has place holders for the unblinded results
- The previous Appendix A (planned work) has been removed. It has been replaced with a comment about the bad runs and COT compromised runs.
- Appendix B (K pi slices) was changed to use the xbhd0d slices (instead of hbot0h).

C.7 Version 1.1

Modifications:

- The margins were modified, to allow more room for text. This results in fewer pages, less trees used for paper.
- Appendix, conclusions, and future work sections were updated.
- Chapter 2 (Analysis Settings) used to be called "Analysis Details", and used to be after chapter 3.
- The first and last paragraphs of Analysis Settings chapter were modified. The 2004 Belle result was added.
- In chapter 3 (background), defined the exact windows used for selecting good D^0s and D^*s. Other small changes were made in wording, especially in reference to figures.
- The table of backgrounds, that used to be in the Conclusion, was moved to the end of the Background's chapter.
- The WS vs RS Scatter plot (figure 6) was replaced. The text dealing with that figure has been rewritten for more detail.
- Figure 7 was moved into the section discussing RS D* background.
- The last section of chapter 3, which dealt with the opposite assignment cut, was removed. That information will resurface in the new chapter dealing with signal optimization.
- The Future Work chapter was moved to the appendix.

Additions:

- Largest addition was the new chapter "Signal Optimization", which deals with finding a set of ROOT cuts for the hbot0h data.
- Added a section called "Analysis Strategy" to the Introduction.
- An appendix section was added, to include $K\pi$ slice fits for the yield results of figure 23.
- Version differences (this appendix) was added, in anticipation of more notes.

(Still to be done:

- Once the note is in good shape, the current version number (1.5) needs to become 1.1.
- Reference all b-hadronic talks

)

C.8 Version 1.0

This version was posted as the first CDF note dealing with this analysis. It has chapters discussing theory, a list of background sources, descriptions of the analysis code settings, and potential future work.

References

[1] Mark Mattson and Paul Karchin, *Initial Status Report on D-Mixing*, B Hadronic Meeting, Sep 15, 2003.

[2] Mark Mattson and Paul Karchin, *Update on Wrong Sign D^0*, B Hadronic Meeting, Nov 24, 2003.

[3] Mark Mattson and Paul Karchin, *Wrong Sign D^0 Decays - Update*, B Hadronic Meeting, March 1, 2004.

[4] Mark Mattson and Paul Karchin, *Wrong Sign D^0 Decays - Update*, B Hadronic Meeting, May 24, 2004.

[5] Mark Mattson and Paul Karchin, *Wrong Sign D^0 Decays - Update*, B Hadronic Meeting, August 23, 2004.

[6] Paul Karchin and Mark Mattson, *Update on the Measurement of Wrong Sign D0 to K+pi- Decays*, B Hadronic Meeting, October 4, 2004.

[7] Mark Mattson and Paul Karchin, *Wrong Sign D^0 Decays - Update*, B Hadronic Meeting, January 24, 2005.

[8] CDF, D. Acosta et al., *Measurement of the Mass Difference $m(D_s^+)$ - $m(D^+)$ at CDF II*, Phys. Rev. **D68**, 072004 (2003), hep-ex/0310043.

[9] S. Giagu et al., *Measurement of Partial Widths and Search for Direct CP Violation in D^0 Meson Decays to KK and $\pi\pi$*, CDF-Note 6989, 2004.

[10] Mario Campanelli and Elena Gerchtein, *Measurement of the D_2 Meson in the $D^{\pm}\pi^{\mp}$ Channel, and Combined Results With $D^{*\pm}$*, CDF-Note 7109, 2004.

[11] CDF, D. Acosta et al., *Measurement of Prompt Charm Meson Production Cross Sections in $p\bar{p}$ Collisions at $\sqrt{s}$ = 1.96-TeV*, Phys. Rev. Lett. **91**, 241804 (2003), hep-ex/0307080.

[12] Alexey A Petrov, *CP-Violation and Mixing in Charmed Mesons*, Continuous Advances in QCD/Arkadyfest (2002), hep-ph/0209049.

[13] Eidelman, S. and others, *Review of Particle Physics*, Physics Letters B **592**, 1 (2004).

[14] Alexey Petrov, *$D^0 - \bar{D}^0$ Mixing and CP Violation*, B Hadronic Meeting, Dec 15, 2003.

[15] Alexey A. Petrov, *On Dipenguin Contribution to $D^0 - \bar{D}^0$ Mixing*, Phys. Rev. **D56**, 1685 (1997), hep-ph/9703335.

[16] K. Abe et al., *A Measurement of the Rate of Wrong-Sign Decays $D^0 \to K^+\pi^-$. ((B))*, (2002), hep-ex/0208051.

[17] BELLE, K. Abe et al., *Search for D0 anti-D0 mixing in $D^0 \to K^+\pi^-$ decays and measurement of the doubly-Cabibbo-suppressed decay rate*, Phys. Rev. Lett. **94**, 071801 (2005), hep-ex/0408125.

[18] BABAR, B. Aubert et al., *Search for $D^0 - \bar{D}^0$ Mixing and a Measurement of the Doubly Cabibbo-Suppressed Decay Rate in $D^0 \to K\pi$ Decays*, Phys. Rev. Lett. **91**, 171801 (2003), hep-ex/0304007.

[19] CLEO, R. Godang et al., *Search for $D^0 - \bar{D}^0$ Mixing*, Phys. Rev. Lett. **84**, 5038 (2000), hep-ex/0001060.

[20] FOCUS, Jonathan M. Link, *$D^0 - \bar{D}^0$ Mixing in FOCUS*, (2001), hep-ex/0106093.

[21] A. Belloni, I. K. Furic, and Ch. Paus, *Multibody Trigger Paths in the Two Track Trigger Data*, CDF-Note 6526, 2003.

[22] S. D'Auria et al., *The CharmMods/DFinder Reconstruction Package Reference Manual*, CDF-Note 6158, 2003.

[23] S. D'Auria et al., *Relative Branching Fractions and CP-violating Decay Rate Asymmetries in Cabibbo Suppressed Decays of the D^0 Meson*, CDF-Note 6391, 2004.

[24] Shin-Shan. Yu et al., *COT dE/dx Measurement and Corrections*, CDF-Note 6361, 2003.

[25] Saverio D'Auria et al., *Track-based calibration of the COT specific ionization*, CDF-Note 6932, 2004.